STRESS-STRAIN BEHAVIOUR

OF REMOULDED LIAS CLAY

SYAWOSH NASSERI

A THESIS SUBMITTED FOR THE DEGREE OF

DOCTOR OF PHILOSOPHY

Department of Civil Engineering
University of Aston in Birmingham

June 1976

SUMMARY

This work is concerned with laboratory investigations of the behaviour of remoulded Lias clay under different stress paths. Basic mechanical properties of the soil were determined and were used in a theoretical study of its stress-strain behaviour based on the strain-hardening plasticity concept and time-dependent strains. Remoulded samples of Lias clay were prepared in a specially developed 100 mm diameter tall oedometer; triaxial and oedometer tests were carried out on 70 mm diameter specimens. Stress-controlled tests were carried out using a specially developed dead loading system in which corrections could be made for change in cross-sectional area of the samples.

The results indicated that the initial mixing (preparation) water content and the one-dimensional consolidation stress-history of the soil affect its subsequent stress-strain behaviour: an increase of the effective mean stress of the order of four times the original consolidation stress is needed to eliminate the stress-history of the soil. The void ratio - mean effective stress plots for isotropic and anisotropic consolidation cases are parallel, and in the latter case approach the state-of-failure line (C.V.R.) as the value of q/p increases. A linear relationship between shear strains from drained and undrained compression tests was obtained which, in conjunction with shear strains from constant stress ratio tests could be used to predict shear strains for any stress increment resulting in plastic strains. It was also found that plastic strain increments and undrained stress paths (for isotropic and anisotropic cases) were not predicted well by the Modified Cam-clay Model. It was confirmed also that the plastic strain increment vector is stress-path dependent; this implies that there is no unique plastic potential surface for a given soil, but its shape is stress-path or stress-history dependent.

ACKNOWLEDGEMENTS

The Author wishes to express his thanks to :

Dr K Starzewski who has supervised the work and for his advice and encouragement.

Mr D H Bennett for frequent discussions and his interest.

The Department of Civil Engineering for providing financial support.

Mr M J Lyons (Soil Technician) for his assistance during experimental work, and the team of technicians in the Departmental workshop for manufacturing some of the apparatus.

Miss D Bailey who patiently and carefully typed the script.

CONTENTS

CONTENTS (contd)

CONTENTS (contd)

CONTENTS (contd)

CHAPTER ONE

INTRODUCTION

1.1 Introduction

Generally, practical load-deformation problems in soil mechanics are dealt with by considering 'deformation' and 'failure' separately. These considerations involve different parameters and different assumptions for the same soil. For example, in stability analysis, a failure criterion is usually postulated based on shear strength properties of the soil, and the ultimate loading is worked out without any consideration of deformations of the soil prior to the failure. On the other hand, consideration of the deformations of soil under working load are usually restricted to the consolidation process or even a quasi-elastic treatment: very frequently the induced stresses within the soil mass due to the applied loading are evaluated according to the elastic theories and then deformations are worked out using the one or three dimensional consolidation theory.

Over the recent years a unified treatment (from small load increments, right up to failure) of load-deformation behaviour of normally consolidated (soft) soils, based on the theory of strain-hardening plasticity has emerged (Drucker et al, 1957 and Roscoe et al, 1963).

In Chapter 2 of the present work existing theories are reviewed briefly and their assumptions and limitations are examined with reference to the normally consolidated Lias clay.

The testing programme and techniques used in this research are described in Chapter 3, which also includes details of conventional and special apparatus used and developed for this project.

Physical properties of Lias clay and the method of preparation of remoulded samples are dealt with in Chapter 4. Detailed test results are presented in Chapter 5, and are reviewed and discussed in Chapter 6, which also includes a description of the effects of the initial one-dimensional consolidation stress-history on the subsequent behaviour of the samples in the triaxial tests and comparison of predicted and observed strains and stress paths of the soil tested.

This work is concluded in Chapter 7 which includes a summary of general conclusions and suggestions for further research.

CHAPTER TWO

DEFORMATION & SHEAR STRENGTH OF NORMALLY CONSOLIDATED CLAY

2.1 Introduction

For many years the approach to the problems of soil as a load carrying material was separately concerned with the determination of the maximum load or stress carrying capacity (i.e. failure), and determination of the working load settlements or deformations. Only in the recent years the attention was focussed on the stress-strain behaviour of the soil up to and beyond the working stress level. Obviously there are a number of familiar difficulties associated with the treatment of the soil as an engineering material. Because of the granular nature of the soils their macroscopic behaviour depends upon the relative movement of the particles under stress, which in turn is controlled by the nature of the particles and of the contacts between them. In addition to the above the stress-strain properties of the soils are generally stress and strain-history dependent.

Therefore, a theoretical treatment of the stress-strain behaviour of real soils is more complicated and practical solutions are more difficult to obtain than for any other engineering material; it is therefore necessary to introduce some idealizations.

Theoretical solutions concerning stress-strain relationships and time-dependent displacements for compressible soil (soft clay) are discussed in this chapter; their application to remoulded Lias clay is dealt with in Chapter 6.

2.2 One Dimensional Consolidation

Over the last 50 years the classical theory of one-dimensional consolidation, developed by Terzaghi (1925), has formed the basis of analytical predictions of settlements from laboratory test results. The theory is founded on the basic assumption of one-dimensional compression of a saturated soil due to one-dimensional Darcean flow of pore water under excess hydrostatic (pore-water) pressure induced by the applied loading.

In more detail, Terzaghi's concept of one-dimensional consolidation involves the following assumptions : (a) the soil is homogeneous and saturated, (b) compression of the soil and flow of pore water are one-dimensional, (c) the flow of water is governed by Darcy's Law, (d) soil grains and pore water are incompressible in comparison with the soil skeleton, (e) for any one load increment the coefficients of compressibility ($a_v = \frac{\delta e}{\delta \sigma'}$) and permeability, k, are constant, (f) at all times the sum of the inter-granular stress, σ', and the excess hydrostatic pressure, u, is equal to the total applied stress, σ, (g) the rate of the consolidation process is entirely governed by the permeability of the soil.

By equating the volume of expelled pore water to the reduction in the void ratio of an element of soil, the following well-known equation of one-dimensional consolidation is obtained :

$$C_v \frac{\delta^2 u}{\delta Z^2} = \frac{\delta u}{\delta t} \qquad (2.1a)$$

Where C_v is the coefficient of consolidation $C_v = \frac{k(1+e_o)}{\gamma_w a_v} = \frac{k}{m_v \gamma_w}$.

The solution to this equation is usually presented as a function of U in terms of independent variables: time t (usually in a dimensionless form known as the time factor, $T = \frac{C_v}{H^2} t$), and depth Z. The settlement in one-dimensional consolidation is obtained from the following equation:

$$\rho_t = m_v(\Delta\sigma - u)h = m_v h U \Delta\sigma' \qquad (2.1b)$$

Where h is the thickness of the sample and U the degree of consolidation.

The results of consolidation tests are usually presented in the form of vertical effective stress vs. void ratio curves. Although the consolidation is generally taken as the principal mechanism in which the time element enters the mathematical calculations of deformation of soils, it does not take into account the time dependent nature of the deforming soil under a constant effective stress, i.e. the relationship between the void ratio and the effective stress is assumed to be independent of time. Results of laboratory tests and observations clearly demonstrate that deformations do not cease at the end of the dissipation of the induced pore pressures; e.g. the tail end of an experimental consolidation curve does not correspond to the theoretical consolidation curve, but exhibits an increase in deformation at a constant effective stress. This rheological or creep phenomenon has been studied by Terzaghi and others and has been termed "secondary consolidation". The part of the deformation controlled by the dissipation of the pore pressure (drainage of pore water) has been termed "primary consolidation".

2.2.1 Secondary Consolidation

Many attempts have been made to develop theoretical or semi-empirical models which would form the basis of analytical predictions of the laboratory consolidation test results, and field settlements of natural clay deposits.

Of the theoretical treatments, the works of Taylor and Merchant (1940), and Biot (1956), were the first rheological studies of the problem of secondary consolidation. Following works of Tan (1957), Gibson and Lo (1961), and Anagosti (1963), on linear rheological models, and of Barden (1965), on a non-linear model, appear to be the most significant ones. The models used mainly consist of Hookean spring and Kelvin dashpot or Maxwell body in series or in parallel. Thus a linear spring and dashpot represent a linear model, and a non-linear dashpot with linear spring form a non-linear model (Gibson and Lo's model is discussed separately in section 2.2.2). Of the semi-empirical treatments, Buisman's (1936) suggestion that the "secondary consolidation increases proportionally to the logarithm of time", is perhaps the best known and has been used in practice. However, it implies a non terminating deformation of the soil which is not acceptable because a sample of soil cannot be compressed to nothingness. A more rational approach based on the logarithmic law is the so called Isotaches method, suggested by Šuklje (1957). Isotaches are graphs relating intergranular stress, σ', to the void ratio, e, for what Šuklje terms a 'constant rate of consolidation' ($\frac{\delta e}{\delta t}$ = constant); it is assumed that the principal effective stress ratio is constant or that its change does not influence the consolidation rate. This approach takes into account the effect of

the thickness of the consolidation layer on the secondary consolidation. An important contribution to the understanding of the secondary consolidation was the Bjerrum's (1967) suggestion that the secondary consolidation process begins immediately on application of the load. He has demonstrated that in one dimensional consolidation, instead of there being a unique relationship between the void ratio and intergranular stress (as assumed in the Terzaghi's theory) a system of approximately parallel curves exists, each representing a void ratio - effective stress relationship at a specific time of sustained loading, i.e. $e = [e(\sigma')]t$ = constant. More recently, Lowe (1974), has analysed the results of gradient-controlled tests, using "the rate of strain" as a third variable in the relationship between the void ratio and intergranular stress. This in fact is another way of expressing the Bjerrum's (1967) concept of 1-day, 10-day, 100-day, etc., lines on the void ratio versus logarithm of stress plot.

2.2.2 Gibson and Lo's Solution

This solution is concerned only with one-dimensional consolidation. The soil skeleton is replaced by a rheological model consisting of a Hookean spring connected in series with a Kelvin element as shown in Fig. 2.1. The process of consolidation has been interpreted in the following way :

When a time dependent stress $\sigma'(t)$ acts on an element of the soil at depth Z, the spring 'α' compresses instantaneously, but the settlement of the compound element 'b'-'λ' is retarded because of the presence of dashpot 'λ'. Since in soils of low permeability the

transference of stress from the pore water to soil skeleton is delayed by the slow rate of drainage, the effective stress $\sigma'(t)$ increases gradually from zero to the full value of the applied stress. Hence, the compression of spring 'a' is also gradual and is fully accomplished only when the applied stress has become fully effective. The process during which the compression of spring 'a' is accomplished is equivalent to the Terzaghi's consolidation. Under the gradually increasing effective stress the Kelvin body commences to compress. Initially the full load is taken by the Newtonian dashpot 'λ' but, as the compression proceeds, it is progressively transferred to the spring 'b'. This phenomenon of transference corresponds to the process of secondary consolidation which occurs under a sustained effective stress. After a very appreciable time has elapsed the full effective stress is transferred to the springs 'a' and 'b', and the dashpot 'λ' sustains no load.

The total strain, ε, is the sum of the strain ε_H of the Hookean spring 'a' and of the strain ε_K of the Kelvin body:

$$\varepsilon = \varepsilon_H + \varepsilon_K \tag{2.2}$$

The strain in 'b' is proportional to its load while in 'λ' the load governs the rate of viscous deformation. The sum of the stress in elements 'b' and 'λ' must be equal to the effective stress $\sigma'(t)$. It follows that :

$$\frac{\varepsilon_K}{b} + \frac{1}{\lambda} \frac{d\varepsilon_K}{dt} = \sigma'(t) \tag{2.3}$$

where both ε_K and $\sigma'(t)$ are functions of the depth Z. The solution of

this equation (for $\varepsilon_K = 0$ at $t = 0$) is :

$$\varepsilon_K = \int_0^t \sigma'(\tau) \bar{e}^{\frac{\lambda}{b}(t-\tau)} d\tau \tag{2.4}$$

and:

$$\varepsilon = a\sigma'(t) + \int_0^t \sigma'(\tau) \bar{e}^{\frac{\lambda}{b}(t-\tau)} d\tau \tag{2.5}$$

The pore pressure dissipation is assumed to be governed by the equation of one-dimensional consolidation (2.1a). Hence substituting

$$d\varepsilon = \frac{-de}{1+e} \tag{2.6}$$

we can write

$$\frac{k}{\gamma_w} \frac{\delta^2 u}{\delta Z^2} = -\frac{\delta \varepsilon}{\delta t} \tag{2.7}$$

Since in one-dimensional compression $du = -d\sigma'$, equation (2.7) becomes :

$$\frac{k}{\gamma_w} \frac{\delta^2 \sigma'}{\delta Z^2} = a\frac{\delta \sigma'}{\delta t} + \lambda\sigma' - \frac{\lambda^2}{b} \int_0^t \sigma'(Z,\tau) \bar{e}^{\frac{\lambda}{b}(t-\tau)} d\tau \tag{2.8}$$

which is the one-dimensional equation of consolidation expressed in terms of the effective stress. The usual boundary conditions used for the solution of equation (2.8) are :

$$\left.\begin{aligned} \frac{\delta \sigma'}{\delta Z} &= 0, \quad Z = h \\ \sigma' &= q(t), \quad Z = 0 \end{aligned}\right\} \; 0 < t \leq \infty \tag{2.9}$$

For the case of step loading, where q(t) is monotonic loading, we have :

$$q(t) = 0 \qquad t < 0$$

$$q(t) = q_o \qquad t > 0 \tag{2.10}$$

The following solutions have been obtained by Gibson and Lo (1961):

(a) For the settlement S(t) at time t:

$$S(t) = (a+b)q_o h \left\{ 1 + \frac{\rho}{\pi^2} \sum_{n=0}^{\infty} \frac{1}{(2n+1)^2} \left[\frac{k-x_1}{x_1-x_2} e^{-x_2 t} - \frac{k-x_2}{x_1-x_2} e^{-x,t} \right] \right\} \tag{2.11}$$

(b) For the pore water pressure :

$$u(Z,t) = \frac{\pi(a+b)}{\pi a} q_o \sum_{n=0}^{\infty} \frac{1}{2n+1} \left\{ \frac{x_1\left(\frac{a}{a+b} - \frac{x_2}{k_1}\right)}{x_1 - x_2} e^{-x,t} - \frac{x_2\left(\frac{a}{a+b} - \frac{x_1}{k_1}\right)}{x_1 - x_2} e^{-x_2 t} \right\} . \sin \frac{(2n+1)\pi Z}{2n} \tag{2.12}$$

The following substitutions have been made :

$$\theta = \frac{k}{a\gamma_w} \tag{2.13}$$

$$\beta = \frac{\lambda}{b} \tag{2.14}$$

$$\alpha = \lambda[\frac{1}{a} + \frac{1}{b}] \tag{2.15}$$

$$k_1 = \frac{(2n+1)^2\pi^2\theta)}{4h^2} \tag{2.16}$$

$$k = [\frac{a}{a+b}]k_1 \tag{2.17}$$

$$\frac{x_1}{x_2} = \frac{(a+k_1) \pm \sqrt{[\alpha+k_1)-4\beta k_1]}}{2} \tag{2.18}$$

For small values of time the solution can be simplified to :

$$S(t) = \frac{2}{\sqrt{\pi}}\sqrt{(\theta t)}\ aq_o[1+\frac{1}{3}\ \frac{\lambda}{a}\ t + O(\frac{\lambda^2 t^2}{a^2})] \tag{2.19}$$

and for large values of time :

$$S(t) = q_o h[a+b(1-e^{-\frac{\lambda}{b}t}] \tag{2.20}$$

For the limit $t \to \infty$

$$S = (a+b)q_o h \tag{2.21}$$

For a soil which is infinitely viscous ($\lambda \to 0$) or when there is no secondary compression ($b \to 0$), equation (2.19) reduces to :

$$S(t) = aq_o\left(1 - \frac{8}{\pi^2} \sum_{n=0}^{\infty} \frac{1}{(2n+1)^2}\ e^{-\frac{h^2\pi^2}{4}\ \frac{\theta t}{h^2}}\right) \tag{2.22}$$

This is identical to the classical solution of the Terzaghi's one-dimensional consolidation problem. For practical application of the theory Gibson and Lo have made the following suggestions:

$\theta = \frac{k}{a\gamma_w}$ is the coefficient of consolidation which can be determined in the conventional way, from a plot of settlement against the square root of time. The parameters a, b, λ, can be found from equation (2.20), rewritten in the following form :

$$\frac{S(t)}{hq_o} = \frac{\varepsilon(t)}{q_o} = (a+b) - be^{-\frac{\lambda}{b}t} \tag{2.23}$$

or from combined equation (2.20) and (2.21) :

$$\frac{\varepsilon(\infty) - \varepsilon(t)}{\sigma'} = be^{-\frac{\lambda}{b}t} \tag{2.24}$$

Taking the logarithim of both sides

$$\log_{10}\frac{\varepsilon(\infty) - \varepsilon(t)}{\sigma'} = \log_{10} b - 0.434\,\frac{\lambda}{b}\,t \tag{2.25}$$

Hence a plot of $\log[\varepsilon(\infty) - \varepsilon(t)]/\sigma'$ against t will yield the intercept b and the slope λ/b. The value of a can be determined either from the final settlement or from the relation :

$$a = \frac{\varepsilon(ta)}{\sigma'} - b[1 - e^{-\frac{\lambda}{b}ta}] \tag{2.26}$$

A typical plot which would be expected from a test data is shown in Fig. 2.2. The straight line, AB, based on equation (2.20) represents the case of no hydrodynamic time lag; in fact equation (2.20) is the solution for the case when the excess pore water pressure has virtually dissipated. This equation holds in the range of the secondary consolidation. Therefore, point A(t = ta) gives the approximate time at which the excess pore water pressure may be considered to have dissipated.

In applying the curve-fitting method the final strain ε_∞ must be known. In order to avoid this requirement an alternative method could be used. In this method, $y = \log_{10}\frac{\varepsilon(t_2) - \varepsilon(t_1)}{\sigma'}$ is plotted against t , where $\varepsilon(t_2)$ and $\varepsilon(t_1)$ are the strains at times t_2 and t_1 respectively. The interval Δt_o being kept constant at any convenient value. The value of b can be computed from the intercept :

$$y_o = \log_{10}\{b[1 - \bar{e}\frac{\lambda}{b}\Delta to]\} \qquad (2.27)$$

and the slope is, $(-0.434\frac{\lambda}{b})$.

According to the basic model, consolidation always starts with the intergranular stress increase being zero, and excess pore water pressure being equal to the applied stress. This may not in general be true except for some thin laboratory specimens of the normally consolidated soil. A more detailed discussion of these assumptions is presented in Chapter 6 when the experimental results are analysed.

2.2.3 Consolidation Process and the Effect of "Rate of Strain"

It was mentioned earlier that the rate at which soil is being strained during the consolidation process can affect the magnitude of the final settlement (or void ratio), as well as the shape of the actual void ratio - intergranular stress curve. This subject has been studied by Crawford (1965), Šuklje (1968), and more recently by Lowe (1974). Lowe has presented a modified Terzaghi theory based on a viscous model consisting of a stack of leaf springs with a viscous material between the leaves. Under very slow rate of compression of such a model, the viscous material can deform readily and each spring acts individually whereas under very fast rate of compression, the viscous material develops shear resistance and the stack of springs acts as a unit. Thus, the resistance to compression when the unit is mobilised under the fast loading is greater than when they act individually. The basic differential equation of the consolidation process (2.1a) is written in the form of strain rate :

$$\frac{k}{\gamma_w} \frac{\delta^2 u}{\delta Z^2} = \frac{\delta \varepsilon}{\delta t} \qquad (2.28)$$

Lowe defines the rate of strain by a dimensionless number, N, and terms it Strain Rate Factor, where :

$$N = \frac{H^2}{u_o} \frac{\delta^2 u}{\delta Z^2} \qquad (2.29)$$

By using this definition in equation (2.28) an expression for strain rate is obtained :

$$\frac{d\varepsilon}{dt} = \frac{k}{\gamma w} N \frac{u_o}{H_2} \tag{2.30}$$

By multiplying both sides of equation (2.30) by $\{(H_o^2/k_o)[\gamma w/p_2-p_1)]\}$ one obtains:

$$\frac{d\varepsilon}{dt} \times \frac{H_o^2 \gamma_w}{k_o (\sigma_2'-\sigma_1')} = N \frac{k}{k_o} \times \frac{H_o^2}{H_o^2} \frac{u_o}{\sigma_2'-\sigma_1'} \tag{2.31}$$

In a natural scale plot of strain, ε, against intergranular stress difference, $\Delta\sigma' = \sigma_2' - \sigma_1'$, equation (2.31) could be plotted (for one increment of loading) as a family of curves corresponding to different values of the strain rate factor N (Fig. 2.3). The basic concept is that the values of m_v, k, H change during the consolidation stage, which also means that the time factor T changes, and it increases by the factor of :

$$\Delta T' = \Delta T \frac{H^2 m_v' k_o}{H_o^2 m_{v_o} k} \tag{2.32}$$

This results in a modified strain - log time factor curve which represents primary as well as secondary consolidation.

In order to write equations (2.31) and (2.32) and plot the strain-effective stress graphs with the strain rate family of curves for a specific soil stratum, the values of $\Delta\sigma'(t)$, k_o, $k(t)$ and $\varepsilon(t)$ must be determined in the laboratory.

For evaluation of settlements of thick layers of clay relevant strain rate curve and initial induced pore water pressures are found from similar graphs obtained from laboratory tests. In this method the effect of thickness of a layer on the secondary consolidation of the soil is accounted for. Initial induced pore pressures smaller than the applied pressure (as might be the case in the field consolidation of a normally consolidated clay) can also be taken into consideration.

2.2.4 Comments on the Experimental Evidence of the Secondary Consolidation

The existing theoretical treatments of consolidation, which take into consideration the secondary consolidation, have certain limitations which include :

(a) It is usually stipulated that the applied load increment should be equal to at least twice the previous load ($\frac{\Delta\sigma'}{\sigma'} > 1$), so that large deformations occur and the initially induced pore pressure is equal to the applied load (as was the case in the Terzaghi's theory). When the incremental load ratio is less than one ($\frac{\Delta\sigma'}{\sigma'} < 1$) the consolidation curve does not follow the same pattern, because the secondary consolidation settlement forms the larger proportion of the final total settlement, and dominates the consolidation process even during the dissipation of the induced pore pressure (see Leonards, et al, 1961, and Crawford, 1965).

(b) The fact that the induced pore pressure may be less than the applied load (especially in thick layers of soil), means that at the start of the consolidation process the increase of the intergranular stress is not zero. This results in an immediate occurrence of the secondary settlements, even during the early stages of the consolidation process, and affects the consolidation settlement at any given time thereafter.

(c) Another factor which influences the void ratio - effective stress relationship of a given soil is the rate of strain which affects the magnitude of both the secondary and total consolidation settlements. This is true for any viscous material, in which the deformation increases with time under sustained load.

(d) Although theoretical treatments have been developed to account for the secondary consolidation of soils, the actual physical process of the creep phenomenon is not fully understood. It has been suggested that it could be due to non-measurable hydrostatic pressures which dissipate under very slow rate. However, a more rational explanation appears to be based on the micro-structural behaviour of the clay (Tan, 1967). The secondary consolidation is considered to be due to either a viscous movement of the soil particles (flakes or plattes) at their point of contact or local breakdown of particles at the contact points. The former results in a structural breakdown and

possible re-orientation of particles, which leads to large strains, whereas the latter in partial re-orientation of particles only, and hence in small strains.

2.2.5 Analysis of Experimental Consolidation curves - the Rate of Strain Approach

The use of the rate of strain as a third parameter in the void ratio - effective stress relationship enables one to take account of the creep (secondary consolidation) deformations.

The three-parameter plots can also be used for investigation of the increase in the intergranular stress due to the increase of strain during the secondary consolidation.

The method can be applied to thin laboratory samples as well as to thick layers of clay deposits (Šuklje, 1968 and Lowe, 1974). Following Šuklje's Isotaches method the three-parameter plot is constructed using the rate of strain parameter $\frac{\delta\varepsilon}{\delta t}$ or $\frac{\delta e}{\delta t}$ as the third variable. From the test results representing ε or e versus t (logarithm of time) the following equation can be written :

$$e_2 - e_1 = \alpha_e \log_{10} t \qquad (2.33)$$

By differentiation of this equation, an expression for the rate of strain is obtained :

$$\frac{\delta e}{\delta t} = \frac{\alpha_e}{2.3026t} \qquad (2.34)$$

which can be superimposed on the graph of e = e(t) (using the common time scale) Fig. 5.12 . By superimposing the effective stress $\sigma' = \sigma'(t)$ on the same plot, again using the common time scale, e, σ' and $\frac{de}{dt}$ can be determined for any given time, t. The results can then be used for obtaining a family of the effective stress-void ratio curves for different constant strain rates, Fig. 5.14 and 5.17.

The family of curves represents the secondary consolidation strains at various time intervals and show the decrease in the rate of strain and increase in the effective stresses with time.

2.3 Three Dimensional Consolidation

The general consolidation equation of a three-dimensional isotropic medium was developed by Biot (1941) using elastic theory. The basic differential equation is deduced from consideration of the continuity of the liquid and solid phases of soil. For a saturated isotropic and linearly elastic soil of constant permeability the general equation is :

$$C_{v3}\nabla^2 u = \frac{\delta u}{\delta t} - \frac{1}{3}\frac{\delta \theta}{\delta t} \qquad (2.35)$$

where $\theta = \sigma_x + \sigma_y + \sigma_z$ is the sum of total stresses at the point under consideration, C_{v3} is the three-dimensional coefficient of consolidation and ∇^2 is the Laplacean operator,

$$\nabla^2 = \frac{\delta^2}{\delta x^2} + \frac{\delta^2}{\delta y^2} + \frac{\delta^2}{\delta z^2} \qquad (2.36)$$

For given boundary conditions the solution of equation (2.35) gives the distribution of the excess pore pressure U at all times t. It is convenient to work in terms of a nondimensional time factor defined by the following equation :

$$T = \frac{C_{v3}t}{L^2} \tag{2.37}$$

where L is the length of the drainage path, and

$$C_{v3} = \frac{k m_v}{\gamma_w} \tag{2.38}$$

m_v is the modulus of compressibility.

This solution defines the problem of dissipation of the pore pressure within the medium and neglects any viscous properties of the material. Some attempts have been made to apply this equation to viscous soils (Tan, 1957 and Anagosti, 1965), by introducing rheological models in which the modulus of compressibility is replaced by appropriate linear viscous parameters.

The resulting analytical solutions are complex, and determination of parameters is so complicated that their application is not practical.

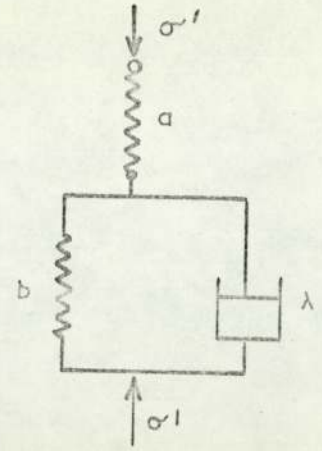

Fig. 2.1

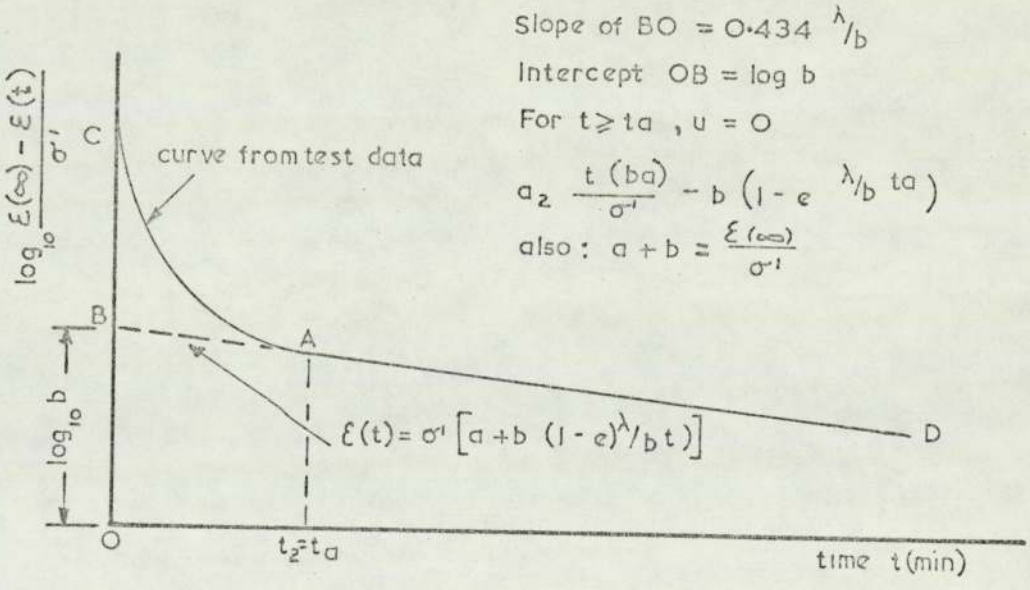

Fig. 2.2 (after Gibson and Lo, 1960)

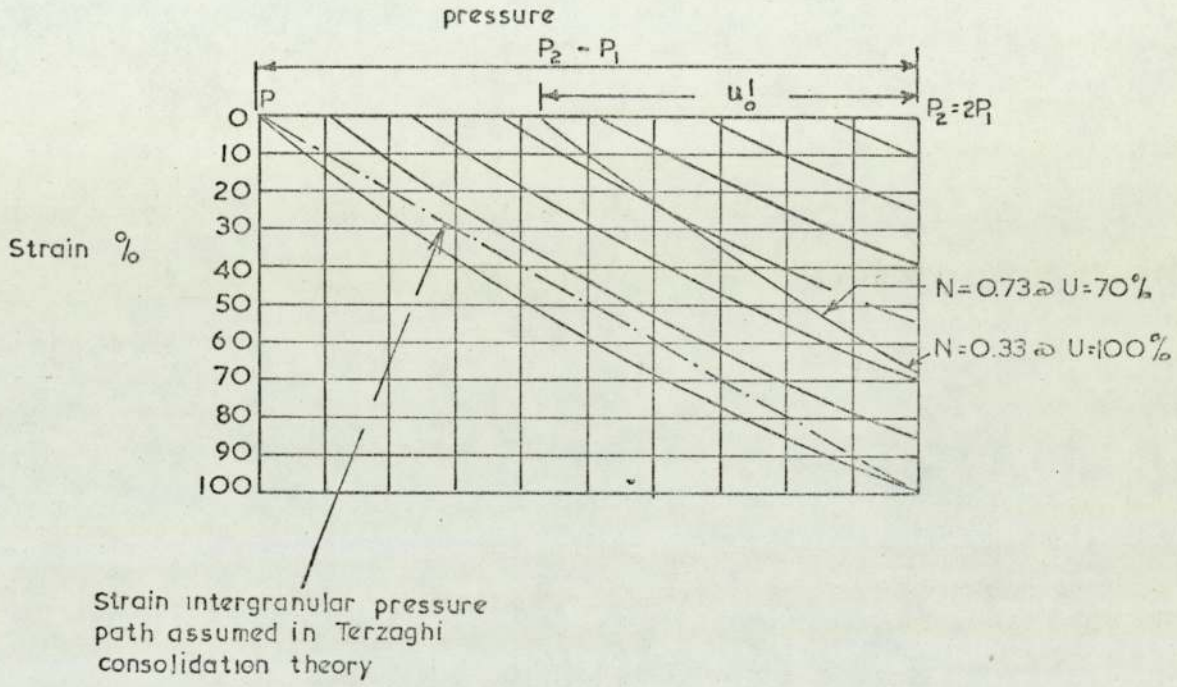

Fig. 2.3 Strain- intergranular pressure path for virtual Terzaghi consolidation (after Lowe 1974)

2.4 Stress-strain relationship for an elastic-plastic strain hardening soil

After more than a decade of research, the soil mechanics group at Cambridge University working under Professor Roscoe has published several theoretical and experimental studies of the three-dimensional stress strain behaviour of soils (Roscoe et al 1958, Scholfield and Wroth 1968, Roscoe and Burland 1968), based on the concept of the theory of plasticity of strain-hardening materials.

The experimental work was mainly concerned with the stress-strain behaviour of soil in the triaxial compression test, which forms a unique surface when plotted in a space relating the void ratio (e) to the mean effective stress (p) and the stress difference (q).

An idealized model of a cohesive soil called Cam-clay model was introduced by Scholfield and Wroth (1968), and was further extended by Roscoe and Burland (1968); it is now referred to as the Modified Cam-clay model. The model pictures the cohesive soil as an isotropic, nonlinear elastic-plastic strain-hardening material, with partially recoverable volumetric strains and irrecoverable shear (distortional) strains. Using the Cambridge notations for the triaxial (axi-symmetrical) compression conditions the stress variables are :

$$p = \frac{1}{3}(\sigma_1' + \sigma_2' + \sigma_3') = \frac{1}{3}(\sigma_1' + 2\sigma_3') \qquad (2.39)$$

and $$q = (\sigma_1' - \sigma_3') \qquad (2.40)$$

(where σ_1' , σ_2' and σ_3' are the effective principal normal stress components), and the strain variables are :

$$\delta v = \frac{\delta e}{1+e} = \delta v_r + \delta v_p \qquad (2.41)$$

where δv_r is the recoverable volumetric strain and δv_p the irrecoverable (plastic) volumetric strain. Considering the principal strain components, the volumetric plastic strain can be expressed as:

$$\delta v_p = \delta v - \delta v_r$$

$$\text{where} \quad \delta v = \delta\varepsilon_1 + 2\delta\varepsilon_3 \qquad (2.42a)$$

and the shear (distortional) strain :

$$\delta\varepsilon = \delta\varepsilon_p = \delta\varepsilon_1 - \frac{1}{3}\delta v = \frac{2}{3}(\delta\varepsilon_1 - \delta\varepsilon_3) \qquad (2.42b)$$

where ε_1 and $\varepsilon_2 = \varepsilon_3$ are principal strains.

For normally consolidated and lightly overconsolidated soils, the triaxial compression tests results plotted in the p, q, e space (Fig. 2.4a) form a unique surface called the 'state boundary surface'. The intersection of the state boundary surface with the q = 0 plane (Fig. 2.4b) gives the spherical consolidation curve which on a semi-logarithmic scale plots as a straight line:

$$e = e_1 - \lambda \log_e p \qquad (2.43)$$

where e_1 is the void ratio corresponding to p = 1 and λ is a soil constant which can be related to the well known index of compressibility C_c ($\lambda = \frac{C_c}{\log_e 10}$). A point in this space is referred to as a 'state point', and a continuous sequence of 'state points' is called a 'state path'. The 'state points' below the state

boundary surface represent admissible states (of stress and corresponding void ratio), whereas those above the surface represent inadmissible states. It is further postulated (Roscoe et al, 1958), that a 'critical state' condition exists on the state boundary surface where an element of soil continues to distort without further change of the void ratio or the state of stress. The projection of the 'critical state' on to the p - q plane (Fig. 2.4c) is a straight line of equation:

$$q = Mp \qquad (2.44)$$

where M is a soil constant.

When projected on the $e = \log_e p$ plane, another straight line is obtained of equation :

$$e = \Gamma - \lambda \log_e p \qquad (2.45)$$

where Γ is the critical void ratio corresponding to $p = 1$: this line is parallel to the isotropic consolidation line (equation 2.43).

2.4.1 Concept of Yield Loci and Normality Conditions

It is assumed in application of the Modified Cam-clay model to a compressible soil that during ordinary loading of the soil the strains are time-independent, with separable elastic and plastic deformations. This means that in compression there is a single stress-strain curve with elastic unloading sharply differentiated from elastic-plastic loading (curves Z and Z' Fig. 2.4b). Moreover, at each stage of deformation a new yield surface, or in two-dimensional stress plot (q, p plane), a new yield curve is reached

(curve AB Fig. 2.4c) which separates the reversible (elastic) paths from those outside it which cannot be reached without some additional plastic deformations; i.e. a shift to a new yield surface such as DE (Fig. 2.4c). Thus on the e - p plane each point on the curve Z (Fig. 2.4b) corresponds to a yield curve (Calladine, 1963), and the yield curve is in fact the projection of the state boundary surface intersection with surface ABC on to the q - p plane (Fig. 2.4a) and is referred to as a yield locus (the vertical surface ABC contains in it the swelling line AC, and is referred to as an 'elastic wall' (Roscoe and Burland, 1968). The yield curve or locus is assumed to be elliptical and is defined in the Modified Cam-clay model by :

$$\frac{p}{p_o} = \frac{M^2}{M^2+\eta^2} \qquad (2.46)$$

where $\eta = \frac{q}{p}$ at any point, and p_o is the value of P when $\eta = 0$. The critical state line (OB Fig. 2.4c) intersects the ellipse at its maximum point, and the critical stress state is defined by an extended Von Mises-type of failure criterion.

Introduction of the basic consideration of stability of materials to soils (Drucker, 1964) leads to two features of the stress-strain relationship in the plastic range : the convexity of yield surfaces and normality conditions; the slope of the normal at any point of a current yield surface gives the ratio of the plastic distortional to volumetric strain increments produced by further loading from that point.

2.4.2 Stress-strain equations

In the Cam-clay model the compression and swelling (rebound) of the isotropic consolidation curve (curve Z and Z' Fig. 2.4b) on the e - $\log_e$p plot are assumed to be straight lines of slope λ and k respectively. Upon the application of small stress increment δp volume change occurs, δv, which is assumed to consist of a recoverable or elastic volume change δv_r and irrecoverable or plastic volume change δv_p; the associated recoverable strain δv_r can be expressed as :

$$\delta v_r = \frac{\delta e_r}{1+e} = - \frac{k}{1+e} \frac{\delta p}{p} \qquad (2.47)$$

whereas the total volumetric strain, δv, as

$$\delta v = \frac{\delta e}{1+e} = - \frac{\lambda}{1+e} \frac{\delta p}{p} \qquad (2.48)$$

The plastic volumetric strain is taken as the difference between δv and δv_r and is equal to :

$$\delta v_p = \frac{(\lambda - k)}{1+e} \frac{\delta p}{p} \qquad (2.49)$$

In the work presented by Roscoe et al (1963) assumption is made that there is no overall recoverable shear distortion, i.e.

$$\delta \varepsilon_r = 0 \text{ and } \delta \varepsilon = \delta \varepsilon_p \qquad (2.50)$$

Derivation of further equation is achieved by application of the normality condition on the current yield locus and consideration of the dissipated work. The work equation states that "the total energy per unit volume transmitted to soil across its boundaries is equal to stored and dissipated energy within the soil skeleton". The expression used for dissipated work by (Burland, 1965) which relates the stress vector $(\vec{p} + \frac{1}{M}\vec{q})$ has the form of :

$$\delta W = p\sqrt{(\delta v_p)^2 + (M\delta\varepsilon_p)^2} \qquad (2.51)$$

At the critical state condition : $\delta W = MP\delta\varepsilon$ (2.52)

and combining equation (2.51) with a previously defined work equation of the Cam-clay in the form of :

$$\delta W = p\delta v_p + q.\delta\varepsilon_p \qquad (2.53)$$

the following equation is obtained :

$$\frac{\delta\varepsilon_p}{\delta v_p} = \frac{2\eta}{M^2 - \eta^2} = \frac{1}{\psi} \qquad (2.54)$$

Where ψ is the slope of the current yield locus AB (Fig. 2.4c) and is related to the stress-increments at the point x (p, q) using the normality condition :

$$-\left(\frac{dp}{dq}\right)_{AB} = \frac{1}{\psi} = \frac{\delta\varepsilon_p}{\delta v_p} \qquad (2.55)$$

by substitution of ψ in the basic differential equation of the yield locus represented by $\frac{dp_o}{p_o} - \frac{dp}{p} - \frac{d\eta}{\psi+\eta} = 0$ (2.56)

and combining with equation (2.49) to eliminate $\frac{dp_o}{p_o}$, the following expressions may be obtained :

$$\delta v_p = \frac{\lambda-k}{1+e}\left(\frac{2\eta\delta\eta}{M^2+\eta^2} + \frac{\delta p}{p}\right) \tag{2.57}$$

$$\delta v = \frac{1}{1+e}\left[(\lambda-k)\frac{2\eta\delta\eta}{M^2+\eta^2} + \lambda\frac{\delta p}{p}\right] \tag{2.58}$$

$$\delta\varepsilon = \delta\varepsilon_p = \frac{\lambda-k}{1+e}\left(\frac{2\eta}{M^2-\eta^2}\right)\left(\frac{2\eta\delta\eta}{M^2+\eta^2} + \frac{\delta p}{p}\right) \tag{2.59}$$

and the yield locus becomes

$$\frac{p}{p_o} = \frac{M^2}{M^2+\eta^2} \tag{2.60}$$

which is an ellipse for a given value of P_o on the q - p plane (p_o is the value of p on the p-axis). It must be noted that the yield locus curve in the q - p plane is different from the undrained loading path (which is the projection of intersection of an $e = e_o$ plane with the state boundary surface on the q - p plane), starting from the same point (e_o, p_o, $q = o$). Nonetheless, the yield locus could be constructed geometrically from experimentally determined undrained loading path (Calledine, 1963).

It is further assumed that in the Modified Cam-clay model the yielding and hardening takes place isotropically (Roscoe and Burland, 1968), so that yield surfaces in the stress space are symmetrical about the space diagonal $\sigma_1 = \sigma_2 = \sigma_3$.

2.4.3. Uniqueness of Yield Surface (plastic potential)

Since the introduction of the strain-hardening plasticity theory into soil mechanics and of the Cam-clay model, the inherent yield surface in soil, its shape and dependence on stress history and prediction of the plastic strains have been a subject of extensive investigations (Lewin, 1973, Roscoe and Poorooshasb 1963). The main observed deviation of the behaviour of real soils from that of the idealized materials is that for different stress paths (from the same yield locus) the measured plastic strain increment directions are different functions of $\eta = \frac{q}{p}$ whereas according to the theory they should be the same.

To overcome some of these difficulties Roscoe and Burland (1968) in their Modified Cam-clay Model postulated that some plastic shear strains (at constant volume) can take place for p, q values beneath the yield locus (Fig. 2.5). Thus the current volumetric yield loci, combined with yield lines parallel to the p-axis, represent revised yield loci, where shear strains, for the stress increments at the corner of the yield loci are the sum of two separate strains:

$$\delta\varepsilon_p = \left(\frac{d\varepsilon_p}{d\eta}\right)_{vp} \delta\eta + \left(\frac{d\varepsilon_p}{dv_p}\right)_{\eta} \delta v_p \qquad (2.61)$$

where the first component is the shear strain under constant volume (corresponding to the straight lines), and the second component is the shear strain associated with plastic volume changes (corresponding to the curved parts).

Again, investigating the uniqueness of the plastic strain increment vector as a function of q/p, Lewin and Burland (1970), performed a careful series of tests on a normally consolidated slate powder, consisting of an anisotropic consolidation stage followed by small stress probes in different directions (in the stress space). The tests showed that the shear strains could be predicted by applying the normality conditions to a yield locus constructed from the results of triaxial compression tests, but the direction of the plastic strain increment vector was partly dependent on the direction of the stress probe.

The subject has been further studied by Calledine (1971) who has used a microstructural model to depict the behviour of a saturated clay; the results suggest in general that the overall yield surface for the clay (according to the Model) is not isotropic, but depends on the previous history of loading.

The influence of the stress history on the yield surface (plastic potential) in triaxial stress conditions was investigated by Lewin (1973, 1975). The experimental results suggest that stress history has a considerable effect on the direction of the strain increment vector even with substantial rise in the stress level. Hence different plastic potentials are obtained for isotropically and anisotropically consolidated samples.

The uniqueness of the plastic potential and application of the normality conditions and predictions of plastic strains in normally consolidated Lias clay will be further discussed in Chapter 6.

2.4.4 Influence of the secondary consolidation on the yield surfaces

The secondary consolidation involves a change in the void ratio, and hence a change in plastic strains under sustained effective stresses. From the family of curves on the e - logp plot (Fig. 2.6a) it is evident that as the secondary consolidation proceeds the 'apparent' consolidation stress increases from p_o to p_{o1} and then p_{o2}, so does the yield stress in the q-p plane increase from p_o to p_{o1} and p_{o2} (Fig. 2.6b).

If there is a yield locus in the q-p plane corresponding to each yield stress p_o, then the increase in the 'apparent' consolidation stress will shift the yield curve from y_o to y_{o1} and y_{o2} respectively (this can be done assuming that according to the theory the yield curves are parallel and symmetrical. It must be emphasised that all laboratory normally consolidated samples of clays are subjected to some secondary consolidation, and therefore, the yield point, i.e. the origin of the yield curve on the p-axis, should be chosen with care (see Chapter 6). The above simple concept is supported by the fact that the undrained shear strength of the soil increases during the secondary consolidation as the void ratio decreases, and hence the time hardening effect appears to produce the same consequences as consolidation of higher stresses (Burland, 1972). It is conceivable that the same effect could take place in the case of anisotropically consolidated samples. This factor will be examined in more detail on presentation of experimental results (Chapter 6).

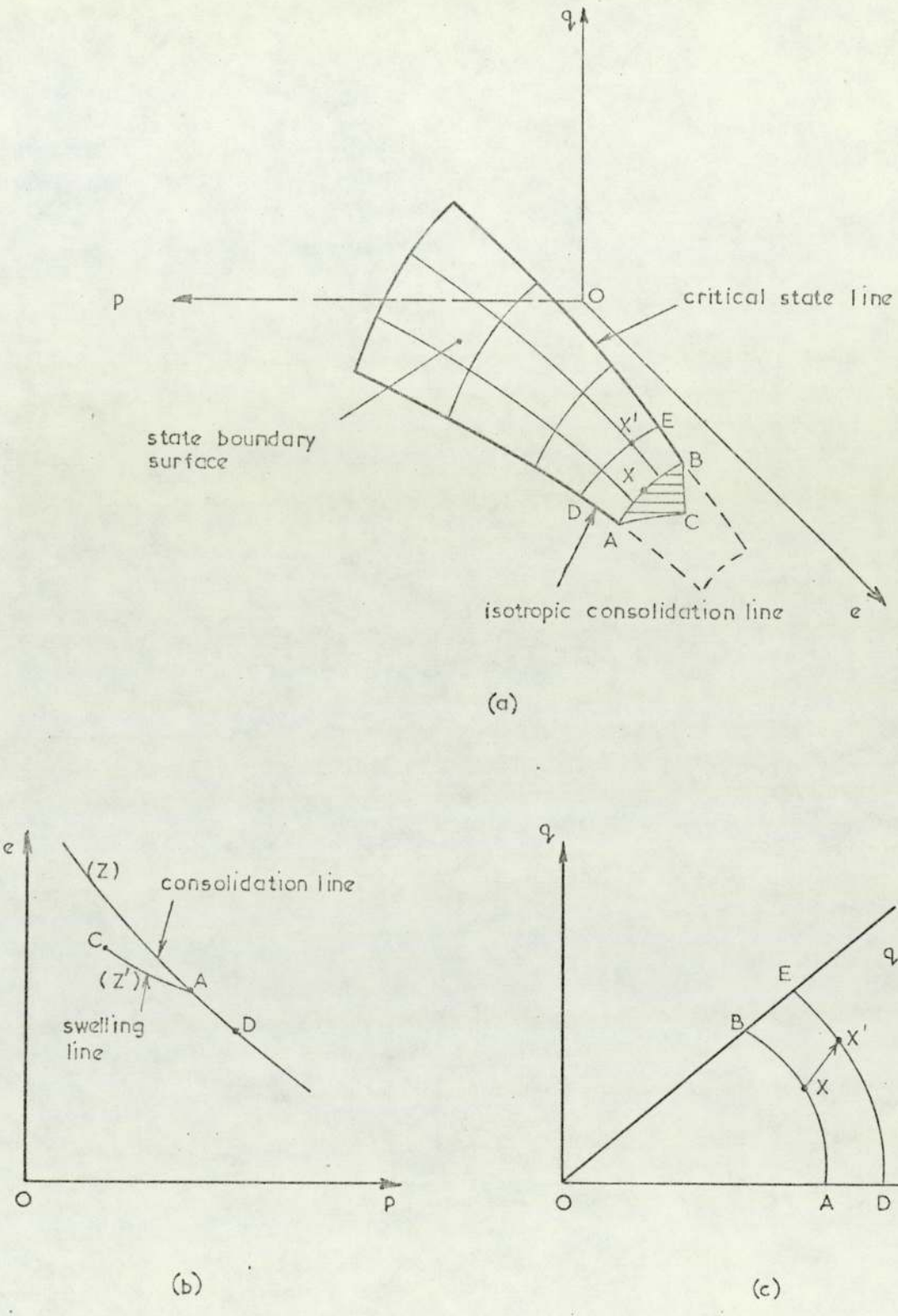
q
p
O
critical state line
state boundary surface
X'
E
B
X
D
C
A
isotropic consolidation line
e
(a)
e
(Z)
consolidation line
C
(Z')
A
swelling line
D
O
p
(b)
q
q = MP
E
B
X'
X
O
A
D
P
(c)

Fig. 2.4

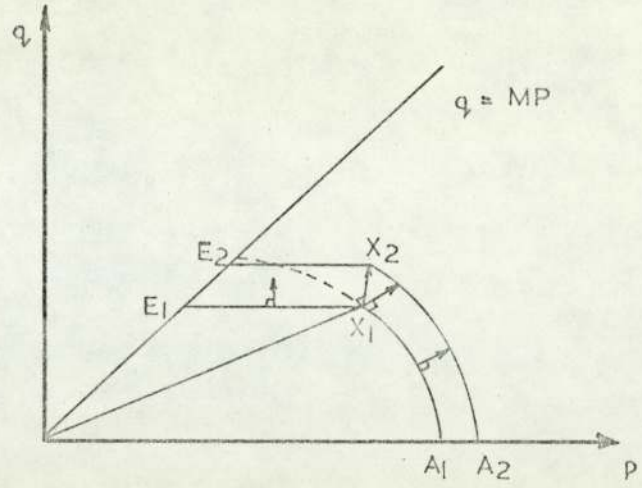

Fig. 2.5

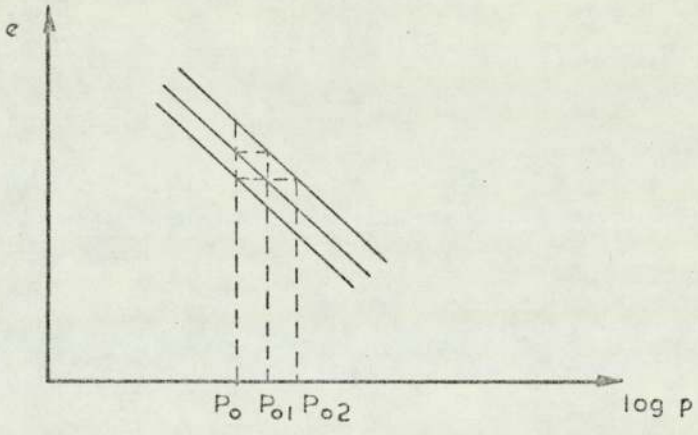

(a)

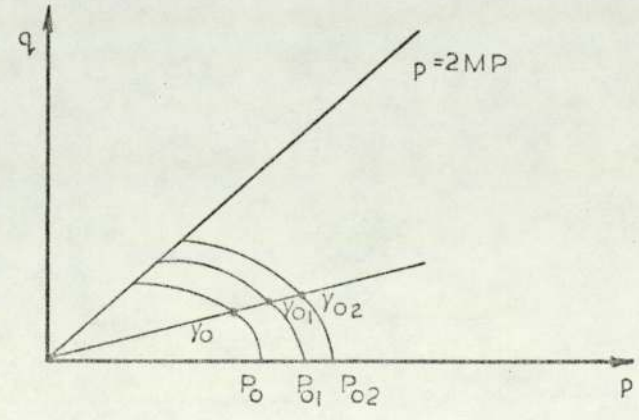

(b)

Fig. 2.6

CHAPTER THREE

TESTING PROGRAMME, DEVELOPMENT OF APPARATUS AND TECHNIQUES

3.1 Introduction

The initial objects of the research project were to study two aspects of the behaviour of a remoulded saturated clay: the creep phenomenon occurring during the consolidation process or the so called secondary consolidation, and the investigation of stress-strain relationships for shearing under different stress-paths. The latter involved the consideration of the effect of creep strains on the shear deformations and stresses. A test programme was worked out and specifications for the necessary apparatus were prepared. An obvious choice for the study of the secondary consolidations was the oedometer apparatus, but certain modifications were necessary to meet the requirements of the proposed more detailed studies. Even with the modifications one could not distinguish volumetric strains from the deviatoric ones in this apparatus and it was therefore decided to use the more versatile triaxial apparatus for the study of both the creep effects and the stress-strain relationships.

In order to study the plastic deformation under different stress-paths, the conventional triaxial compression apparatus was used in parallel with a specially designed stress controlled apparatus which was specifically developed for this research and could be used for both the anisotropic consolidation and undrained shearing of soils.

An attempt was also made to use an "independent stress cell" developed by Thomas (1973) but preliminary tests have shown that it was not suitable for testing of soft clay specimens.

3.2 Testing Programme

It was decided that before commencing the study of the deformation, hardening and secondary consolidation of remoulded Lias clay, its basic conventional parameters must be determined first. A test programme was therefore prepared which involved oedometer and triaxial tests (Fig. 3.1).

The first series of conventional tests were carried out on 70mm diameter specimens. The apparatus was then modified and several series of special tests were performed on samples of the same diameter. The description of the test programme can best be done by division of the tests into two categories : (1) oedometer tests, and (2) triaxial tests, involving both conventional and special tests.

3.2.1 Oedometer Tests

The main object of the oedometer tests was to measure the secondary consolidation strains and their dependence on the incremental stress ratio ($\Delta p/p$) and time. At the same time, however, these tests were used to determine the values of the compression and swelling indexes (C_c and C_s) for the soil under consideration. Some of the tests were performed with measurement of pore pressure at the base of the sample.

The oedometer tests can be divided into two series :

(i) S O Tests

This series consisted of the conventional oedometer tests on samples of soil prepared in the tall oedometer.

The ratios of the stress increment to the initial stress ($\Delta p/p$) were taken to be 1, 0.5, 0.33 and 0.25 and were kept the same for the first loading, unloading and reloading cycles.

(ii) P O Tests

In this series of tests pore pressure measurements were taken at the base of the specimen to study the dissipation of the pore pressure and its influence on the secondary compression. The same incremental stress ratios were used as in the S O tests and each load increment was left on for up to 7 days.

3.2.2 Triaxial Tests

The object of triaxial tests was threefold :

(a) - Study of the deformations during consolidation and subsequent secondary compression at different stress levels.

(b) - Study of the shear and plastic deformations during application of different stress-paths to failure.

(c) - Evaluation of the basic soil parameters (M, ϕ', C_c), and study of the influence of the stress-paths on them. To carry out this work a comprehensive test programme was worked out and is shown in Fig. 3.1. The involved tests consisted of two stages:

(i) isotropic or anisotropic consolidation and

(ii) shearing along a predetermined stress-path.

The two stages of the tests are described under separate headings.

(i) Consolidation Stage

All the samples were initially subjected to one-dimensional consolidation in the tall oedometer. When they were set up in the triaxial apparatus the samples were reconsolidated under a mean effective stress of 50 KN/m^2, which usually was higher than the pre-consolidation stress to which they were previously subjected. Subsequent stress levels were p = 100, 200 and 300 KN/m^2. Isotropic and anisotropic consolidation stages were carried out under the same mean effective stresses.

Three different consolidation stages were used :

(a) I C A Series

In this series incremental stress loading was applied and the samples were subjected to isotropic consolidation, with top and radial drainage and measurement of pore pressure at the base. This series could be best compared with that of the stage loading in the oedometer test.

(b) I C B Series

In this series of isotropic consolidation tests the cell pressure was increased at a constant rate until a new stress level was reached. Drainage conditions were virtually the same as in the I C A series, and when the cell pressure was stopped pore pressure of up to $\frac{1}{5}$ of the cell pressure increment was recorded at the base. It dissipated when samples were left under a constant cell pressure for investigation of the secondary compression strains.

(c) A C Series

The samples in this series were anisotropically consolidated under different ratios of the axial to radial stresses. The values of mean effective stress p under which secondary compression took place were the same as the ones used in isotropic tests, i.e. p = 100, 200 and 300 KN/m^2. These tests were carried out in the stress-controlled triaxial apparatus. The anisotropic stresses were achieved by increasing the cell pressure at a constant rate and by increasing the axial load to reach the desired stress ratio. Drainage conditions were the same as in the other series, and pore pressure was measured at the base; the maximum value recorded was less than $\frac{1}{5}$ of mean effective stress increment (less than 20 KN/m^2).

(ii) Shearing Stage

On completion of the consolidation stage the samples were sheared in compression under three different stress-paths :

(a) I C D Series

In this series of tests both types of the isotropically consolidated samples were sheared under free drainage from the sides and the top of the samples. In order to establish a suitable rate of strain the dissipation of pore pressure was monitored at the bottom of the sample.

(b) I C U Series

This series consisted of undrained tests of istropically and anisotropically consolidated samples. The shearing was carried out either at a constant rate of strain, or by incremental increase of the deviator stress; pore pressure was measured at the top and bottom of the sample.

(c) I C P Series

In this series of drained tests the isotropically consolidated samples of the I C B series were sheared under constant mean effective stress p and a gradually increasing deviator stress.

3.3 Oedometer Apparatus

A mechanical oedometer of the standard Bishop type supplied by Wykeham Farrance Limited was used. A screw support was added at the back of the main frame, to support the loading arm at the time of application of load increment and thus eliminate shock loading. The vertical dial gauge was coupled to a linear transducer for 24 hour automatic recording of readings at predetermined time intervals.

3.3.1 Oedometer with measurement of pore pressure at the base

A conventional oedometer was used for the evaluation of compression and swelling indexes (C_c and C_s) of the remoulded Lias clay, and for the initial study of the secondary consolidation. For more detailed studies of the secondary consolidation under different load increment ratios and dissipation of the induced pore water pressure, an oedometer set up was needed in which top and bottom drainage were separated so that one could measure the pore pressure at the bottom, and allow drainage from the top.

To achieve this a modified consolidation cell was used in which the sample ring was fixed inside the cell and sealed at the middle of the ring with a rubber O-ring. This allowed drainage through the top cap, whereas the bottom end was utilised for pore pressure measurement. A new base plate was made of aluminium with a 20mm diameter ceramic porous disc fitted at its centre. Another O-ring was used to obtain an effective seal between the ring and the base;

the whole assembly was then placed inside the cell and sealed. A pressure transducer was screwed into the bottom of the base plate immediately below the ceramic disc, against a rubber O-ring. Leads to the transducer were taken through a hole in the base of the cell and through the bottom member of the loading frame of the oedometer as shown in Plate 3.1. The transducer leads were then connected to a digital data logger for automatic recording of the pore pressure at the base of the sample at all stages of loading.

3.4 Oedometer Testing Techniques

The oedometer samples were cut from large samples prepared in the tall oedometer (see Chapter 4). In conventional oedometer tests a 76mm diameter, 20mm high, stainless steel confining/cutting ring was used: prior to cutting of the samples the ring was thoroughly greased. It was then placed on a 25mm high sample, extruded from the tall oedometer, and was gently pushed down to cut through it. The top and bottom surfaces of the soil were then trimmed flush with the ring, which was placed on the porous stone inside the cell. After putting on the top porous stone and centering the ring, the assembled cell was placed in the oedometer, filled with distilled water, and loading was commenced.

Filter paper was not used between the sample and porous stones, because it had been shown by Bennett (1975) that filter paper's compressibility could affect the results, especially when small deformations during the secondary consolidation stage were investigated.

To avoid penetration of the clay particles, fine grade porous stones (A 80 KV) were used.

For oedometer tests with pore pressure measurments a 65mm dia. and 20mm high brass ring was used. The initial preparation of the sample followed the procedure described above, but after the sample was placed on the base, it was pushed into the chamber through the bottom. The base plate of the cell was then screwed into the main body of the cell to obtain a watertight seal between the two ends of the sample. The top porous stone and cap were placed from the top, and the cell was positioned in the machine in contact with the loading frame. It was absolutely essential to ensure that the bottom porous stone was fully saturated before placement of the sample. As it was a high air entry value (H.A.E.V.) ceramic stone, it was easy to ensure that no air would penetrate it during the few seconds in which the ring was placed on top of the base. With the cell placed in the oedometer the pressure transducer fixed in the base was connected to the data logger. Initial tests with the pore pressure measurements, using back pressure facilities with a short length of Saran tubing for connecting the transducer to base, proved that the system was too flexible, resulting in delays in the build up of pore pressure. On the basis of these tests the transducer was mounted in the base of the oedometer cell, immediately below the porous stone. In spite of this the recorded rise of the pore pressure was still less than expected, but reaction of the system was almost instantaneous.

3.5 Triaxial Apparatus

Two types of triaxial apparatus were basically required: one for the isotropic consolidation of samples, i.e. for q/p = 0, and another for the anisotropic consolidation in which the q/p ratio would be varied. In both cases large cells (for 100mm samples) were used, but were modified for testing of 70mm dia. samples. For anisotropic loading a stress-controlled loading device was designed and developed as part of the research programme.

3.5.1 Standard triaxial apparatus

The isotropic consolidation in the ICD, ICU and ICP series of tests, was carried out in a standard Wykeham Farrance triaxial cell for 100mm samples. Top and bottom platens were altered to 70mm diameter and fitted with H.A.E.V. ceramic discs. Drainage and pore pressure measurement facilities were available at both the top and bottom platens. Internal load cell was used for measurement of the axial load.

3.5.2 Independent stress triaxial cell

This cell was designed and manufactured in the department (Thomas 1973) for testing of undisturbed samples of Lias clay. The main feature of the cell was the facility for separate application of the radial and axial stresses; the latter could either be applied at a 'constant rate of strain' or in a 'stress-controlled' manner.

The axial load was measured with a load cell which was mounted beneath the bottom platen (Plate 3.2). There was a 5mm gap between this platen and cell base which was sealed with a silicon (silco-set) rubber ring. The top cap was attached to the plunger and moved in the upper chamber of the cell - the seal between the upper and main chamber was achieved with a pair of rubber O-rings.

This cell was originally designed for laboratory testing of heavily overconsolidated soils using stress-paths comparable to the in situ conditions. In the initial stages of the present work the independent stress cell was used for stress-controlled tests on remoulded normally consolidated samples of the Lias clay. A new plunger was made in order to reduce friction, all seals were redesigned and the method of setting up of the sample was completely modified. However, after a few tests, it was found that this cell was not suitable and could not be adapted for testing of samples of firm to soft soils. The difficulties were mainly due to the following factors :

(a) The effect of plunger friction.

Friction on the plunger was acting at two points, firstly around the plunger itself and secondly around the top platen, at the seal between the upper and main chamber. The latter was of greater magnitude, especially when the axial deformation was greater than a few millimetres. To investigate the friction a silicon rubber sample was made and tested. The tests showed that plunger friction was considerable, and was not constant. To overcome the static friction an extra pressure of between 70 and 105 KN/m^2 was needed in the upper chamber. However, when the plunger started moving downwards, there

was a sudden decrease in the friction and the load cell reading would suddenly increase to a value much greater than expected.

(b) The effect of decrease in the diameter of a sample.

During consolidation of a sample in this cell its volume and consequently its cross-sectional area were decreased. As the axial load was measured by a load cell beneath the bottom platen, any decrease in the cross-sectional area of the sample, exposed a small portion of the top surface of the platen to the cell pressure and resulted in an increase in the readings of the axial load. This effect was detected when dummy samples of different diameters were tested (70, 65 and 60mm).

Obviously, such uncontrollable fluctuation of loading could not be tolerated, and hence it was decided to abandon the use of this cell and to develop a new method of 'stress-controlled' loading of cylindrical specimens.

3.5.3 Development of a dead loading 'stress-controlled' triaxial apparatus

In order to be able to carry out anisotropic consolidation and stress-path controlled compression tests, it was necessary to develop a stress-controlled triaxial apparatus. This was achieved by addition of a lever arm to a conventional 10 T compression frame and adaptation of a standard cell for 100mm diameter specimens. The lever arm consisted of two spaced-out aluminium sections, attached to a pivot on a rigid fulcrum which in turn was fixed to the cross beam of the machine (Plate 3.3). The main weight hanger was positioned at the

end of the long arm of the lever whereas a movable counter weight was attached to the other end.

The transfer of load from the lever to the ram of the load cell was achieved through a steel ball, positioned at the top of the ram, and free to slide in a groove in a plate connecting the two aluminium sections. Either knife edges or ball bearings were used to ensure efficient transfer of the dead loading to the specimen. A stop screw was fixed to one of the columns of the machine to support the lever arm during the process of application of the load increments. Along with the stop screw an 'on-off relay' switch was mounted which operated the drive motor of the compression machine. This enabled automatic raising of the cell to ensure that at all times the lever arm was kept horizontal (Fig. 3.2). With a 6:1 lever ratio axial loads of up to 150 Kg could be applied to the specimen.

The axial load was measured using an internal 450 Kg load cell. A rotating bush at the top of the cell ensured minimal fluctuation of the reading due to plunger friction at the top of the cell. Calibration of the load cell against either dead loading or external proving ring had shown that the plunger friction was almost eliminated. The movable counter balance was used for the adjustment of the applied load necessary to compensate for the change in the cross-sectional area of the sample resulting from volumetric and axial strains during the tests. In order to reduce the amount of leakage castor oil seal was maintained in the bush by connecting it to an oil supply under the same pressure as the main cell.

For carrying out strain-controlled tests in the same apparatus, and for anisotropically consolidated undrained tests, a ram was fixed to the centre of the main cross-beam of the compression frame and a steel ball was placed between it and the above mentioned connecting plate in the lever arm. Thus the sample could be strained against the cross-beam by raising the cell to make contact between the plate and the ram.

3.5.4 Subsidiary devices

Axial deformations were measured with dial gauges reading to an accuracy of 0.002mm per division. They were fitted externally to the load cell and measured deflection with reference to the triaxial cell.

Volume changes were measured using a device designed by the B R S and supplied by Wykeham Farrence Ltd. It had a $10cm^3$ capacity and could be read to an accuracy of $0.001cm^3$. The volume change device consisted of a piston mounted inside a perspex cylinder and coupled, via a dial gauge, to a small electric motor. The two ends of the cylinder were separately connected to the drainage system, in parallel with a mercury and oil filled U-tube through which no flow took place but which operated as an on-off switch for the electric motor. A slightest movement of water in the drainage system would switch the motor on and hence activate the piston to allow the water into one of the chambers of the cylinder and register the amount of movement on the connected dial gauge.

During consolidation of 70mm diameter specimens, volume changes of up to 40cm^3 were recorded. This was achieved simply by repeated repositioning of the piston; drainage was shut off during these operations. Care had to be taken in connecting the device into the drainage system to ensure flow in the right direction. Whenever the device was not in use, the by-pass tap had to be left open and small back pressure had to be maintained in order to prevent migration of air or oil within the device.

Finally all the dial gauges were coupled with linear transducers for automatic recording of the deformations via a digital data logger.

3.6 Triaxial Testing Techniques

A series of provisional tests were carried out in order to decide upon an appropriate method of testing of 70mm diameter and 140mm high specimens. As the result of these tests, the following procedure was adapted :

(a) Setting up procedure

The whole system was thoroughly de-aired and a specimen was placed on the bottom platen. A filter paper was then placed around the sample and a single rubber membrane (previously soaked in the water for at least 24 hours) was placed over it, and sealed to the pedestal with two O-rings (Plate 3.4). In order to remove as much air as possible from between the rubber membrane and the specimen, a small amount of water was flushed through the bottom and the rubber

membrane was gently stroked in an upward direction. The top sealing, O-rings (previously threaded over the top drainage connection) were positioned using a split stretcher.

The cell was assembled and filled with de-aired water up to the top of the load cell; the castor oil was then introduced through an inlet mounted in the rotating bush. When the oil overflowed, the cell-clearing tap was shut, connections were made ready for application of the cell pressure.

(b) Cell pressure was gradually increased to 200 KN/m^2 while the top and bottom drainages were kept shut and the pore pressures on both ends were recorded. The pore pressure rise was almost immediate and equal to the applied cell pressure (see Chapter 5 for the results), which indicated presence of free water at the top and bottom during the setting up procedure. At this stage the cell pressure was increased to 220 KN/m^2 and a back pressure of 200 KN/m^2 was applied to the drainage system. The drainage tap to the top platten was opened for a few minutes to expel the excess water accumulated during the setting up of the sample. The back pressure of 200 KN/m^2 was maintained in all tests to ensure that any trapped air could be dissolved.

(c) From here on the cell pressure or cell pressure and axial load, were then increased to achieve the required stress-path. The initially applied 20 KN/m^2 cell pressure was well below the preconsolidation pressure of the samples in the tall oedometer, and the first stage of the consolidation was for all tests started from $p = 50\ KN/m^2$.

In the drained tests drainage was from the sides and top of the specimens, while the dissipation of the pore pressure was monitored at the bottom. In the undrained stages of tests both top and bottom pore pressures were recorded.

(d) In some initial tests greased rubber membrane sandwiches were used at both ends of the samples, in order to decrease the end friction. Although this resulted in more uniform deformation of the samples, it was found that with tall samples (height to diameter ratio of 2:1) residual excess pore pressure (above back pressure) was induced in the bottom of the samples. It was decided, therefore, to test all samples without the lubricated ends. Following prolonged preliminary tests* on dummy samples, all tests were carried out using single standard rubber membranes.

* Less than 0.1cm^3 leakage was recorded after 7 days of testing, and as this was equivalent to 0.0002 volumetric strain, it was considered to be negligible.

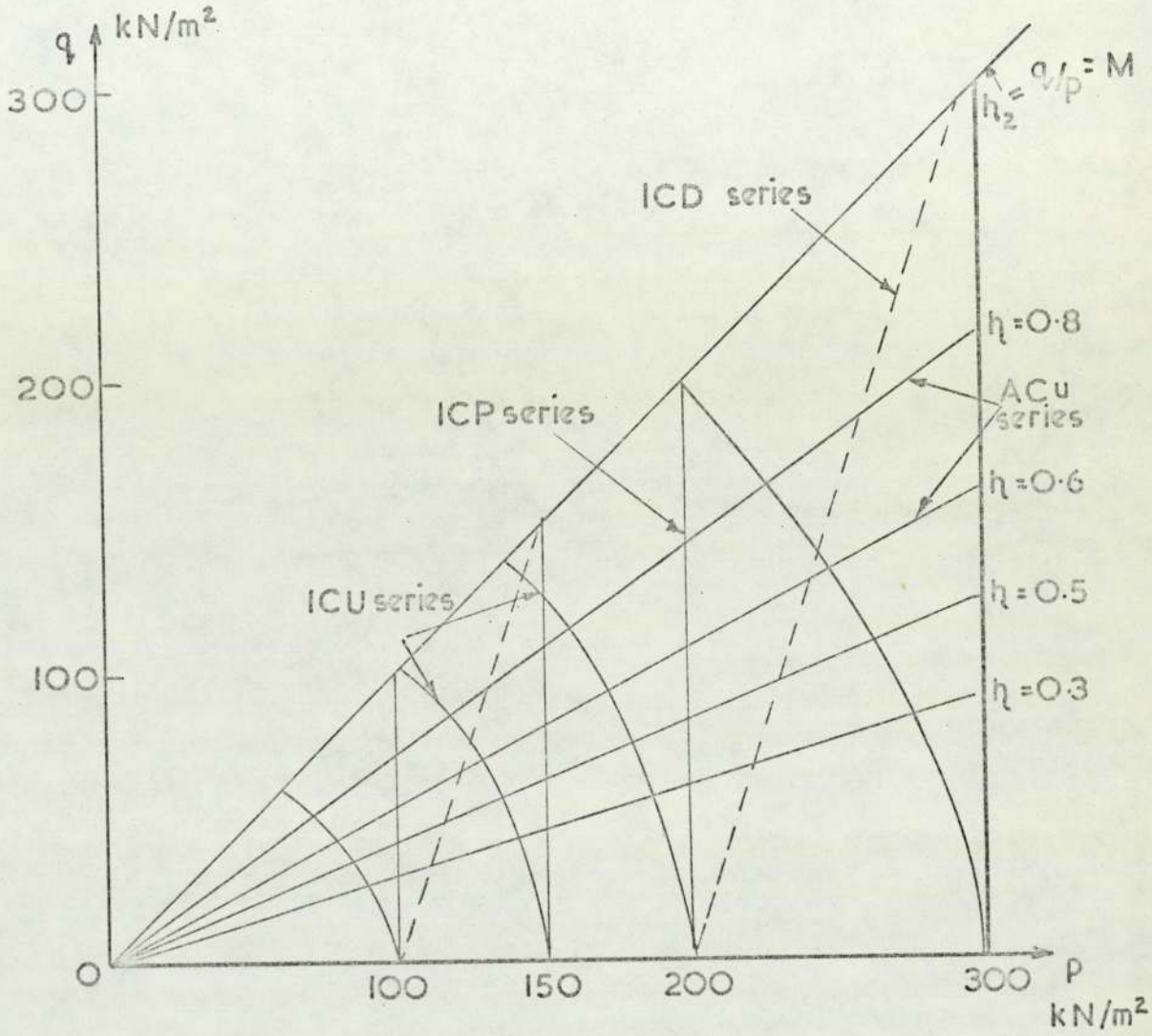

Fig. 3.1. Stress paths in different triaxial test series

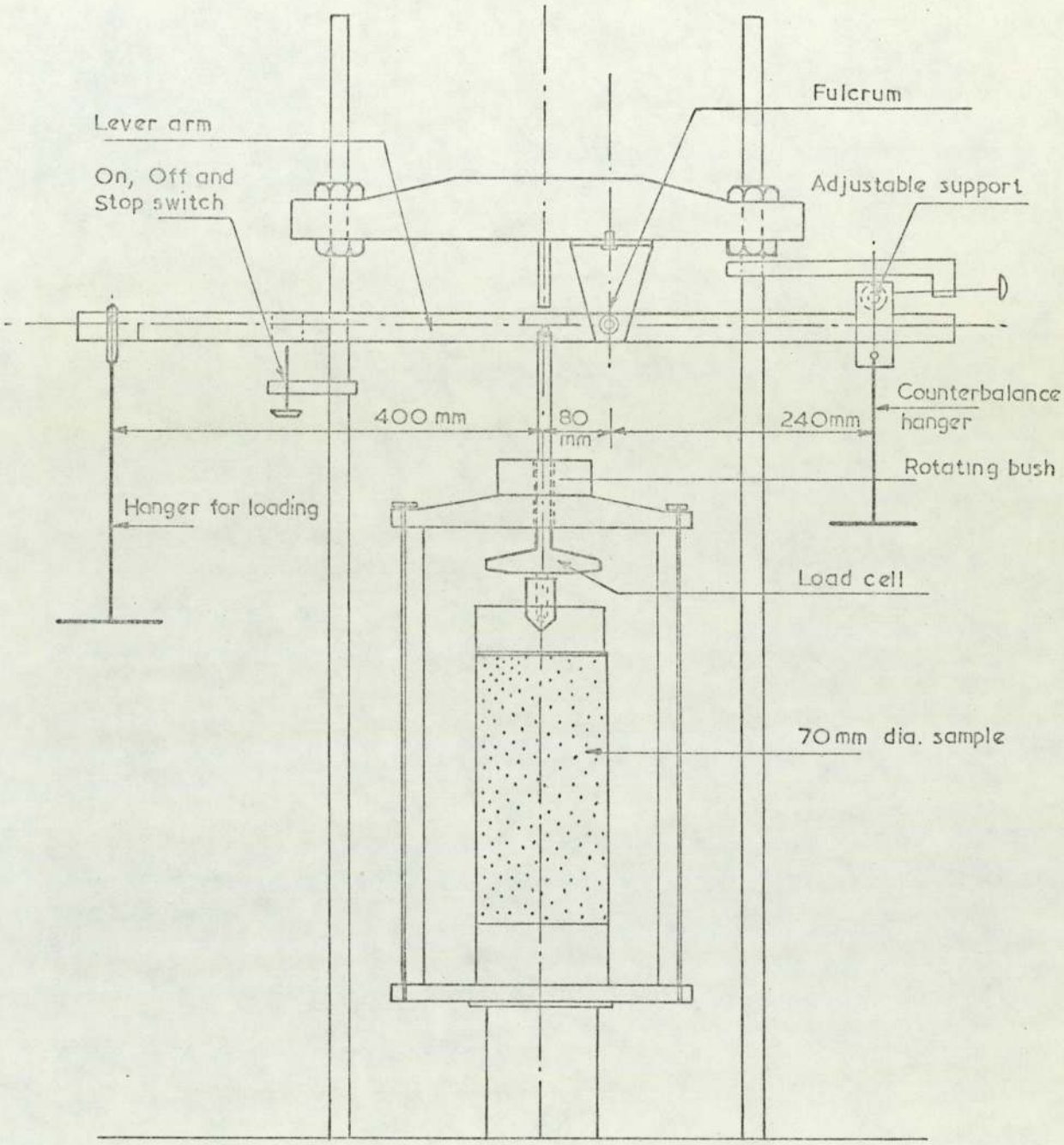

Fig . 3.2 Layout of the stress controlled triaxial cell

PLATE 3.1 Oedometer cell with the pressure transducer attached to the base

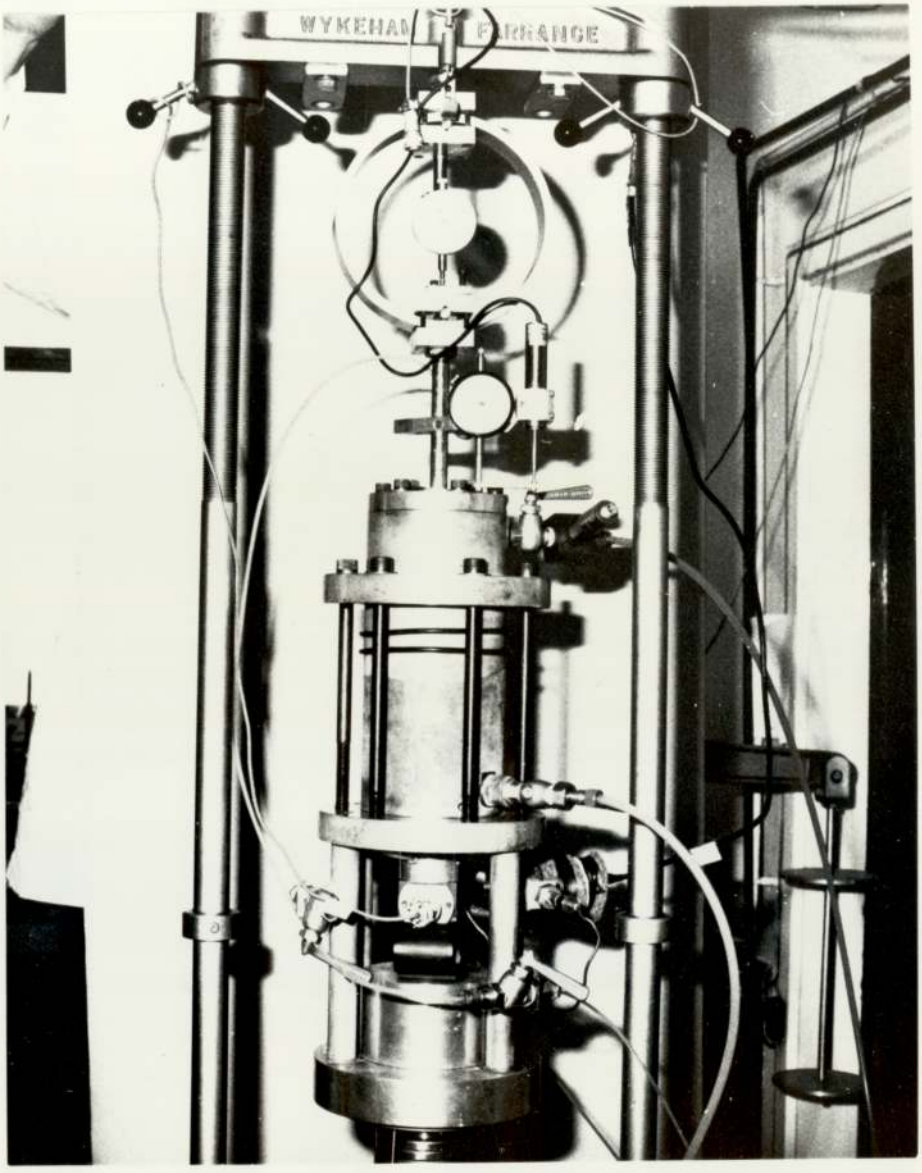

PLATE 3.2 Independent stress triaxial cell

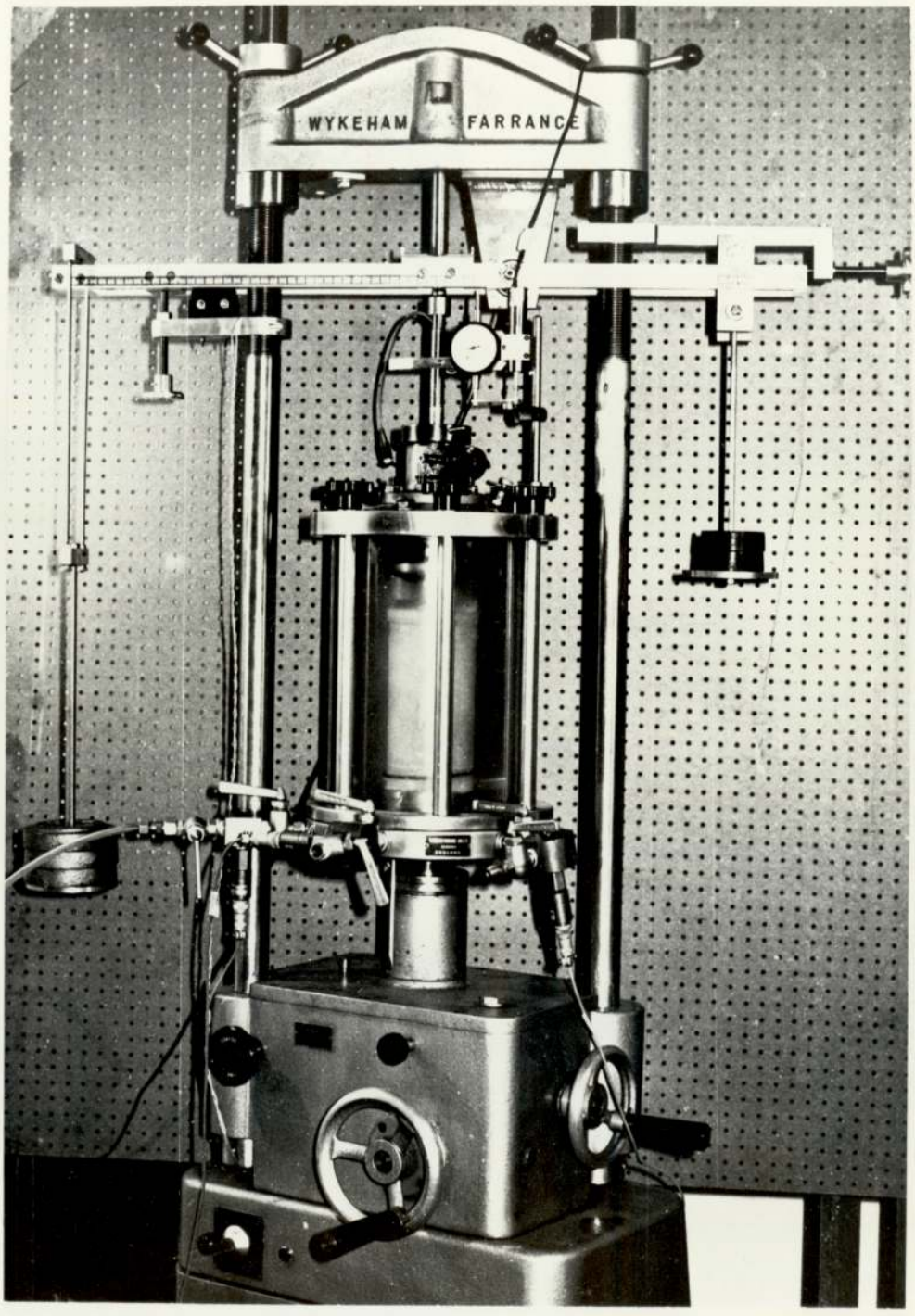

PLATE 3.3 'Stress-controlled' triaxial set up

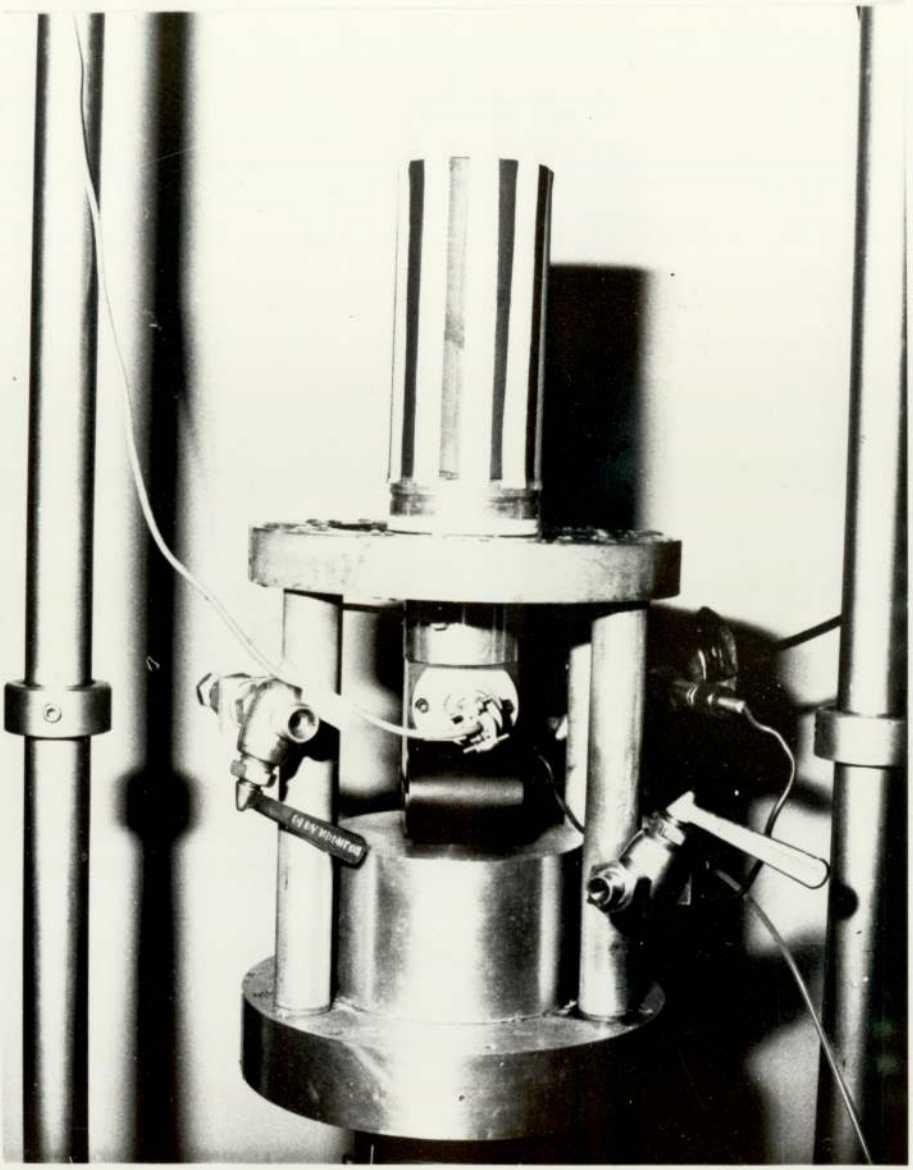

PLATE 3.4 Setting up of the 70mm diameter triaxial sample

CHAPTER FOUR

CHOICE OF MATERIAL & PREPARATION OF SAMPLES

4.1 Introduction

Detailed study of the mechanical properties of natural soils is generally made difficult by a wide scatter of results due to normal variation of their physical properties, even in the most homogeneous of the natural deposits. It is therefore reasonable to start investigations of mechanical properties of a material by elimination of as many of the natural variations as possible. In the case of a soil this can be achieved by preparation of an homogeneous, remoulded, sample of it. It is, of course, recognised that differences, particularly in the structure of the soil, exist between the natural material and the remoulded soil. However, detailed study of the remoulded material can provide data which may further the understanding of the behaviour of the natural soil during shearing, if not at small, then at large deformations.

Comparisons could be made between the effect of different stress histories on the mechanical properties of the material, and the effects of deformation under sustained loading could be investigated.

Bearing this in mind, an attempt was made to prepare a high quality, remoulded sample of homogeneous composition and consistency. In all cases samples of slurry consistency ($w = w_{\ell} + 20\%$) were prepared from a well mixed dry bulk samples and were reconsolidated to reach a water content at which the soil could be handled with ease. The material used was an unweathered Lias clay, available in the departmental soil mechanics laboratory, in the form of

block samples excavated on site by Thomas (1973). Consolidation of the slurry samples was carried out in a "tall oedometer" (see Section 4.5) until the required consistency was obtained. Care was taken at all stages of the preparation of samples to achieve a fully saturated material; the obtained degree of saturation was generally greater than 98%.

4.2 Lower Lias Clay (Geology)

Lias is the name given to the Lower Jurassic system of rocks of the Mesozoic era. The Lower Jurassic is divided into Upper, Middle and Lower Lias. The Lias was deposited under marine conditions which existed over much of England and Europe during the Jurassic era.

The Lower Jurassic comprises of argillaceous rocks, clay, shales and thin muddy limestones, and it is from the alteration of shales and limestones that the name is derived. Since its deposition, some 190 million years ago, the Lower Lias clay has become overconsolidated; in some parts overburden of the order of 700m was estimated (Caulthard, 1975). By the end of the Jurassic era the deposits were elevated above sea level and were subjected to erosion. Subsequent subsidence of the majority of the British Isles below a shallow sea led to deposition of chalk above the Lias, which in turn was elevated and eroded away. Samples of the Lias clay for the present work were obtained from a site in Blockley (Gloucestershire in the Severn Basin), from a depth of about 10m below the G.L. The tested material can be

described as a heavily overconsolidated fissured very hard clay, which, in spite of some deep weathering on the site, has not been affected by it; the tests described in this thesis were carried out on remoulded samples of the above material.

4.3 Physical Properties

A number of tests were carried out to measure the consistency limits and particle size distribution of the Lias clay. A summary of the results and of data available from other sources is given in Table 4.1. Consistency limits tests were carried out according to the B.S. 1377 (1967), on samples of air dried soil passing through a B.S. No. 36 sieve (440 μ). Some samples were wetted and left in a saturated state for a week to see if this had any effect on the index properties, but no significant differences were detected.

Particle size analysis carried out by Caulthard (1975) had shown the clay content to be between 40% to 44%, whereas x-ray diffraction analysis indicated clay contents of twice the above values. Major minerals present were Illite and Kaolinite (between 70% and 90%) with Quartz, Pyrite and Calcite as subsidiary minerals.

Table 4.1

W_L%	W_p%	I_p%	G	Clay Fraction CF%	Activity $\frac{IP}{CF}$
53-63	25-29	28-31	2.72	40-44	0.65-0.86

4.4 Preparation of remoulded samples of Lias clay

Remoulded samples of the soil were prepared from several block samples of unweathered Lias clay from Blockley. Air-dried lumps of the undisturbed soil were ground down to a powder, which was then sieved through a B.S. No. 36 sieve (440 μ). The passing fine silty clay was thoroughly mixed to form the bulk sample from which individual samples were prepared. The powdered soil was mixed with distilled water to a water content of 74%, i.e. 20% above the average liquid limit. The high water content was chosen to ensure a high degree of saturation of the soil. The mixing was carried out in an electric food mixer for at least 30 minutes. The mixture was then placed in a desiccator and was de-aired by connecting it to a vacuum pump. After de-airing the container was closed and the soil was left for 24 hours to allow equalization of the water content in the soil. At the end of the equalization period, the soil was again subjected to vacuum while being gently vibrated and occasionally stirred; this was done to improve saturation or de-airing of the soil.

The consistency index of the soil at this stage was less than zero (i.e., it was of liquid consistency), and it could easily be poured into the tall oedometer, where it was consolidated.

4.5 Development of the "tall oedometer" for initial consolidation of remoulded soil

The bulk sample was prepared at a water content above the liquid limit and therefore its consistency was too soft for handling and preparation of triaxial samples. Hence the soil had to be

consolidated prior to further preparation of samples. This was done in a specially built oedometer (referred to as a "tall oedometer") which was previously used by the author (Nasseri 1972). On the basis of previous experience the original tall oedometer was modified to facilitate easier placement of the soil and obtain a more homogeneous sample. It was found in the previous studies that because the initial height of samples was nearly 400mm, the side friction for samples compressed from one end produced a significant variation in water content over their length.

To improve the uniformity of the water content the original apparatus was modified to facilitate compression from both ends of the sample, i.e. from top and bottom. To achieve this a bottom piston (identical to the top piston) was introduced; both were mounted in sleeves fitted with ball-race bearings. The bottom sleeve was attached to the base. A simple pulley system was devised for a simultaneous application of loading to both pistons, as shown in Plate 4.1. Top and bottom drainage outlets were connected to separate volume change devices and a back pressure was applied to ensure saturation of the system, the whole apparatus was mounted on a frame as shown in Plate 4.1 and Fig. 4.1.

4.5.1 Consolidation of remoulded soil in the tall oedometer

The tube of the tall oedometer (100mm internal diameter and 500mm height) was greased and fixed to the base. The bottom piston was pushed through and after drainage connections were made, the whole system was flushed and saturated. A small amount of distilled water was poured into the tube to cover the bottom. A de-aired

batch of soil slurry was then slowly poured into the tube which was continuously tapped during this operation. A layer of free water was maintained on the surface of the rising slurry. When the slurry level had reached the desired height, filling was stopped and the bottom piston pushed upwards until the slurry started to overflow. The top of the slurry was then levelled off and the top piston was placed in position and together with the bottom piston was pushed down the tube to the starting position. At this stage the top sleeve was put on and the top loading beam was then fixed to the hanger rods. The wires attached to the bottom loading beam were then tightened and contact was made (via ball bearings between the loading beams and the piston plungers).

Loading of up to 150Kg was applied, usually in three increments, each doubling the previous load intensity. The load increments were added when the settlement from the previous loading had virtually ceased. Two conventional 100ml paraffin volume change devices were used to measure separately the amount of water draining from the top and bottom of the samples. Axial movement was measured with a 50mm dial gauge.

Measurements of the preconsolidation stress during triaxial and oedometer tests had shown that there was a considerable friction in the tall oedometer, mainly due to the seals (rubber O-rings) between the piston and the tube; the initial load necessary to induce movement of the piston was approximately equal to 20 Kg. The rest of the frictional losses were due to the side friction between the sample and the tube. The side friction produced a moisture content variation between the sides and centre of the

samples, which at most was about 0.5%. The vertical variation of the moisture contents between the ends and middle of samples was of the order of 1%. In 140mm high (70mm dia.) triaxial samples the differences were proportionally smaller.

Measurements of moisture content in some of the tall oedometer samples are summarized in Table 4.2.

Consolidation curves for one of the samples and void ratio - calculated effective stress curve are shown in Fig. 4.2 and 4.3 Because of the friction in the tall oedometer the value of the compression index evaluated from this curve is rather high (C_c= 0.55) compared with the results obtained from triaxial and oedometer tests. However, the extruded samples had a moisture content of between 38% and 41% and were sufficiently firm for handling and preparation of triaxial samples without visible disfiguration.

The degree of saturation evaluated from small (quality and control) triaxial samples, was generally higher than 98%.

4.6 Preparation of triaxial and oedometer samples

At the end of the consolidation of samples in the tall oedometer the load was removed and the top loading beam and sleeve were dismantled. An extension was fitted to the bottom piston so that the 100mm dia. sample could then be extruded. This was simply achieved by placing a small load on the hanger, sufficient to push gently the piston and sample upwards. When the top of the sample emerged from the tube, the movement was halted and the top piston

was removed. A 10mm slice of the sample was then cut off and the surface was smoothed.

Following this two 25mm high oedometer samples were cut off with a thin wire; final samples were then cut using the containing rings. A special 70mm dia. cutter was then attached to the top of the tube through which a triaxial sample of the same diameter was extruded. Again, it was sufficient to place a small load on the hanger to push the sample upwards at a steady speed until the required length of sample was extruded, as shown in Plate 4.2. The soil was then cut off at the bottom with a cheese wire. The wire was threaded through two holes in the outer ring and the so formed loops were retained inside a groove formed by the oedometer tube and the outer ring. The cutting action was achieved by pulling the two ends of the wire with the inner ring acting as a guide for the wire. The sample was then transferred to the base of a triaxial cell where, before it was mounted, its length and diameter were accurately measured.

Table 4.2

Final water content of tall oedometer samples
(Initial W ≃ 74%)

Sample No. and Final Applied Stress KN/m^2	Position of samples for determination of W%						Triaxial Samples W%
	Top		Middle		Bottom		
	Side	Centre	Side	Centre	Side	Centre	
No. 101 σv = 84	39.34	39.52	39.83	39.96	39.51	38.74	39.93
No. 104† σv = 84	39.70	39.82	40.54	41.63	41.62	41.50	41.60
No. 109 σv = 94	37.93	38.27	38.27	-	37.83	38.08	38.08
No. 110 σv = 84	38.02	-	38.50	-	38.16	38.21	38.20
No. 115 σv = 84	39.14	-	39.46	-	38.56	38.94	39.03

† At the end of the second increment, wires had snapped and drainage from the bottom slowed down

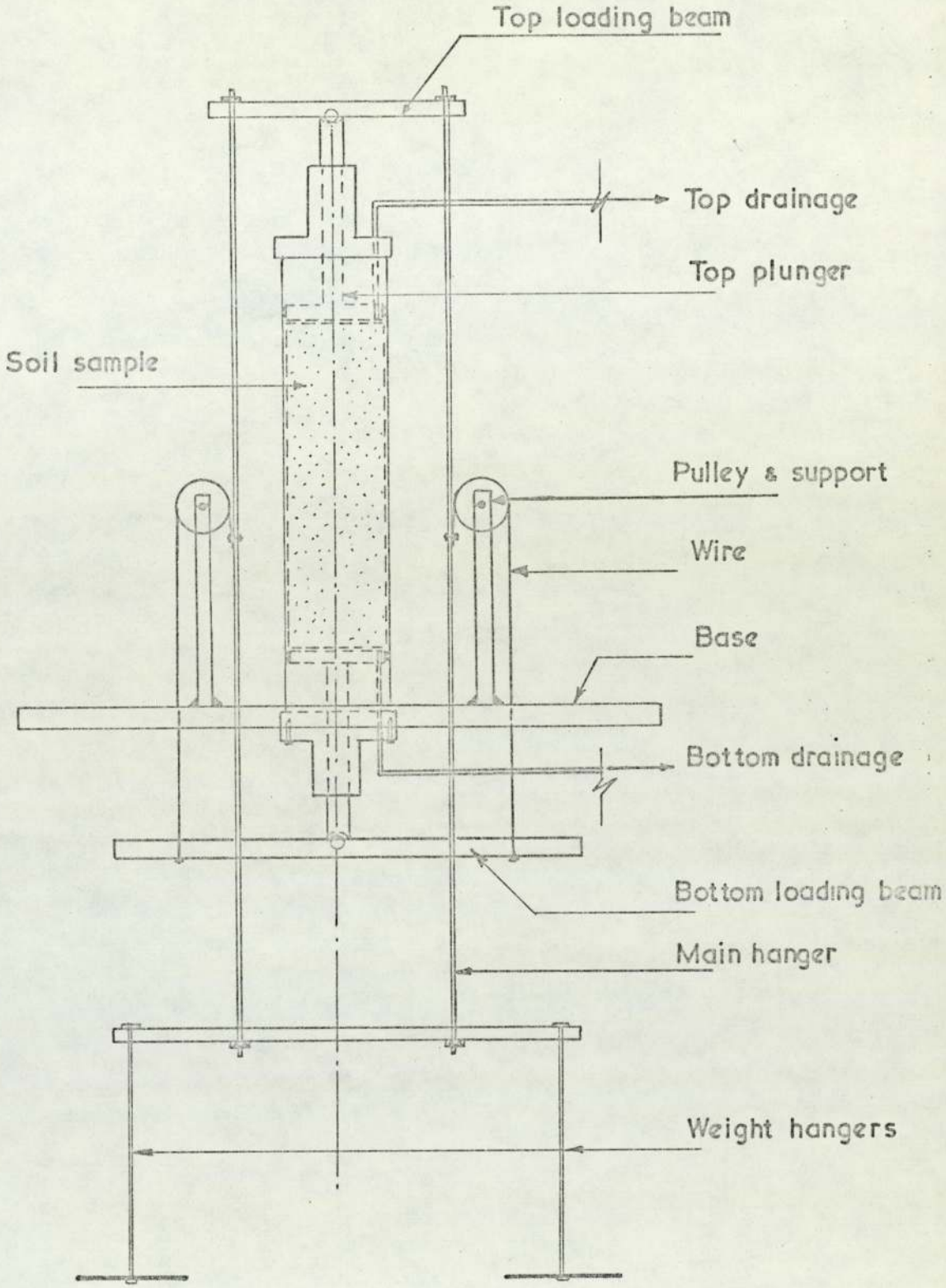

Fig. 4.1 Layout of the tall oedometer with top and bottom drainage connections

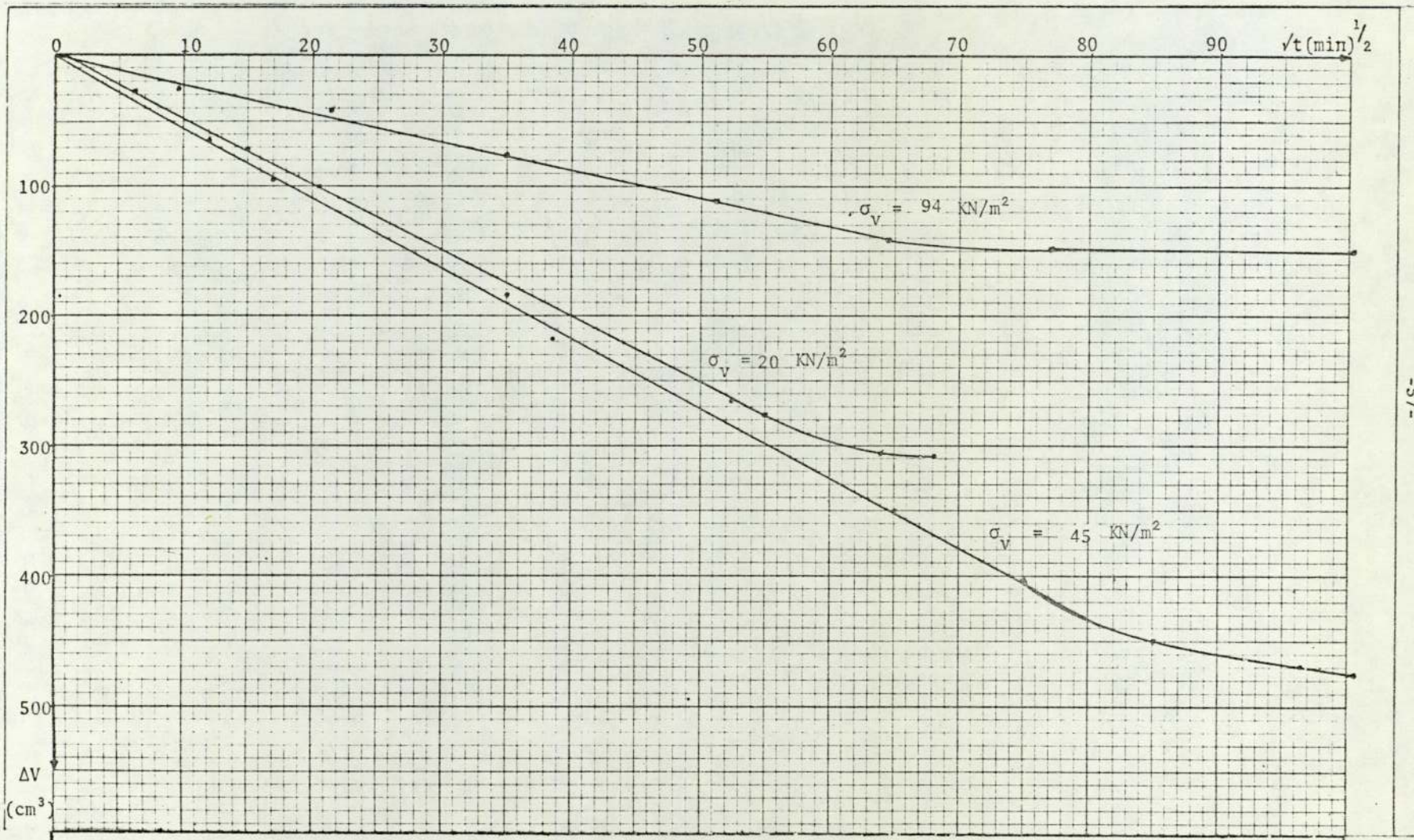

Fig. 4.2 Compression vs Root Time (Sample No 109)

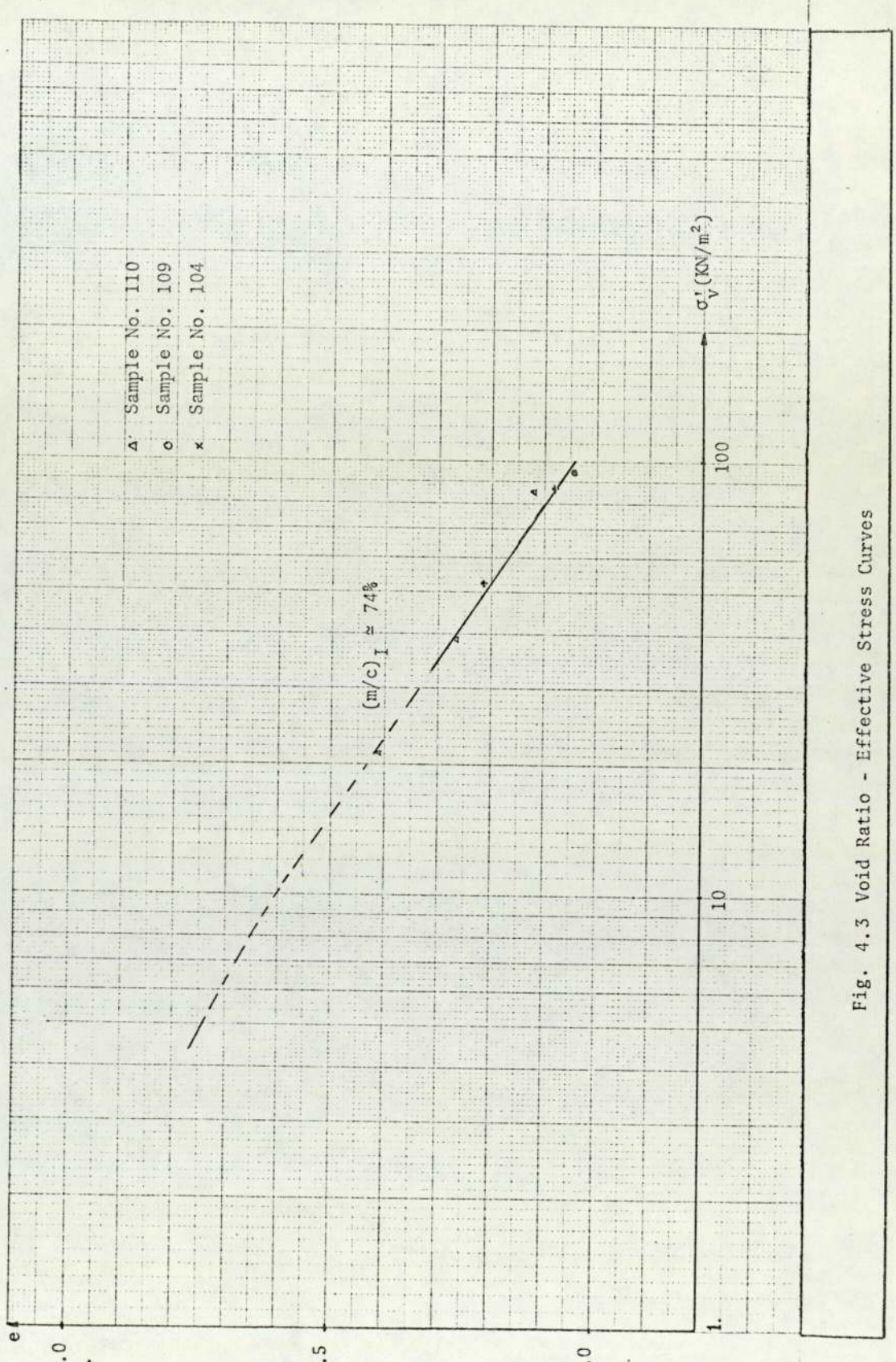

Fig. 4.3 Void Ratio - Effective Stress Curves

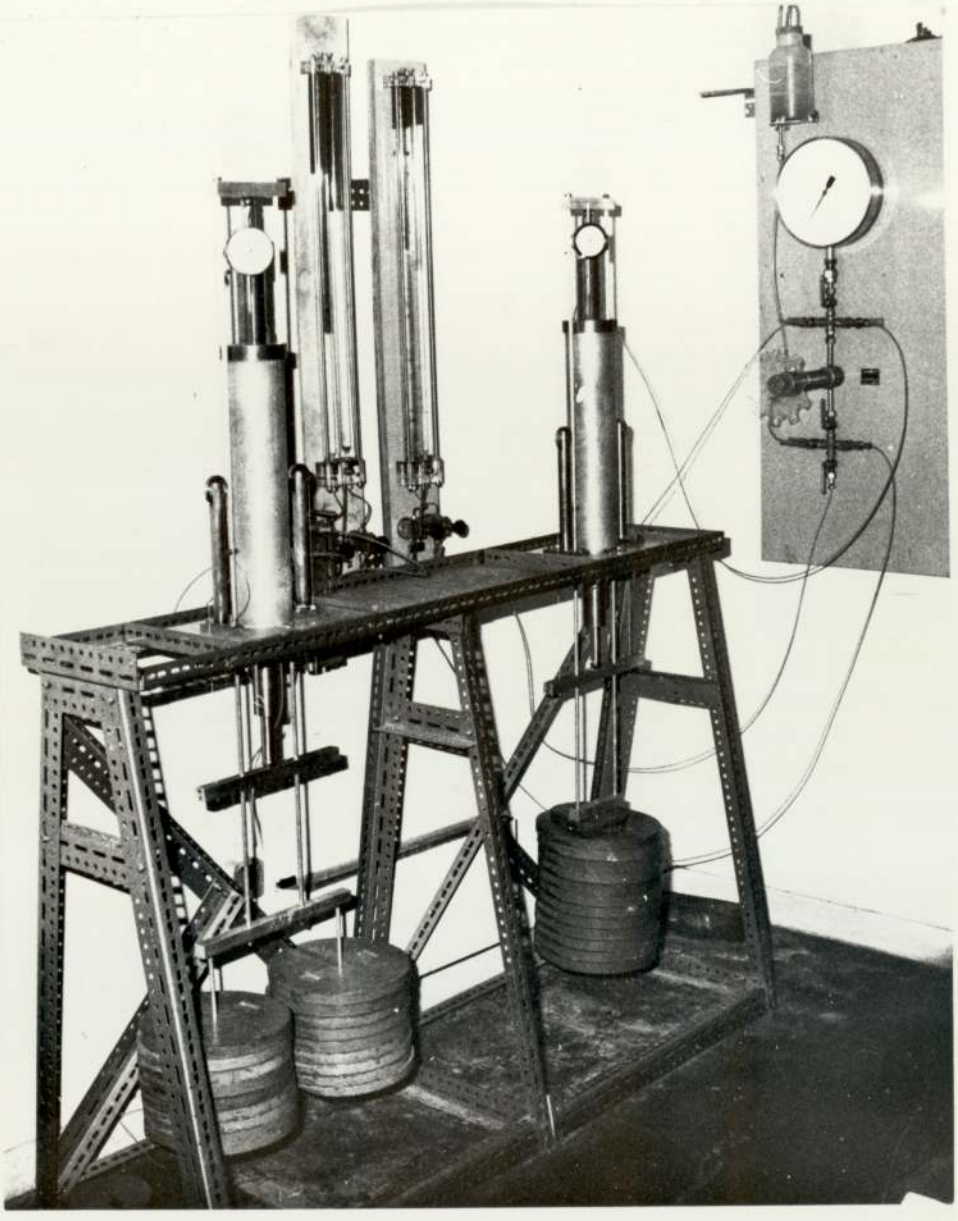

PLATE 4.1 'Tall oedometer' apparatus

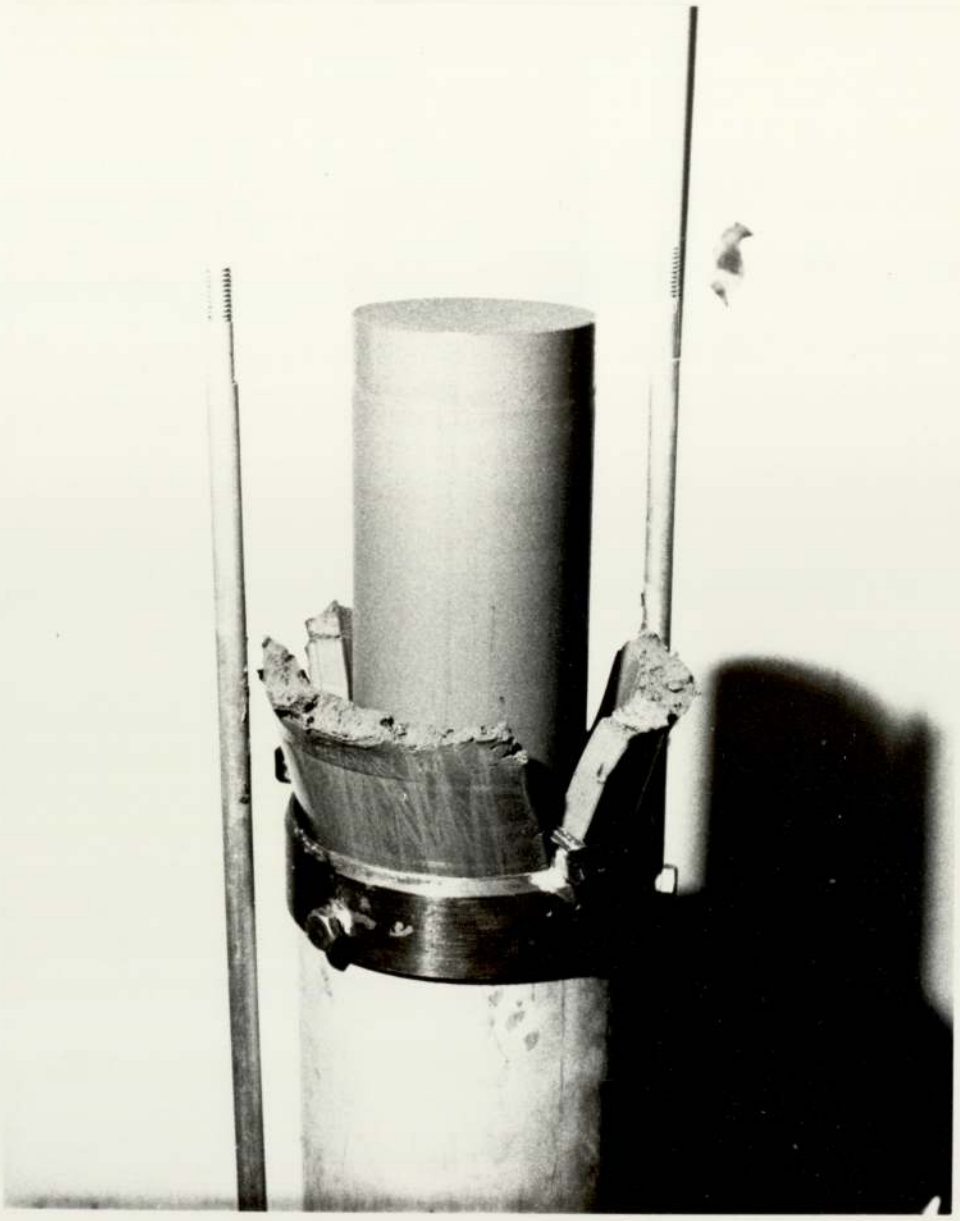

PLATE 4.2 Cutting of a 70mm dia. triaxial sample from the tall oedometer sample

CHAPTER FIVE

TEST RESULTS

5.1 Oedometer Test Results

For clarity the results of the oedometer tests presented in this chapter include four representative test results for samples initially prepared in the tall oedometer (see Chapter 4) and two more results for samples prepared and consolidated directly in the oedometers at 61% moisture content (Bennett 1975). For each test the compression has been plotted versus the square root and logarithm of time (Figs. 5.1 to 5.8). Origin correction for each stress increment was evaluated from compression - square root of time plots, but no correction was made for the range of the machine error (Thomas 1973). For the loading cycles, with the exception of the first loading cycle, the origin correction was generally less than 10% of the total compression, whereas for some of the unloading cycles it was as high as 50%. With the exception of tests SO1 and SO2, filter papers were not used because calibration tests with steel block and filter papers proved inconsistency in their compression (Bennett 1975).

In the analysis of test results the actual compression was taken as the recorded compression less the origin correction. The coefficient of volume compressibility m_v was adopted as a measure of compressibility of the soil instead of using Terzaghi's coefficient of compressibility $a_v = de/d\sigma'$:

$$m_v = \frac{a_v}{1+e} = \frac{de}{(1+e)d\sigma'} = \frac{d\varepsilon_v}{d\sigma'} \qquad (5.1)$$

The values of the coefficient of consolidation, C_v, were calculated from 50% and 90% consolidation time obtained, respectively, from the plots of compression against logarithm and square root of time.

5.2 S O Series

Results of three tests in this series are given in Table 5.1. Compression-time curves for test SO7 are shown in Fig. 5.1 and Fig. 5.2, and void ratio - effective vertical stress curves are plotted in Fig. 5.3 for Tests SO1, SO2 and SO7.

5.3 P O Series

Five tests were carried out in this series with pore pressure measurement at the base. All samples were preconsolidated in the tall oedometer and were then set in the oedometer in the usual manner. Results of three of the tests are tabulated in Table 5.2, and compression - time curves are shown in Figs. 5.3 to 5.8. For samples PO2 and PO3 a flexible connection (polythene tube) was used between the base of the sample and the pressure transducer. Observed ratios of the induced pore pressure Δu to incremental stress, $\Delta\sigma$, against time, are in Fig. 5.9. In Test PO2 an initial back pressure equal to applied stress was applied to the measuring system. Fig. 5.10 shows the plot of the pore pressure ratio $\Delta u/\Delta\sigma$ against time for Test PO4, in which the pressure transducer was attached directly to the base of the cell in order to minimize flexibility of the measuring system. The

void ratio versus vertical effective stress plots for the PO series of tests, and Test SO7 are shown in Fig. 5.11. It should be noted that the values of the void ratio in these graphs are the final values under the relevant stress increment. The initial height of samples in all the tests was between 19mm and 20mm, thus the drainage path, for the PO series was twice that of the SO series.

5.4 Rate of Consolidation Curves

In order to introduce the rate of consolidation as an additional variable in the void ratio - effective stress relationship the test results must be analysed in the manner described in Chapter 2. The void ratio - time curves for four loading stages of Test SO7, are shown in Fig. 5.12 and the derived rate of consolidation $\frac{de}{dt}$ - log time relationship is shown in Fig. 5.13. Finally the results of Test SO7 are replotted in Fig. 5.14 in the form of void ratio - effective stress curves for different rates of consolidation $\frac{de}{dt}$. The results of Test PO4 are presented in Figs. 5.15 to 5.17 in a similar form.

5.4.1 Determination of Soil Parameters for Gibson and Lo's Theoretical Soil Model

In order to obtain soil parameters for the theoretical soil model as described in Section 2.2.2 graphs of $\log \frac{\varepsilon(\infty) - \varepsilon(t)}{\Delta\sigma}$ versus time were plotted in Figs. 5.18 and 5.19. Table 5.3 was compiled using parameters obtained from these two graphs. Fig. 5.20 and 5.21 show the comparison of experimental and theoretical results for Tests SO7 and PO4 respectively.

Test No.	Increment No.	σ' KN/m^2	$\frac{\Delta\sigma'}{\sigma'}$	C_v cm^2/sec x 10^{-4}		m_v m^2/KN x 10^{-4}	C_c
				t_{50}	t_{90}		
	2	50	1	9.59	12.44	8.80	0.156
	3	100	1	3.97	4.67	8.19	0.291
	4	200	1	5.19	3.77	5.78	0.398
S07	5	400	1	4.14	4.66	3.03	0.389
	6	800	1	4.22	4.11	1.53	0.345
	13	1200	½	2.13	3.68	0.77	0.30
	4	53.56	1	2.61	3.89	15.67	0.309
S01	5	107.3	1	3.51	4.25	9.39	0.355
	6	214.6	1	4.12	4.39	5.42	0.389
	7	429.2	1	4.48	5.04	3.0	0.400
	3	26.27	2.5	5.28	6.45	39.9	0.373
	4	53.65	1	4.84	5.20	12.83	0.243
S02	5	107.30	1	4.22	6.72	9.56	0.356
	6	214.60	1	5.21	6.86	5.37	0.380
	7	429.2	1	6.44	8.45	3.0	0.396
	8	859.4	1	10.30	7.78	1.41	0.353

Table 5.1

Test No.	Increment No.	σ' KN/m^2	$\frac{\Delta\sigma'}{\sigma}$	C_v cm^2/sec x 10^{-4}		m_v m^2/KN x 10^{-4}	C_c
				t_{50}	t_{90}		
P02	2	150	$\frac{1}{2}$	4.22	9.32	5.75	0.327
	3	200	$\frac{1}{3}$	2.86	3.67	4.79	0.388
	4	300	$\frac{1}{2}$	6.74	7.42	3.61	0.399
	5	400	$\frac{1}{3}$	1.48	1.92	2.53	0.378
	6	600	$\frac{1}{2}$	3.80	2.97	1.56	0.328
	7	800	$\frac{1}{3}$	1.32	2.44	1.24	0.357
	13	1200	$\frac{1}{2}$	2.71	2.44	0.79	0.313
P03	2	200	1	6.27	8.22	4.92	0.326
	3	300	$\frac{1}{2}$	4.45	7.57	3.17	0.340
	4	400	$\frac{1}{3}$	3.09	4.45	2.36	0.344
	5	600	$\frac{1}{2}$	5.13	5.90	1.75	0.356
	6	800	$\frac{1}{3}$	3.84	5.19	1.33	0.368
	7	1200	$\frac{1}{2}$	4.29	6.82	0.77	0.286
	8	1600	$\frac{1}{3}$	2.91	4.92	0.68	0.356
P04	2	100	1	13.5	9.56	9.06	0.342
	3	200	1	4.74	4.52	5.46	0.363
	4	400	1	5.42	7.15	3.13	0.397
	5	800	1	6.57	7.14	1.07	0.387

Table 5.2

Test No.	Increment No.	σ' KN/m^2	a m^2/KN	b m^2/KN	$1/\lambda$ $KN/m^2/min$	λ/b $1/min$	θ cm^2/min
	3	100					
	4	200	4.67×10^{-4}	1.2×10^{-4}	1.9×10^{7}	4.38×10^{-4}	
S07	5	400	2.0×10^{-4}	1.05×10^{-4}	2.58×10^{7}	3.69×10^{-4}	0.142
	6	800	1.24×10^{-4}	2.85×10^{-5}	4.48×10^{7}	7.83×10^{-4}	
	2	200	5.8×10^{-4}	7.95×10^{-5}	2.66×10^{7}	4.72×10^{-4}	0.090
P04	3	400	2.82×10^{-4}	4.74×10^{-5}	4.40×10^{7}	4.80×10^{-4}	0.114
	4	800	1.5×10^{-4}	4.50×10^{-5}	4.82×10^{7}	4.61×10^{-4}	0.130

Table 5.3

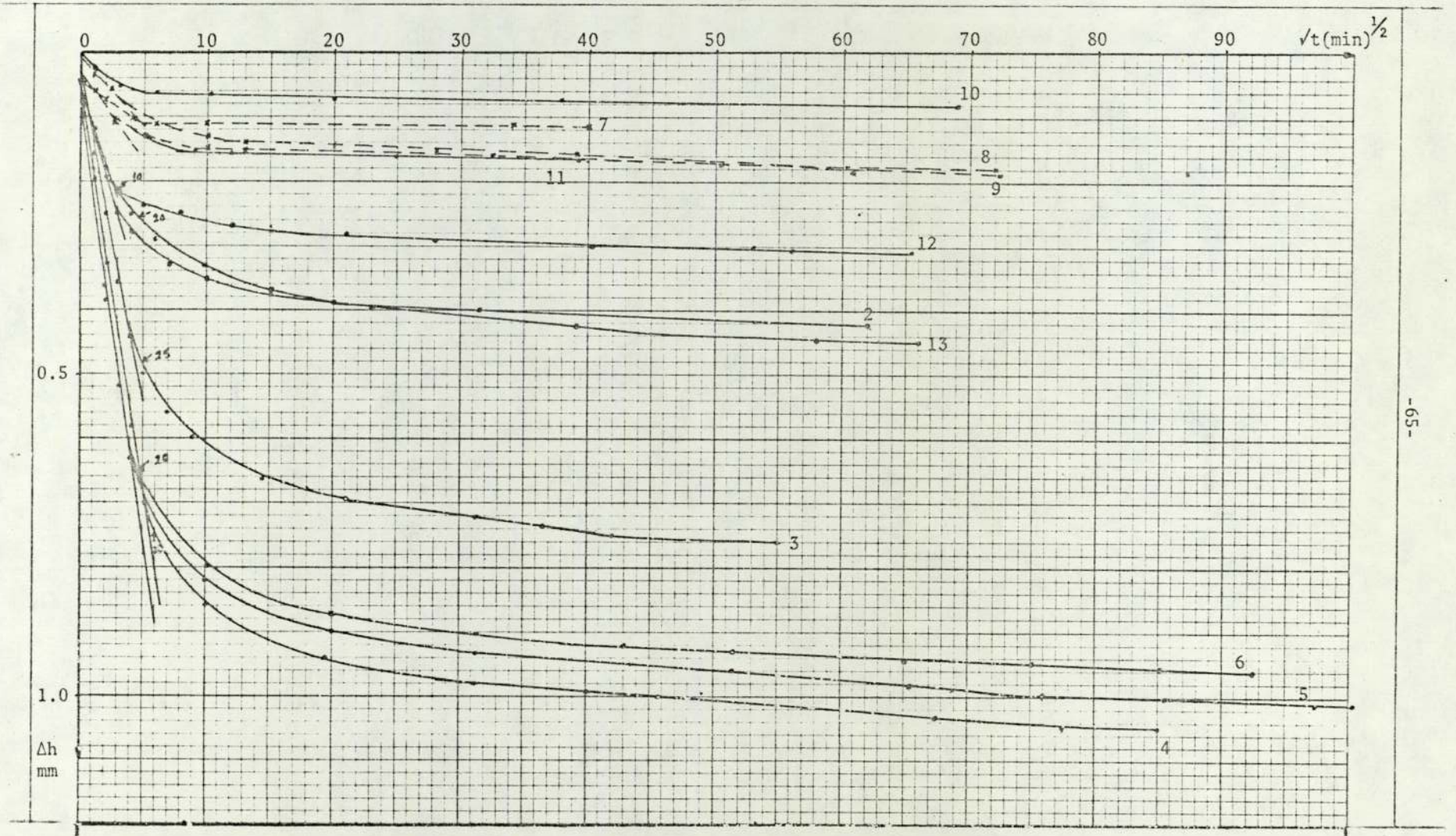

Fig. 5.1a Compressions - Square Root Time Plot for Test S07

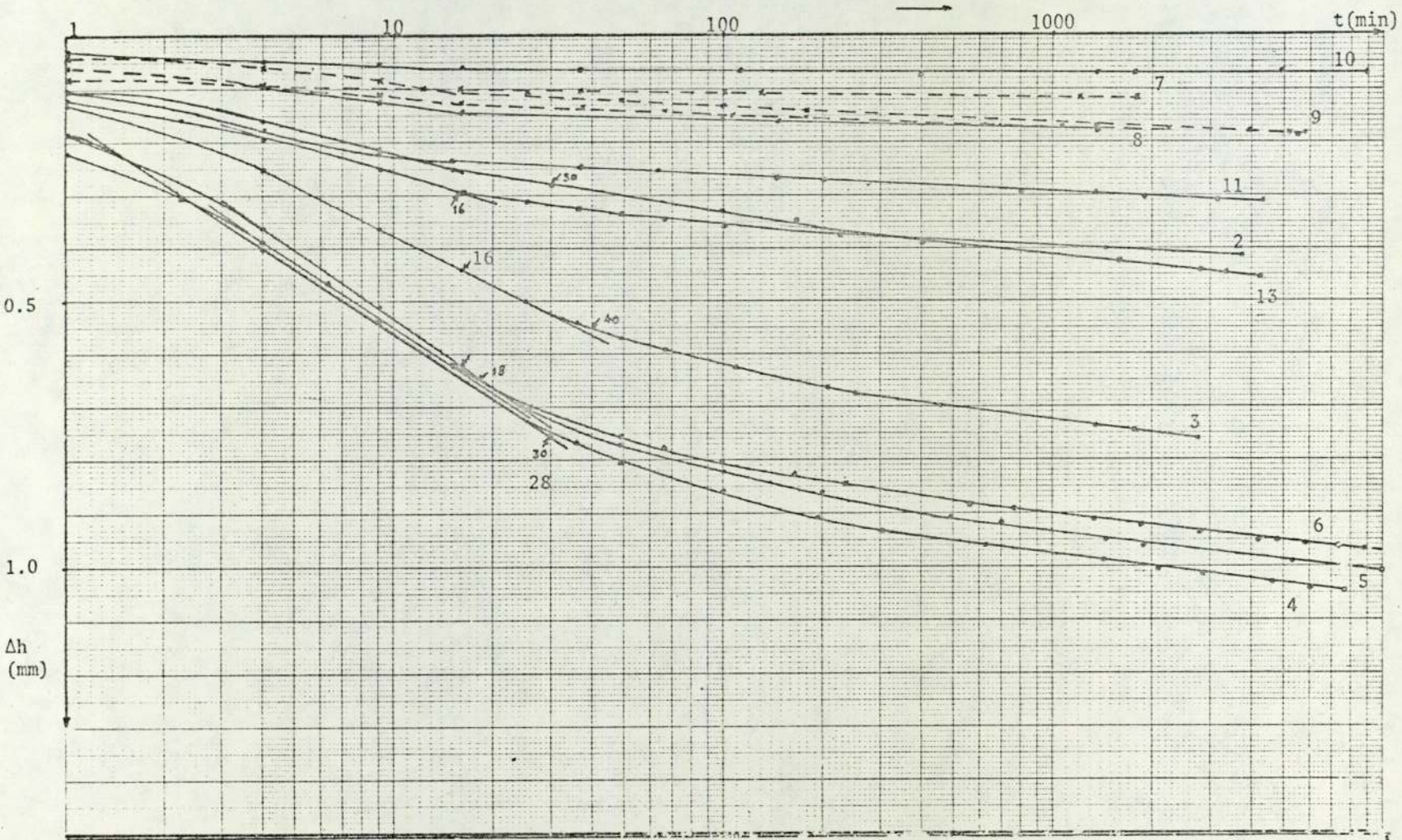

Fig. 5.1b Compression - Logarithm of Time Plot for Test S07

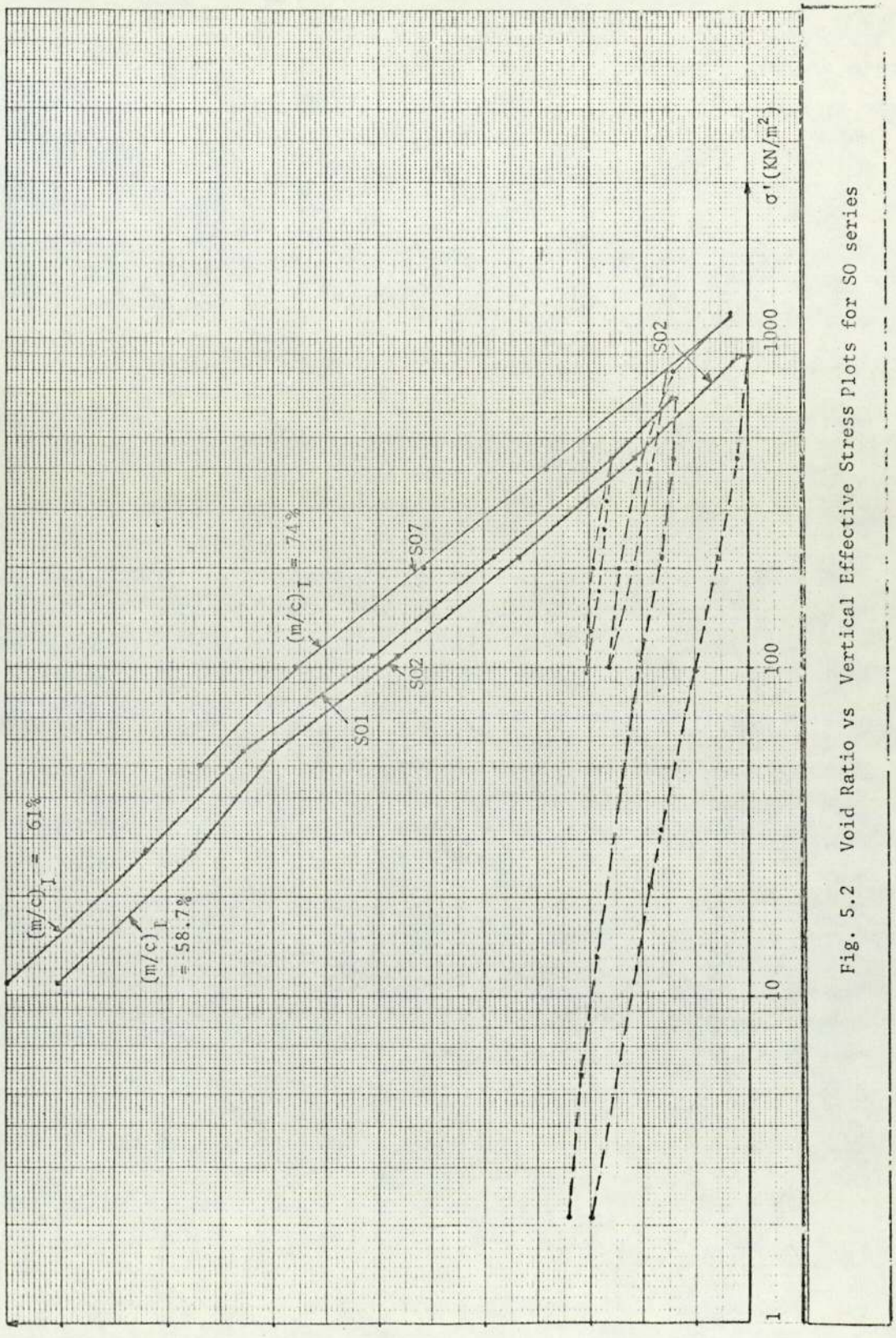

Fig. 5.2 Void Ratio vs Vertical Effective Stress Plots for SO series

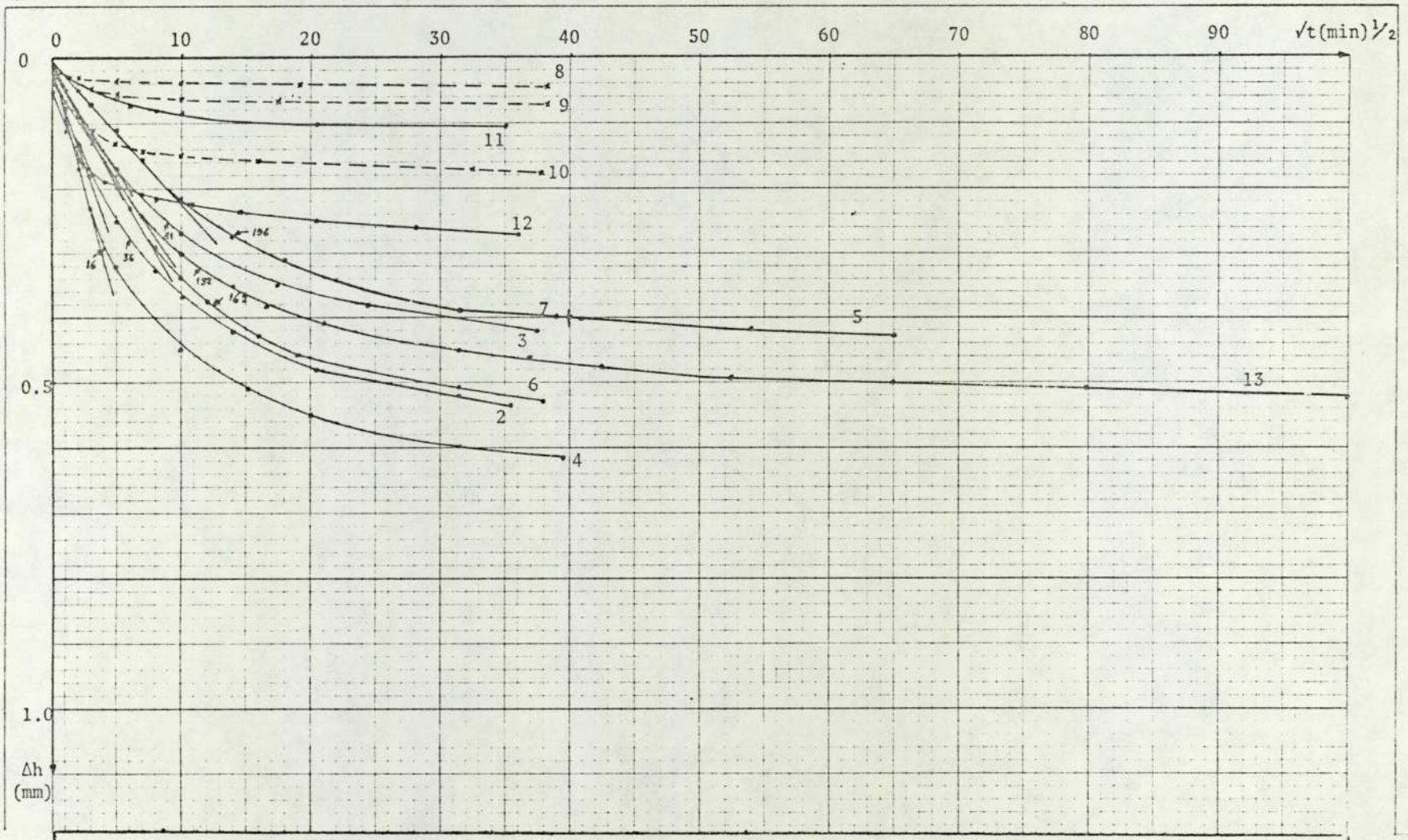

Fig. 5.3 Compression - Square Root Time Plot for Test P02

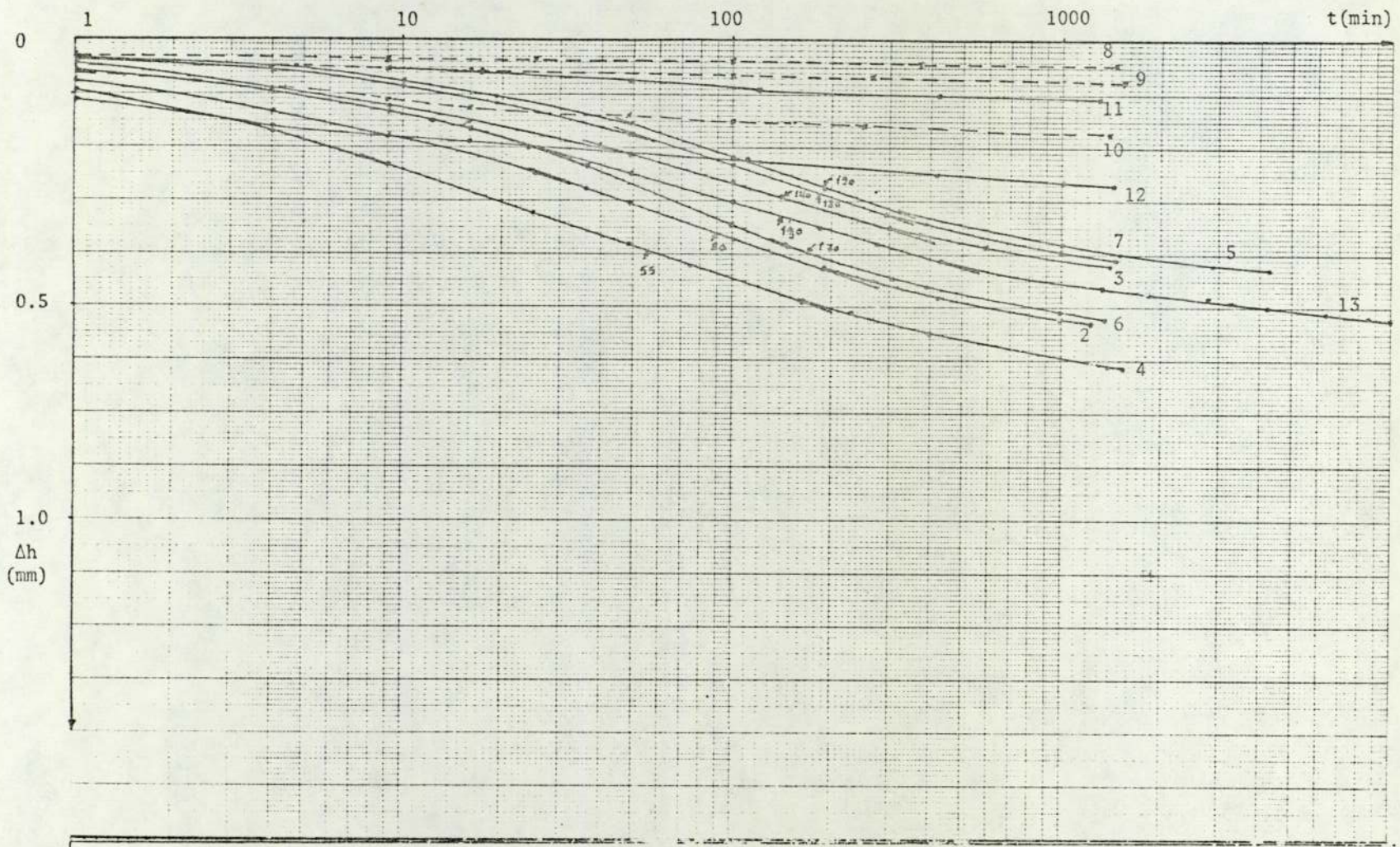

Fig. 5.4 Compression - Logarithm Time Plot for Test P02

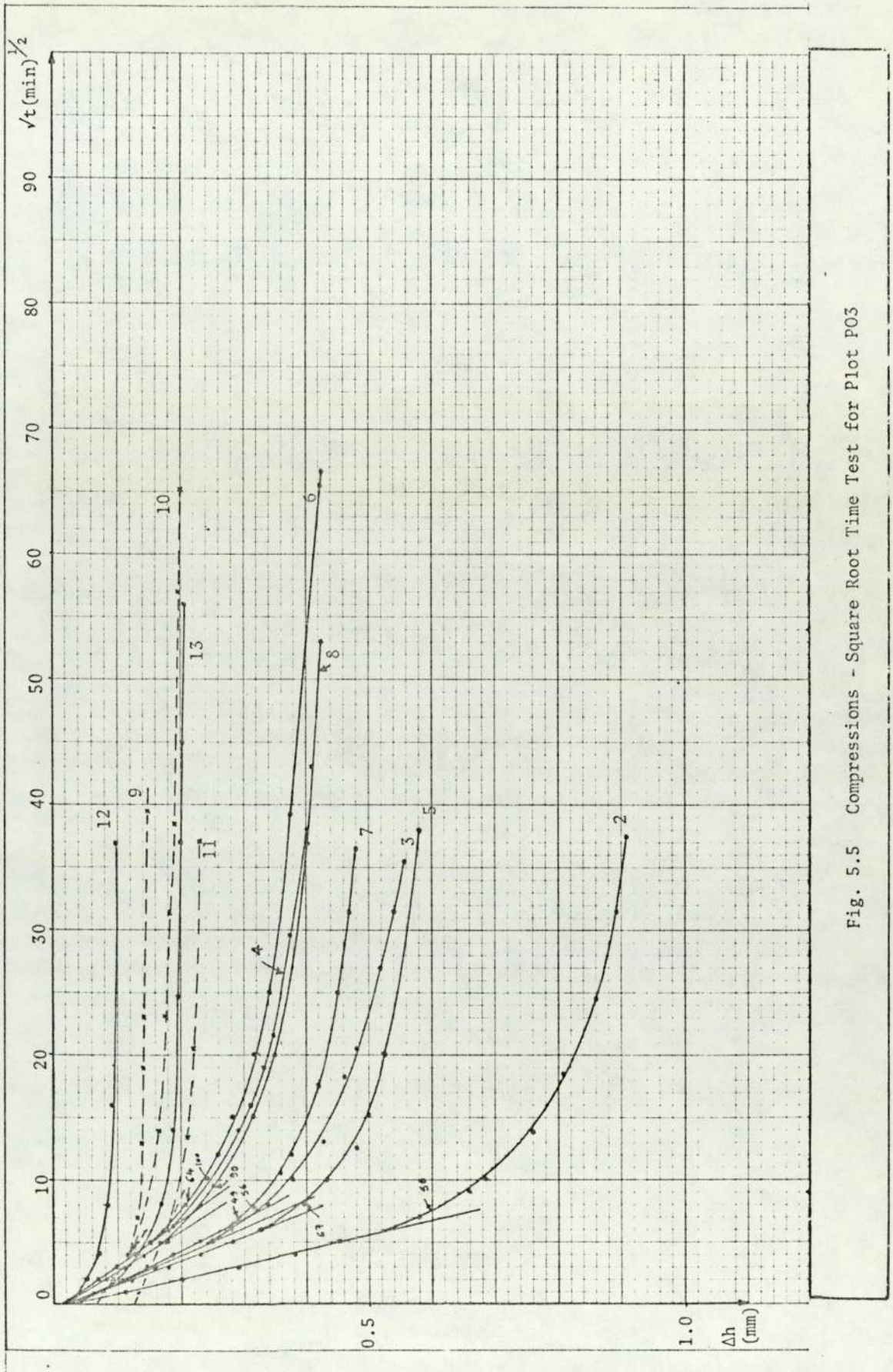

Fig. 5.5 Compressions - Square Root Time Test for Plot P03

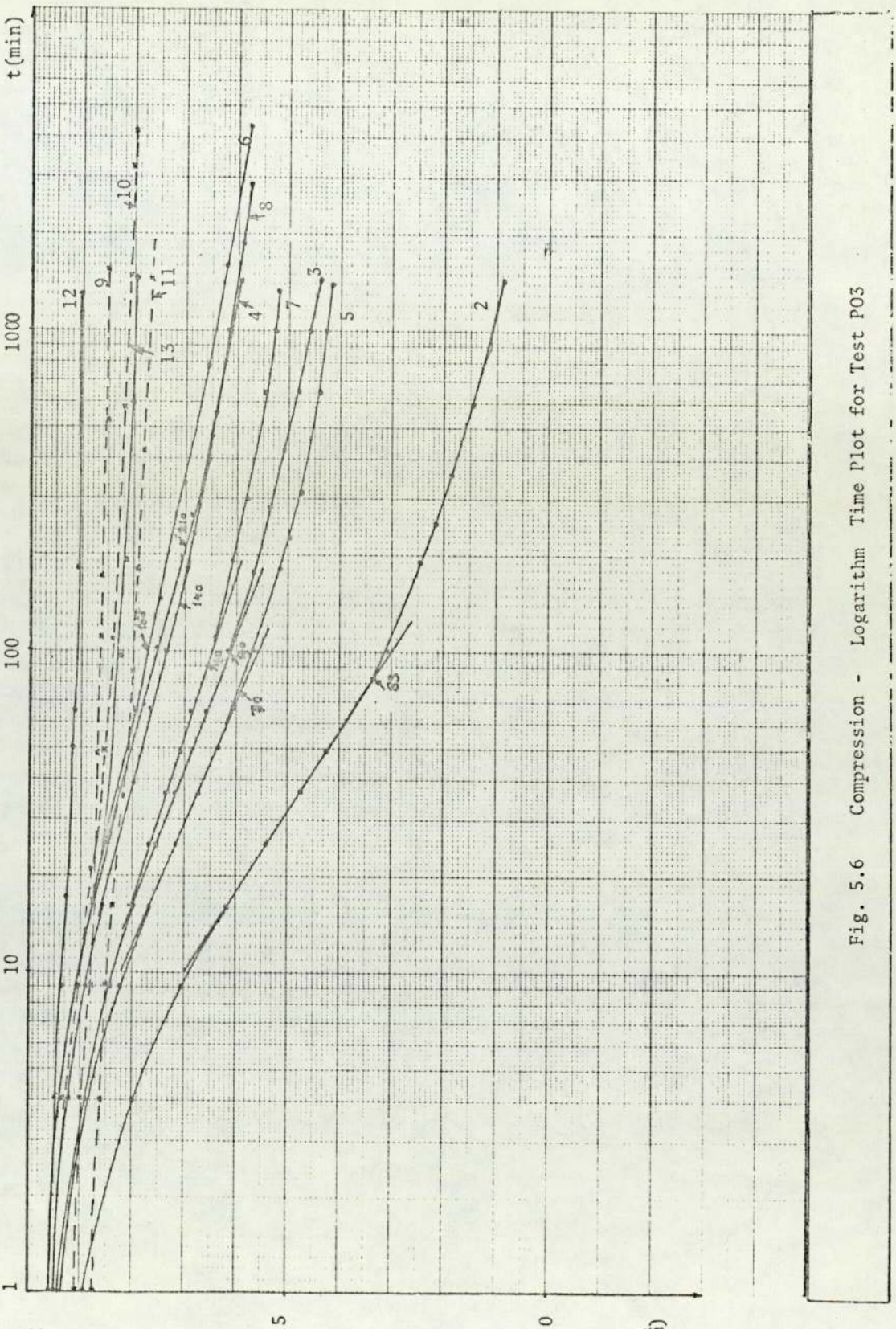

Fig. 5.6 Compression - Logarithm Time Plot for Test P03

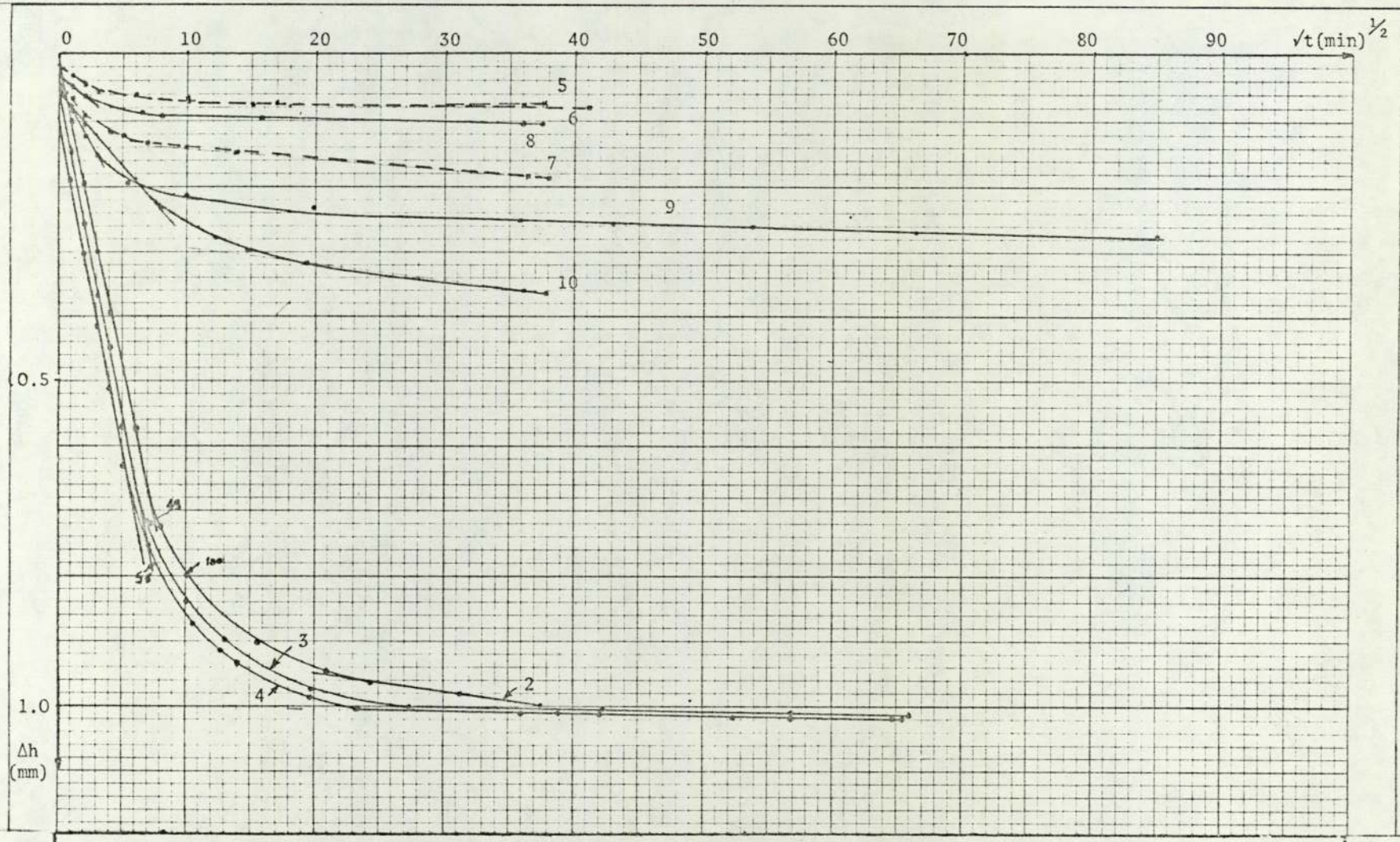

Fig. 5.7 Compression - Square Root Time Plot for Test PO4

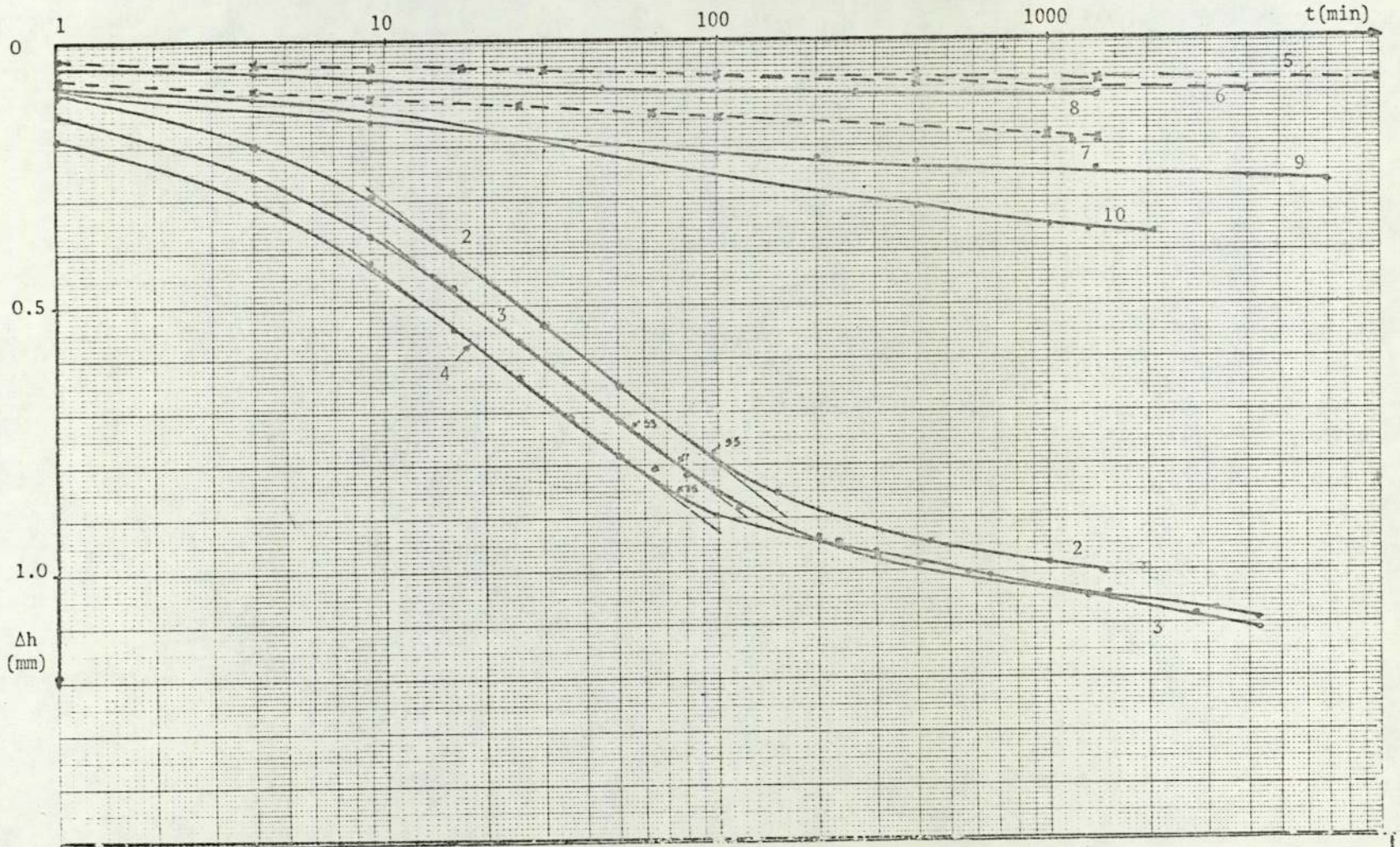

Fig. 5.8 Compression - Logarithm Time Plot for Test P04

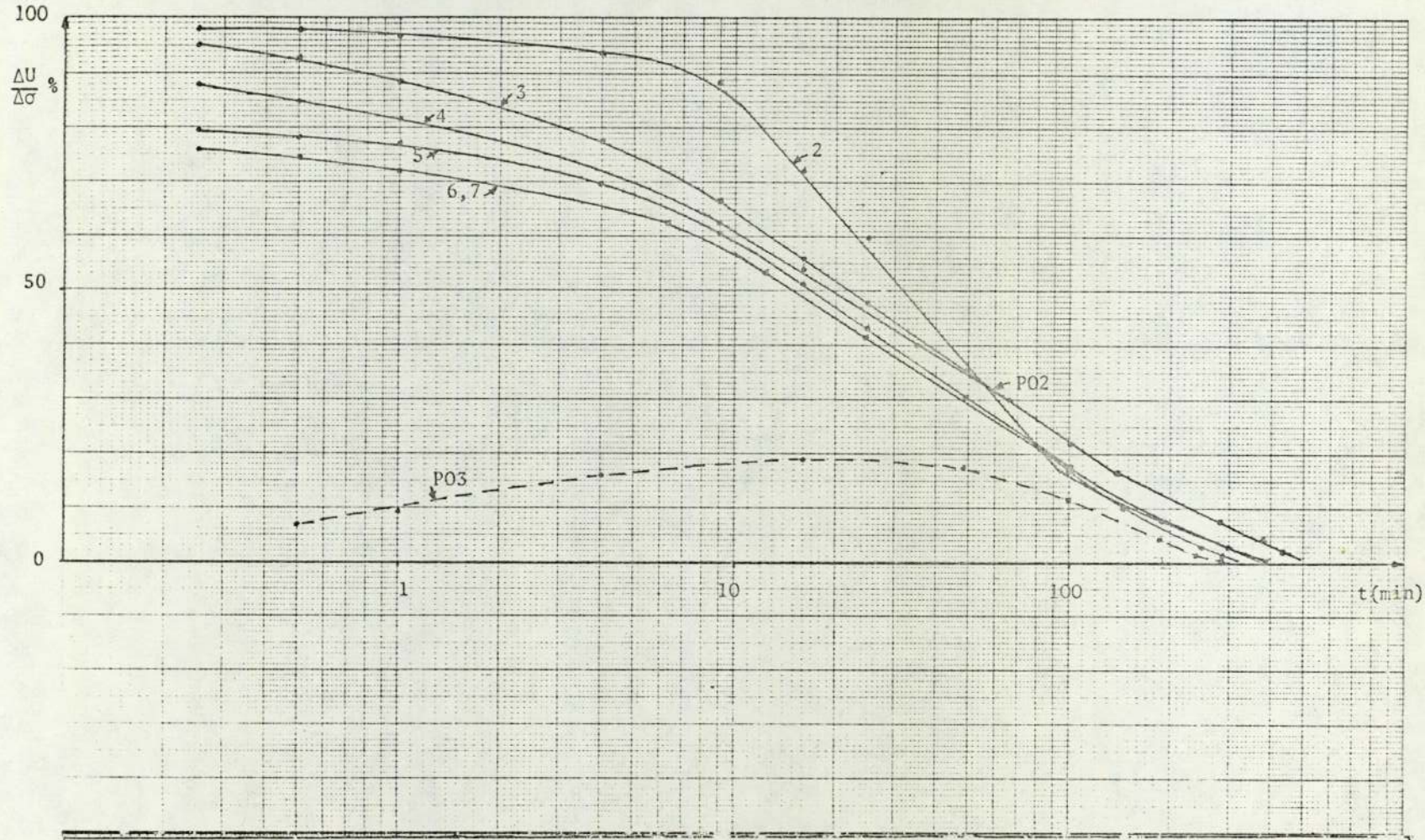

Fig. 5.9 Pore Pressure Ratio - Time Curves Test P02 and P03

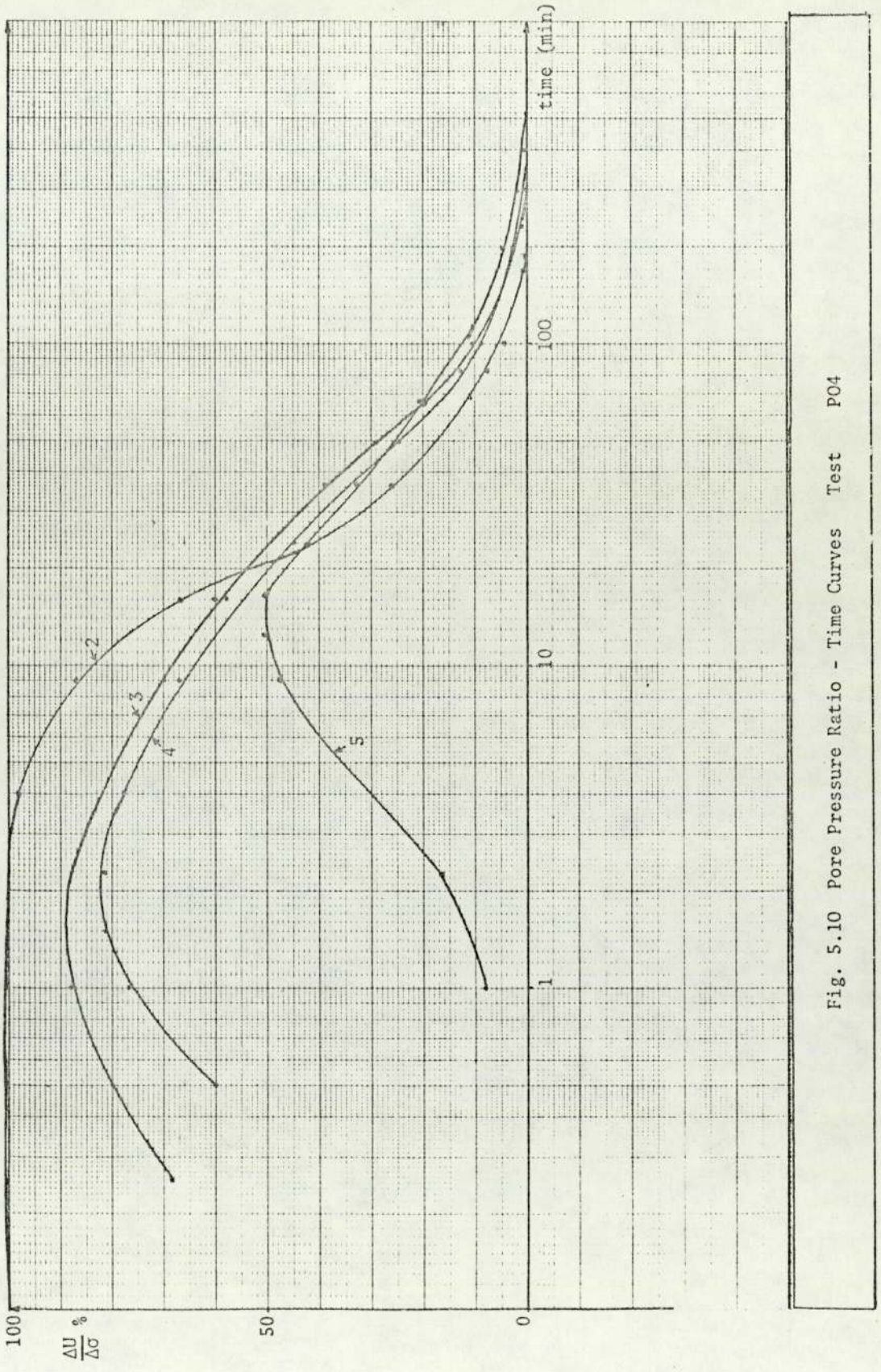

Fig. 5.10 Pore Pressure Ratio - Time Curves Test P04

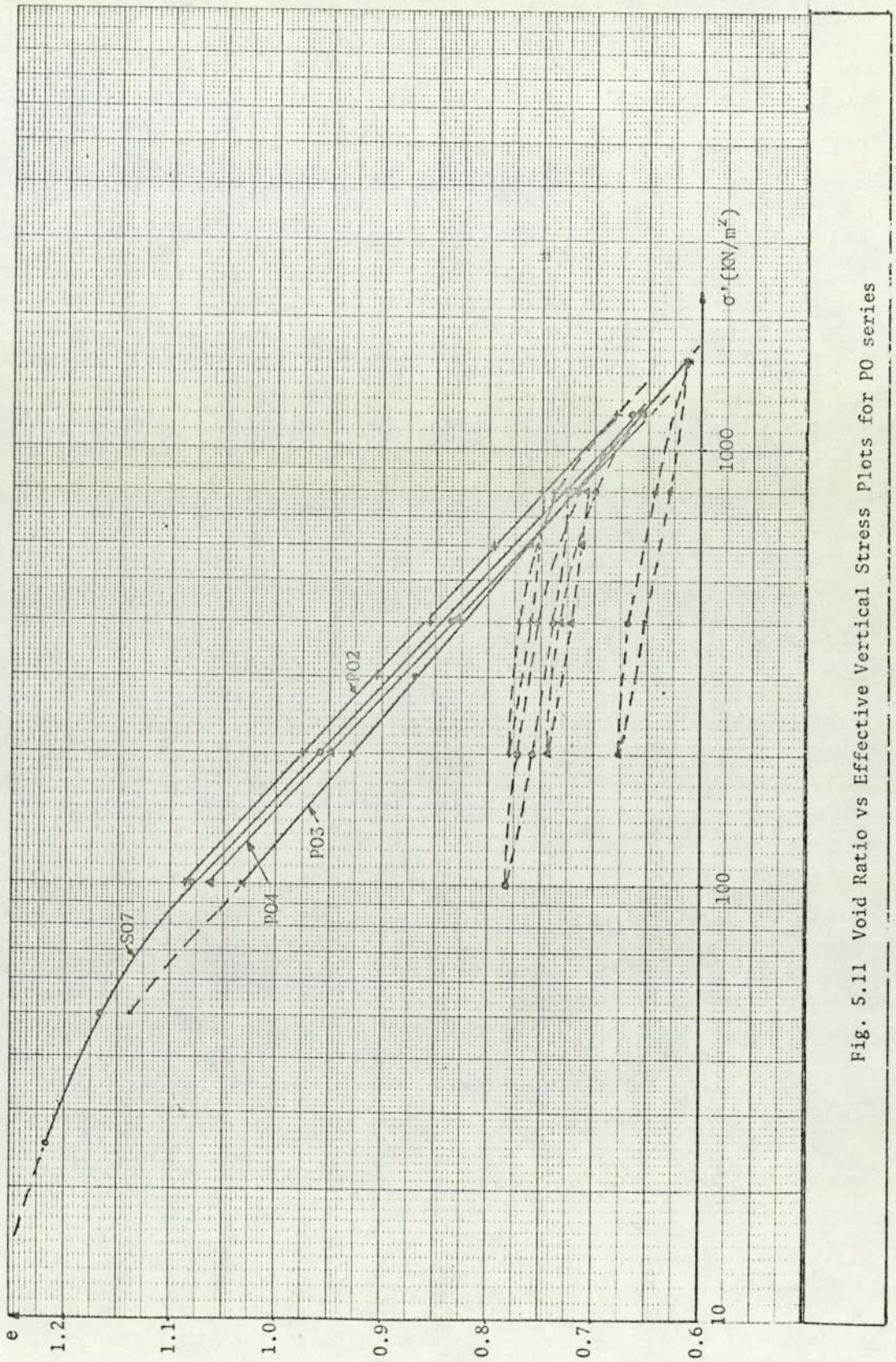

Fig. 5.11 Void Ratio vs Effective Vertical Stress Plots for PO series

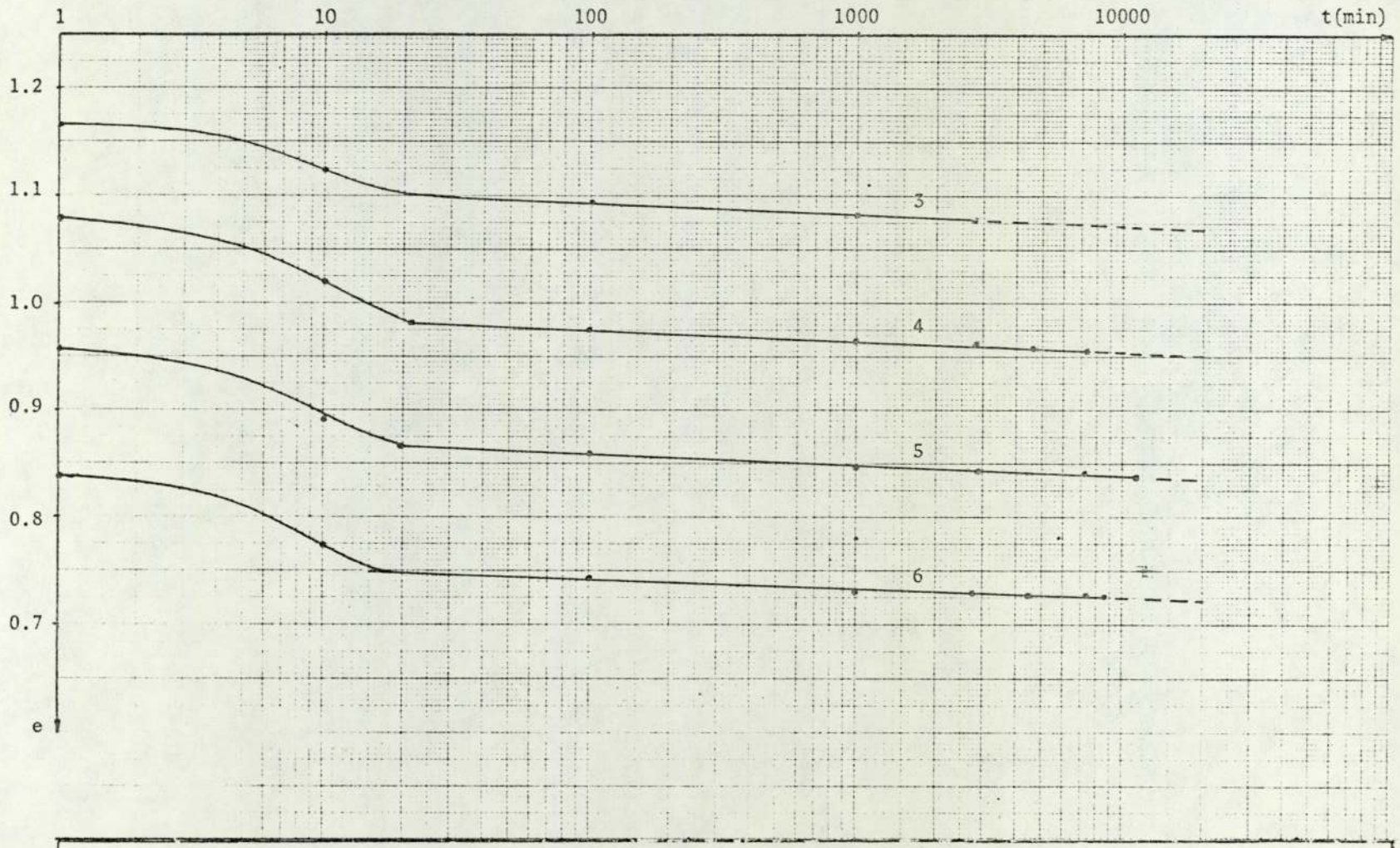

Fig. 5.12 Void Ratio vs log t Curves Test S07

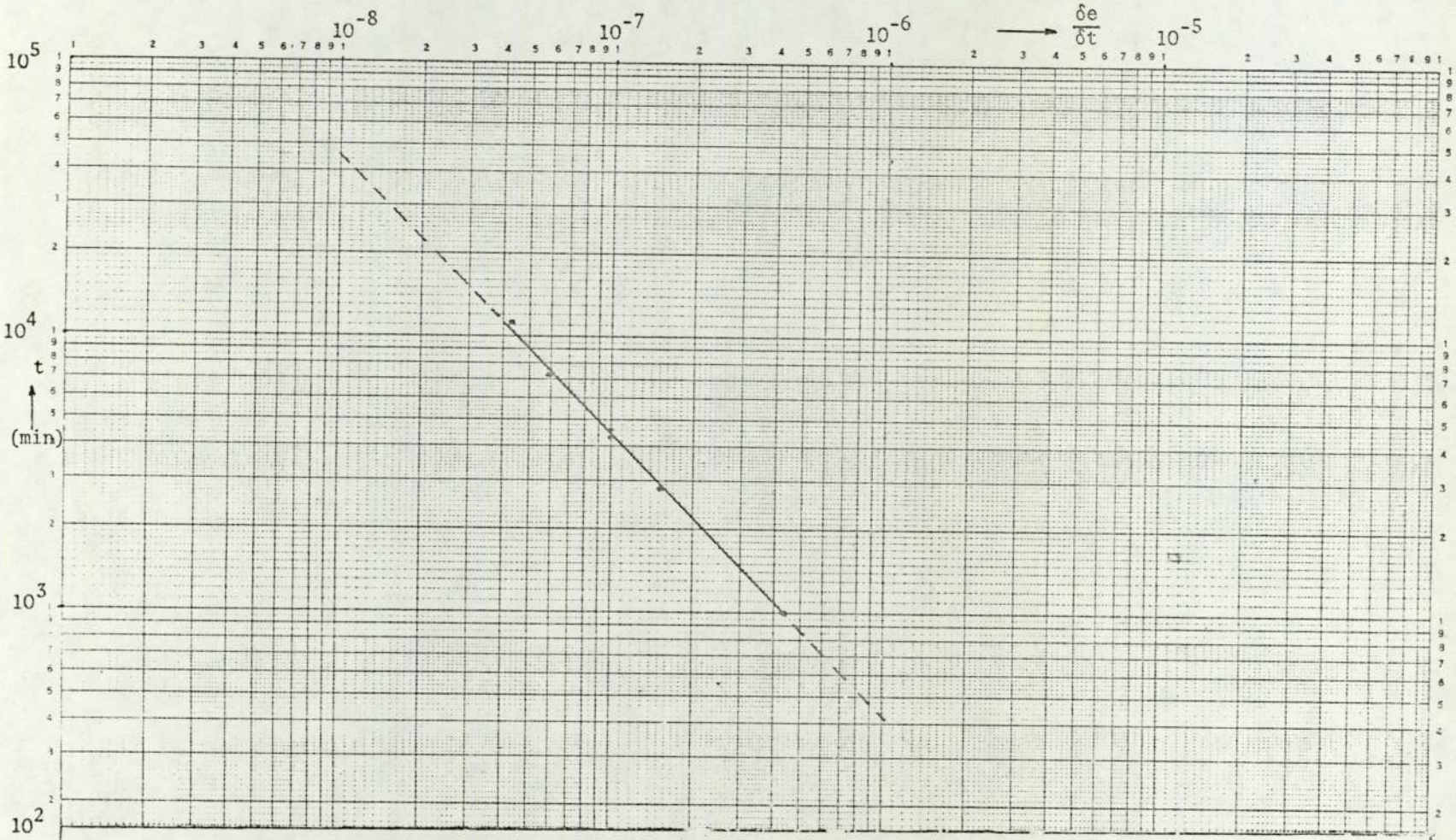

Fig. 5.13 Rate of Consolidation vs Time Test S07

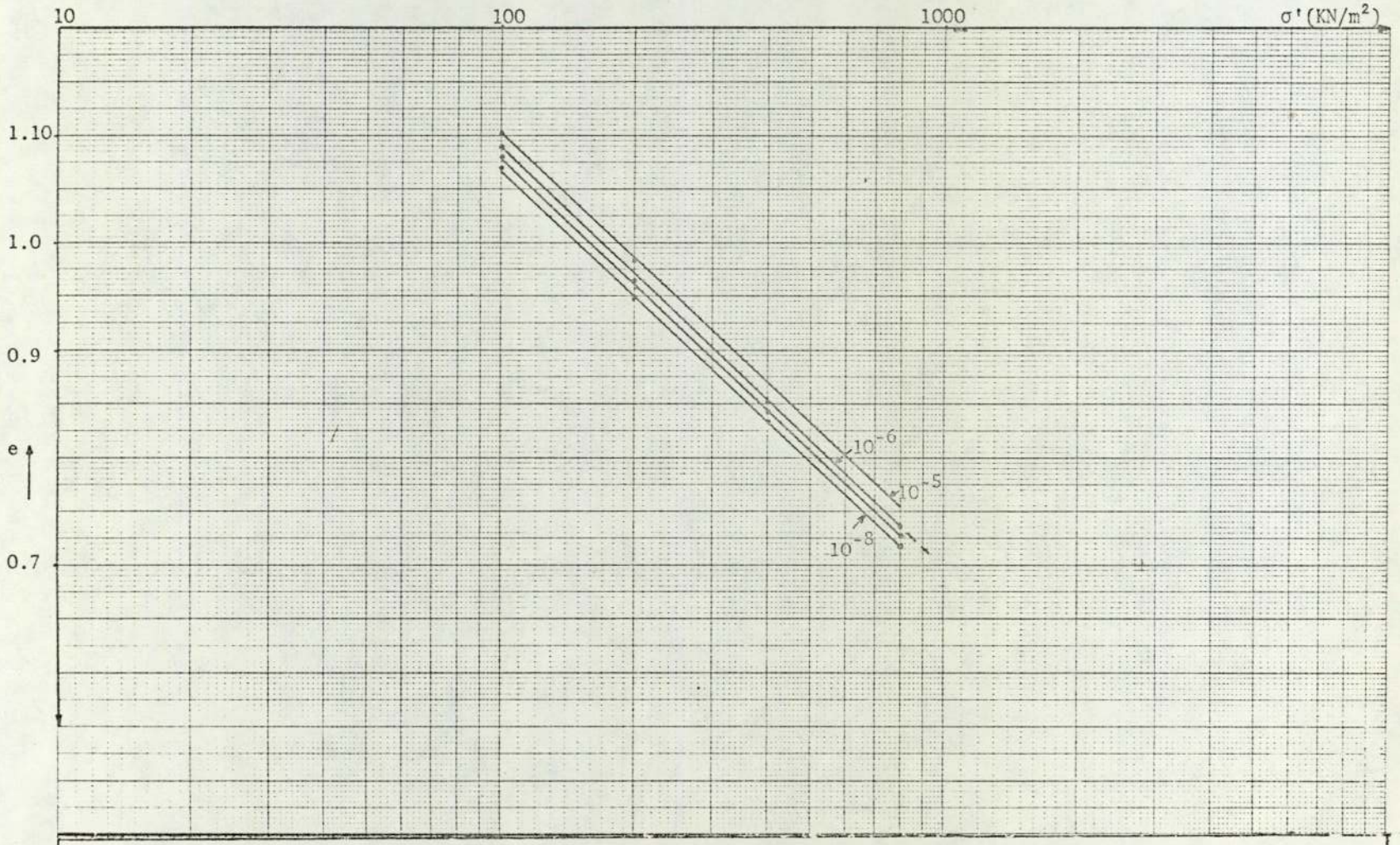

Fig. 5.14 Void Ratio - Effective Stress Lines with Consolidation Rate Parameter .
Test S07

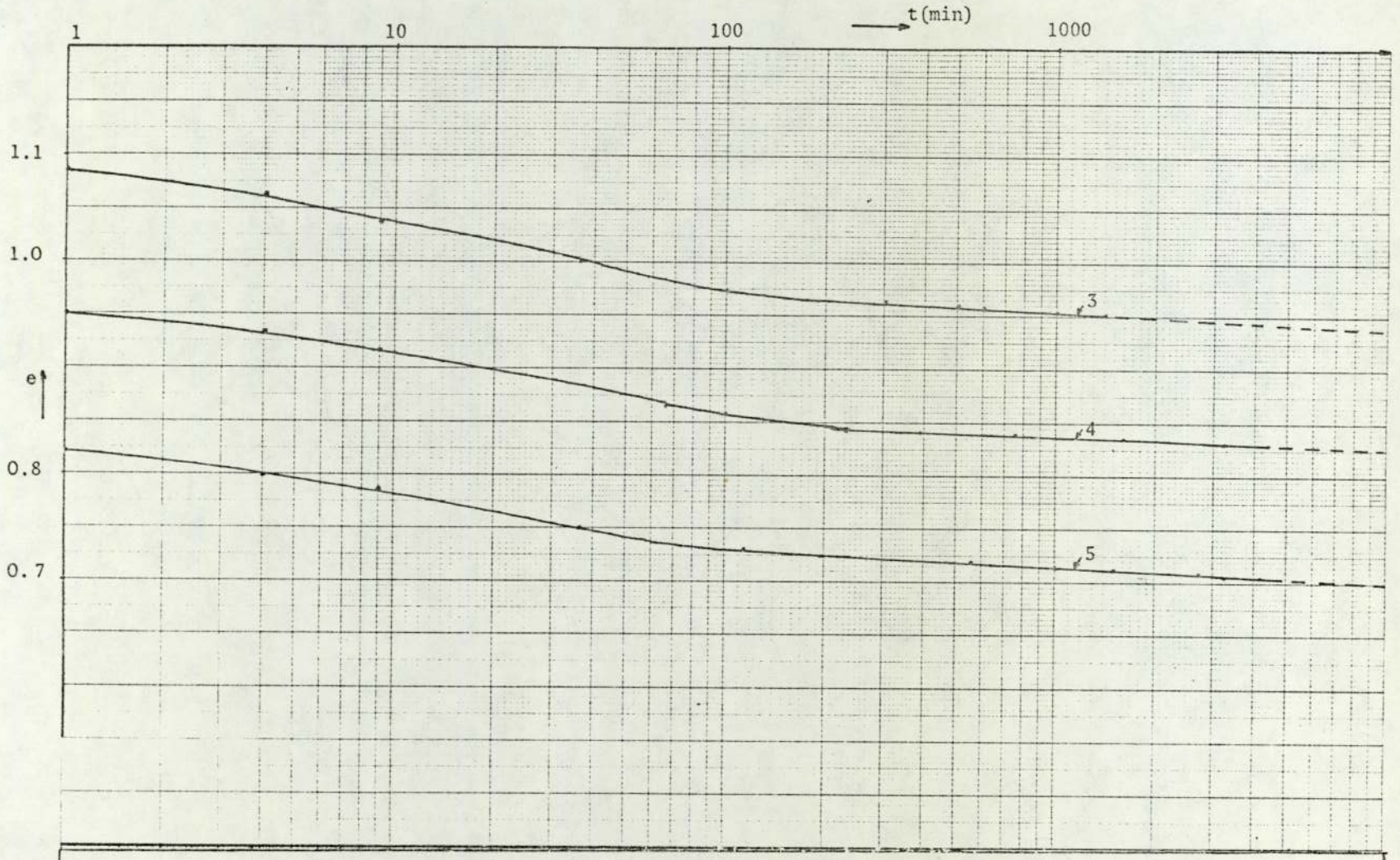

Fig. 5.15 Void Ratio vs log t Curves Test PO4 .

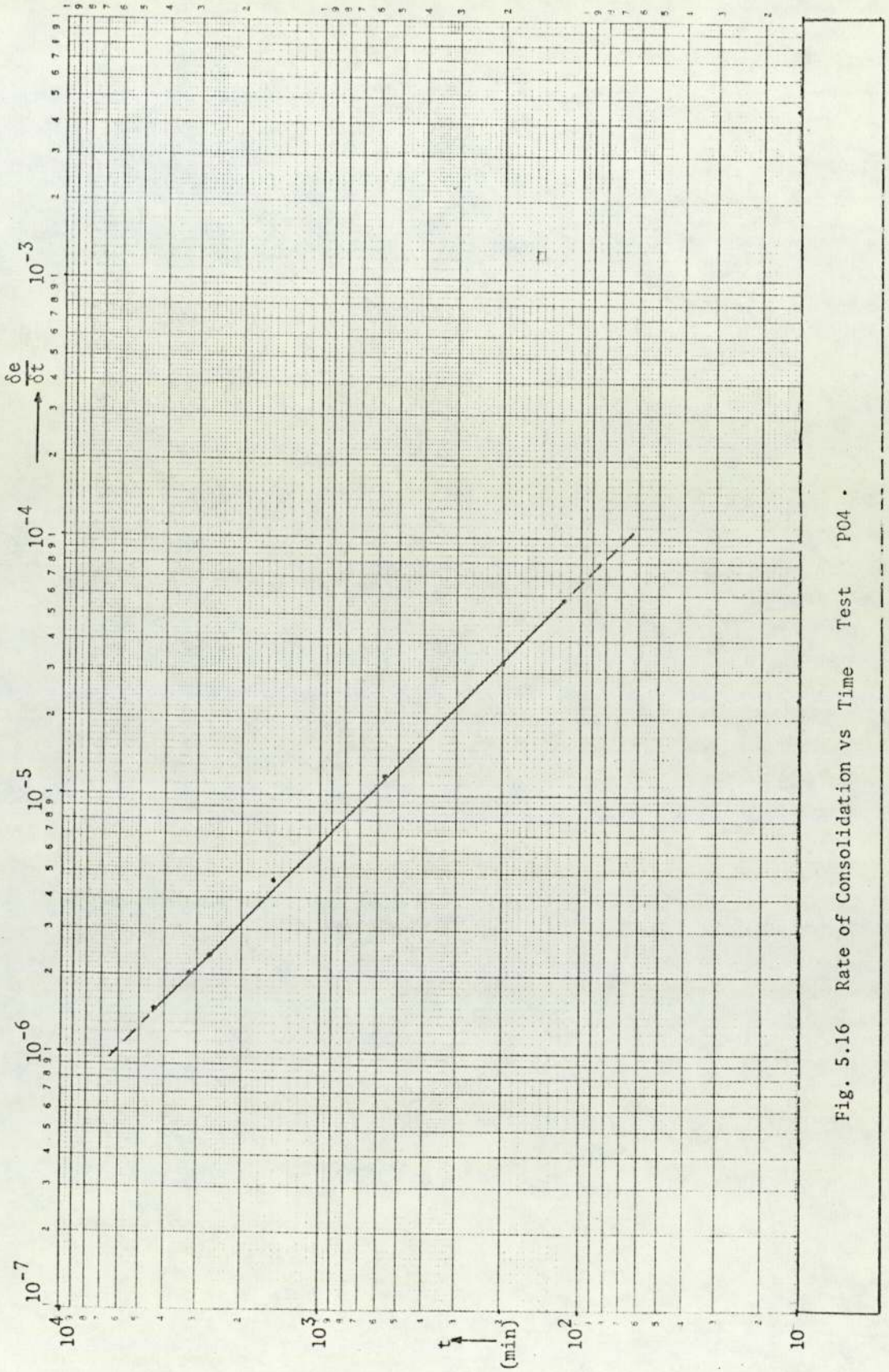

Fig. 5.16 Rate of Consolidation vs Time Test P04 .

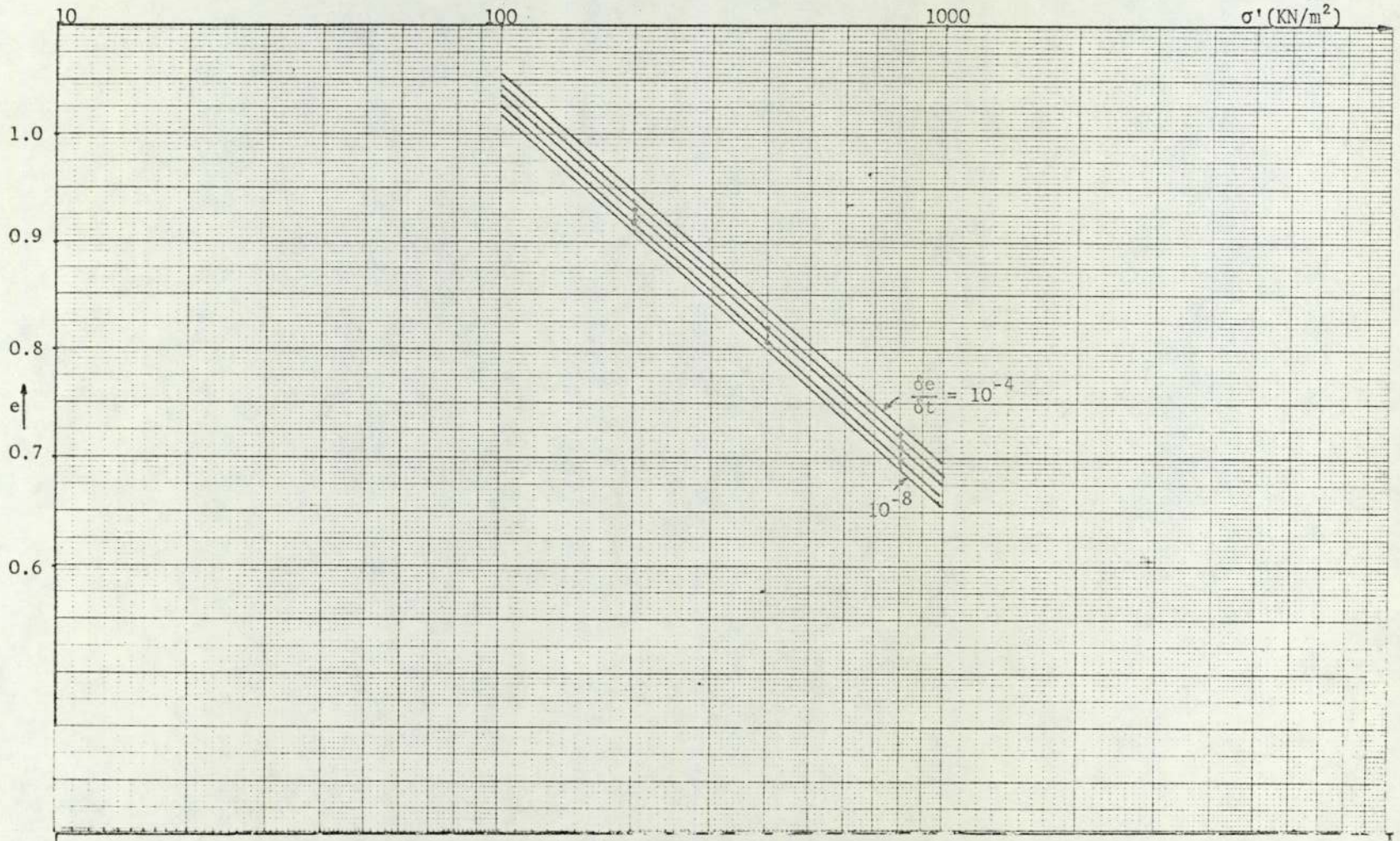

Fig. 5.17 Void Ratio - Effective Stress Lines with Consolidation Rate Parameter Test P04 .

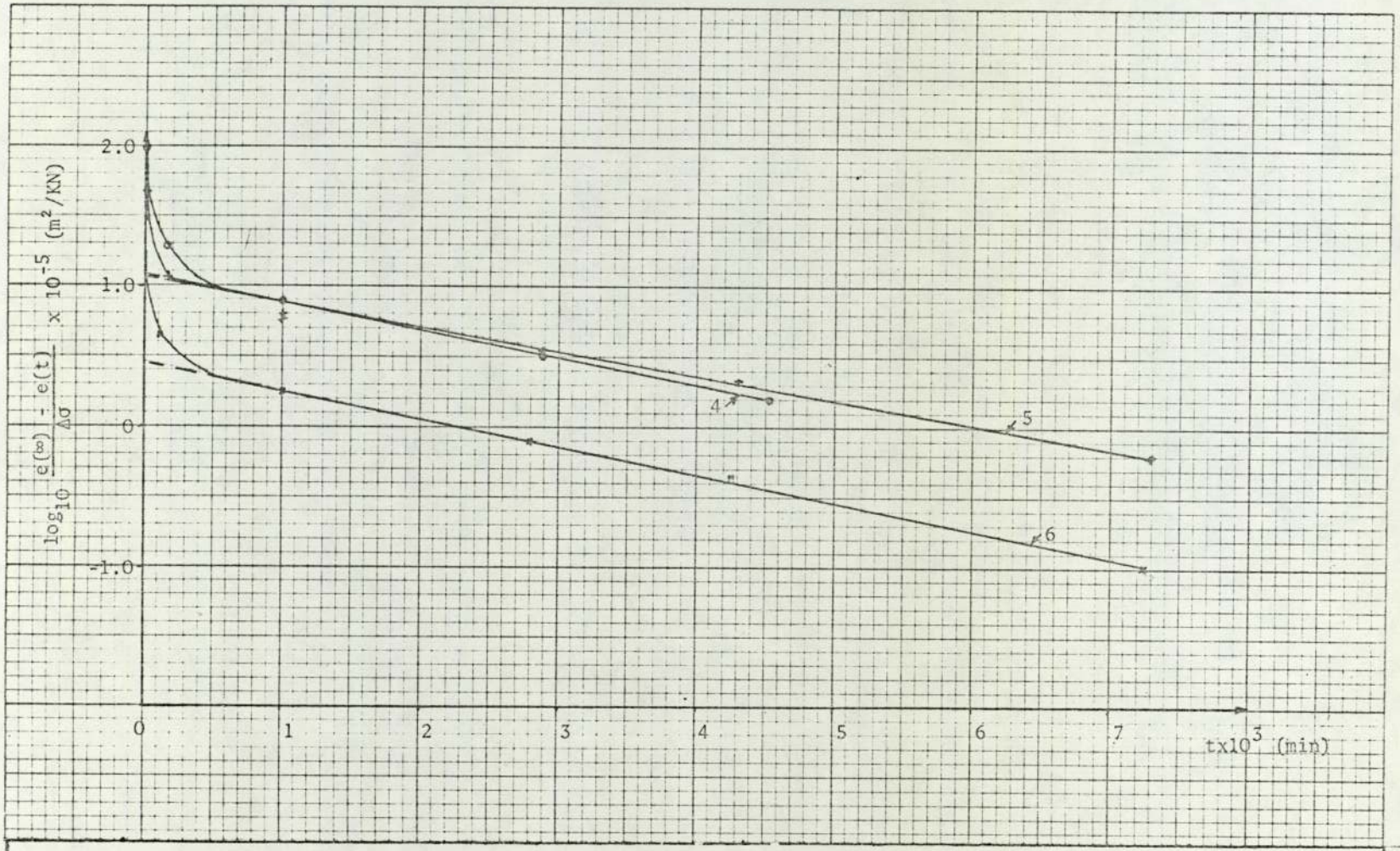

Fig. 5.18 Determination of Soil Parameter Test S07 .

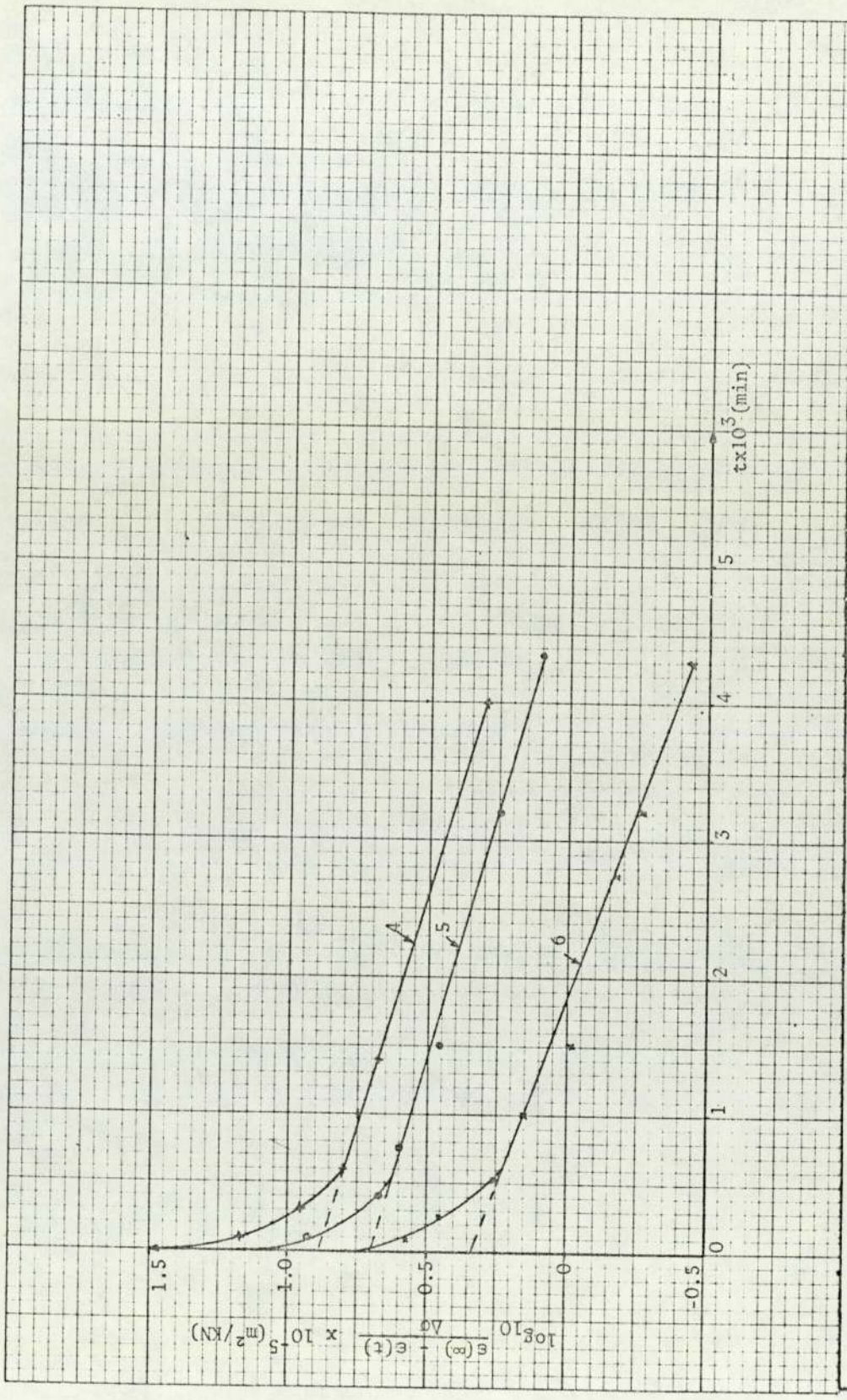

Fig. 5.19 Determination of Soil Parameter Test PO4 .

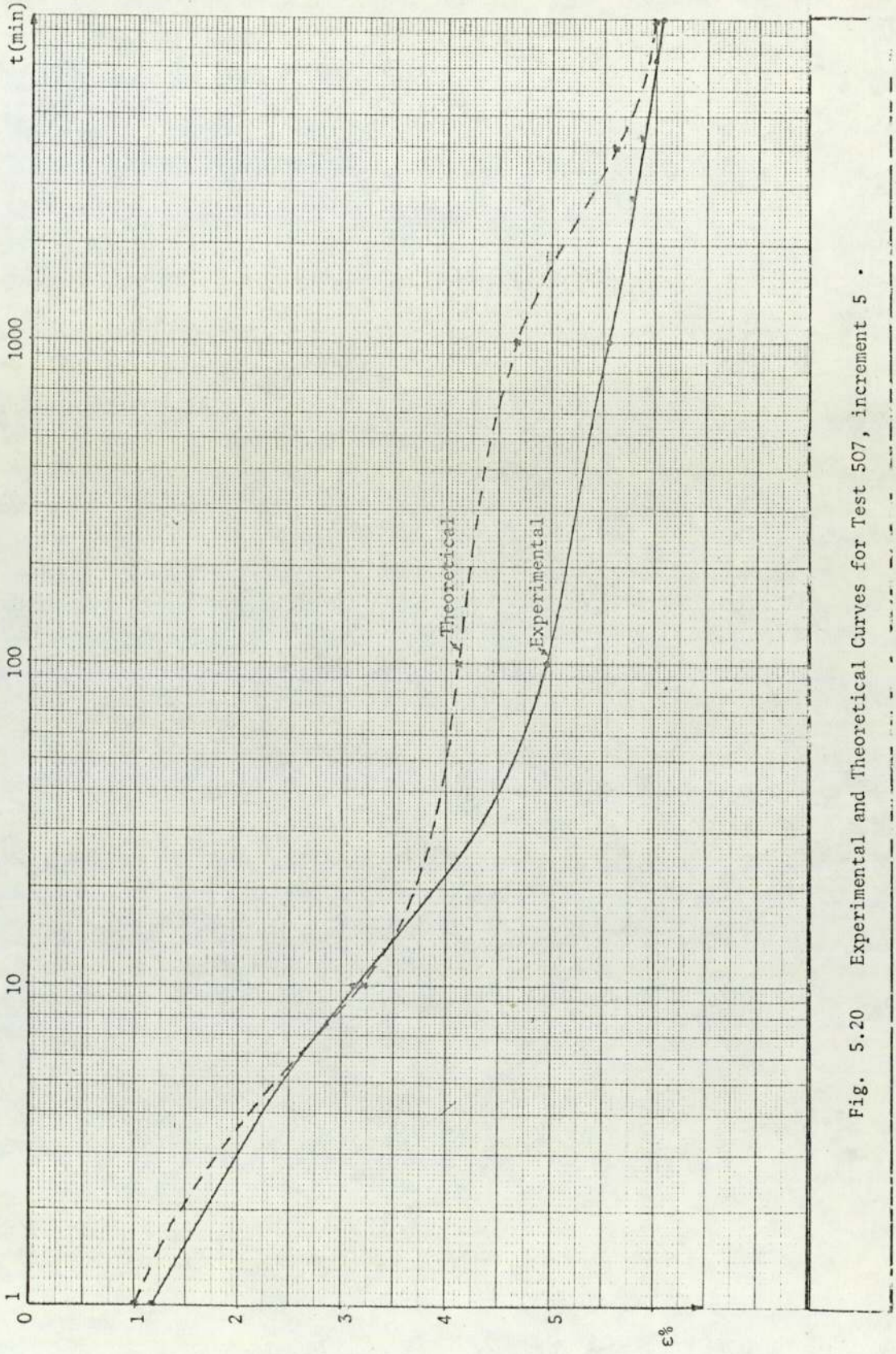

Fig. 5.20 Experimental and Theoretical Curves for Test 507, increment 5 .

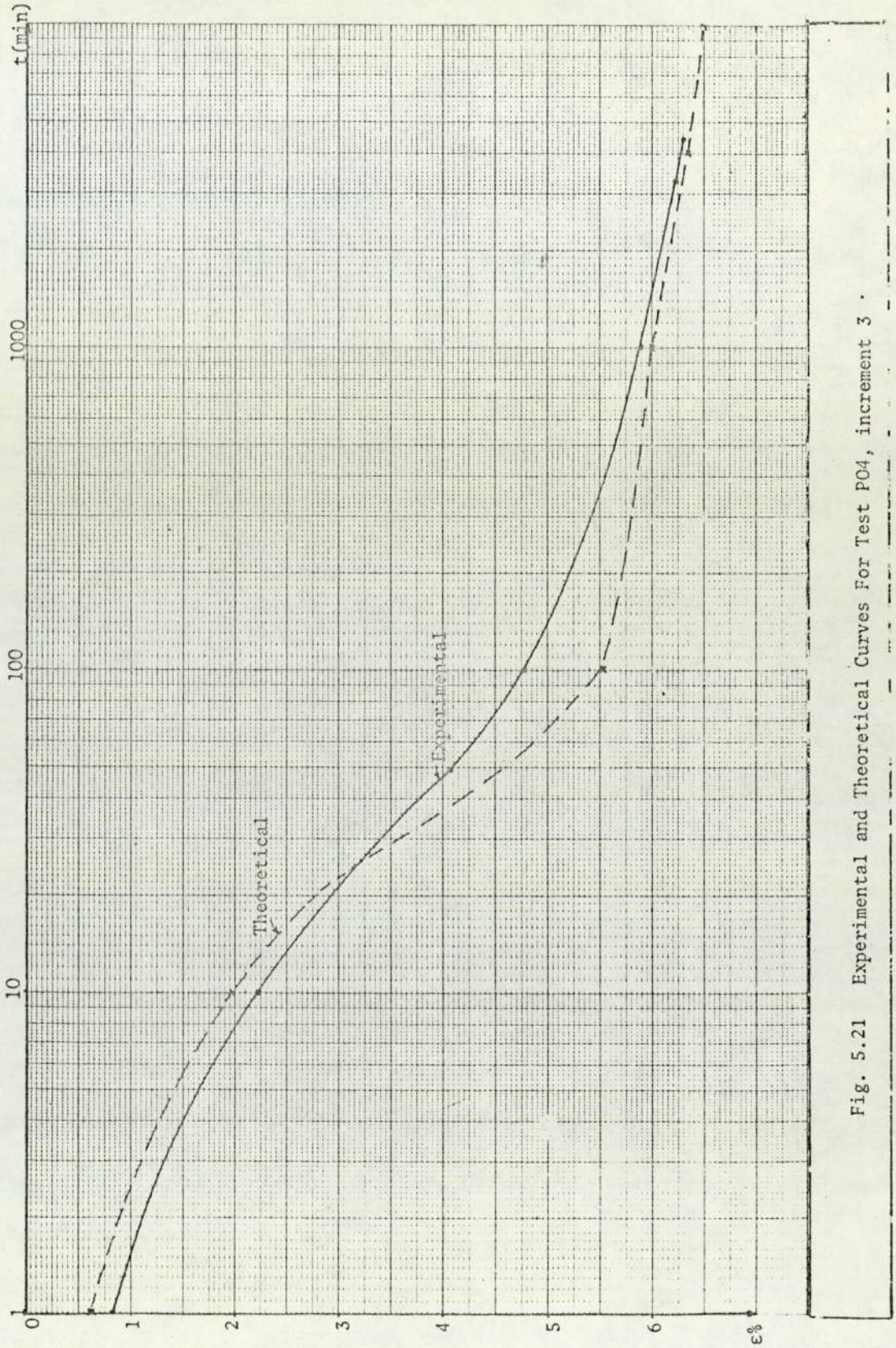

Fig. 5.21 Experimental and Theoretical Curves For Test P04, increment 3 .

5.5 Triaxial Test Results

The triaxial test results presented in this Chapter are grouped under two headings: (a) triaxial consolidation stage (isotropic and anisotropic) and (b) shearing stage. The results are described in accordance with the programme outlined in Chapter 3. Discussion of the results is contained in Chapter 6.

5.6 Triaxial Consolidation Stage

The samples of soil in all triaxial tests were prepared in the tall oedometer from which they were extruded and transferred to triaxial cells (see Chapter 4); the height to diameter ratio H/2R for most of the test specimens was 2. In some of the tests top and bottom lubricated membrane sandwiches were used.

From the analysis of the consolidation stage of the tests, axial and radial coefficients of consolidation were computed; these are denoted $(C_v)_a$ and $(C_v)_r$ respectively. The time to 90% consolidation $(t_a)_{90}$ and $(t_r)_{90}$ were respectively obtained from compression versus square root time curves which were plotted for both the axial deformations and volume changes for each test. For axial drainage the time factor T was taken in accordance with one-dimensional consolidation of the Terzaghi's theory: $(T_a)_{90} = 0.848$ and $(C_v)_a = \frac{TH^2}{t}$. For radial drainage the time factor was taken from the three dimensional theory of consolidation (McKinlay, 1961, Scott, 1963): $(T_r)_{90} = 0.335$ and

$(C_v)_r = \frac{TR^2}{t}$. For comparison purposes the values of the shear strain ratio $\varepsilon_v/\varepsilon_1$ were obtained from the tail ends of the $\varepsilon_v - \varepsilon_1$ plots of the compression curves, i.e. after almost full dissipation of the pore water pressure was achieved. The results are presented for three different consolidation stages : numbers on the curves indicate the stress increment stage as referred to in the tables.

(a) I.C.A. Series

The results of tests in this series (incremental increase of cell pressure) are shown in Figs. 5.22 to 5.24 and the derived data is presented in table 5.4. Fig. 5.25 shows the compression-logarithm of time plots and Fig. 5.26 the pore pressure ratio $\frac{\Delta u}{\Delta p}$ versus time, i.e. pore pressure dissipation curves.

(b) I.C.B. Series

In this series the isotropic consolidation of the soil was taking place under a constant rate of increase of the cell pressure.

The compression-square root time plots are shown in Figs. 5.27 and 5.28 and summary of the results is given in table 5.5.

(c) A.C. Series

The test specimens in this series were anisotropically consolidated with differing $\eta = q/p$ ratio; results are shown in Figs. 5.29 to 5.32 and detailed results are given in table 5.6. In Figs. 5.33 and 5.34 the

volume changes for the same stress increment of $\Delta p = 100$ KN/m^2 from $p_1 = 100$ KN/m^2 to $p_2 = 200$ KN/m^2, from all the tests, are plotted against the logarithm and square root of time.

The void ratio-mean effective stress plots for the ICA and ICB series are shown in Fig. 5.35, and for the AC series in Fig. 5.36.

5.7 Shearing Stage of Triaxial Tests

The results of shearing stages of the triaxial tests are presented under three headings as outlined in Chapter 3.

(a) I.C.D. Series

Four drained tests were carried out in this series and a summary of the results is given in Table 5.7. The specimen in test C.D.13 was consolidated under a constantly increasing cell pressure (see also table 5.5), followed by a drained shearing stage the results of which are shown in Fig. 5.37, where the values of q, ε_v and $\eta = q/p$ are plotted against axial strain ε_1. The results of the other three tests in this series are presented in the same form and are shown in Figs. 5.38 to 5.40 respectively (see also table 5.7). In test C.D.19 lubricated top and bottom membrane sandwiches were used and only side drainage was provided; height to diameter ratio H/2R for this specimen was 1.5. The H/2R ratio for C.D.13 and C.D.15 was 2 and for C.D.17 -1.

(b) C. U Series

In this series the consolidated undrained tests are sub-divided into three groups :

(i) Isotropically consolidated samples in the 'independent stress triaxial cell' were sheared in an undrained manner; the results are shown in Figs. 5.41 to 5.43. Four test results are presented and summarised in table 5.8.

Undrained shear results consist of plots of q, Δu and q/p or $\Delta u/\Delta q$ against the axial strain ε_1. In Fig. 5.44 q is plotted against P for the test in this group, and Δu against $\Delta\sigma_3$ for all tests in the C.U. series.

(ii) Five isotropically consolidated samples in the standard 100mm triaxial cell were sheared and the results are given in table 5.9 and plotted in Figs. 5.45 to 5.49. In this group one short sample was used (C.U.16) for which the ratio of H/2R was 1; for all other samples this ratio was approximately 2.

The specimen in test C.U.11 was sheared in two stages, firstly under σ'_3 = 100 KN/m^2 and then it was consolidated to a higher stress (σ'_3 = 300 KN/m^2) and sheared to failure.

(iii) This group consisted of five anisotropically consolidated samples (in the stress-controlled triaxial cell) which were sheared in an undrained manner; sample ACU14 was an exception because the cell developed a leak. A summary of the results is given in table 5.10 and plots of q, Δu and q/p or $\Delta u/\Delta q$ versus axial strain ε_1 are shown in Figs. 5.50 to 5.53.

(C) I.C.P. Series

In this series two isotropically consolidated samples were sheared under constant mean effective stress P (in a drained manner). The specimen in test C.P.18 failed prematurely. The results of both tests are given in table 5.11 and plotted in Fig. 5.54.

(d) The overall results for I.C.D., I.C.U. and A.C.U. series are shown in Fig. 5.55, Fig. 5.56 and 5.57 respectively.

Test No.	Drainage	H mm	R mm	Increment No.	P KN/m^2	$\frac{\Delta P}{P}$	t(min)		$cm^2/sec \times 10^{-4}$		C_c	$\frac{\varepsilon_v}{\varepsilon_1}$
							$(ta)_{90}$	$(tv)_{90}$	C_a	C_r		
C.V.8	Top & Side	140.0 138.0 136.64	35.0 34.90 34.75	1 2 3	50 150 300	- 2 1	156 1521 1764	196 1444 1444	- 17.67 14.82	- 0.467 0.417	- 0.276 0.286	- 3.28 3.21
C.V.9	"	128.5 127.69 126.35	35.0 34.30 33.70	1 2 3	50 100 200	 1 1	 841 961	 625 900	 27.40 23.48	 1.05 0.70	 0.266 0.302	 5.70 3.20
C.V.16	"	 64.0 63.44	 33.84 32.87	1 2 3	50 100 150	- 1 0.5	 1089 798	 841 798	 5.32 7.13	 0.70 0.76	 0.352 0.392	 5.0 3.8
C.V.19	Side	106.5 105.32	34.17 32.50	1 2	50 200	- 3	266 961	266 1024	60.2 16.31	2.45 0.576	- 0.419	8.0 4.77

Table 5.4 I.C.A. Series

Test No.	Drainage	H mm	R mm	Increment No.	P KN/m^2	$\frac{\Delta P}{P}$	t(min)		$cm^2/sec \times 10^{-4}$		C_c	$\frac{\varepsilon_v}{\varepsilon_1}$
							$(ta)_{90}$	$(tv)_{90}$	C_a	C_r		
C.D.13	Top & Side	132.90 131.05	33.93 33.23	1 2 3	50 100 200	1 1	2116 4225	1806 4226	11.80 4.65	0.36 0.146	0.340 0.333	3.58 3.11
C.P.20	"	128.62 126.42	34.32 33.29	1 2 3	50 100 200	1 1	6400 4422	6400 4422	3.65 5.11	0.103 0.140	0.371 0.400	4.52 3.99

Table 5.5 I.C.B. Series

Test No.	Drainage	H mm	R mm	Increment No.	P KN/m^2	$\eta = q/P$	$\frac{\Delta P}{P}$	t(min)		$cm^2/sec \times 10^{-4}$		C_c	$\frac{\varepsilon_v}{\varepsilon_1}$
								$(ta)_{90}$	$(tv)_{90}$	C_a	C_r		
	Top			1	50	-	-	-	-	-	-	-	3.45
A.C.U.	&	127.50	34.40	2	200	0.3	3	1296	1296	17.73	0.509	0.382	1.91
10	Side	123.94	33.90	3	300		0.5	3025	3249	7.18	0.197	0.340	1.73
				1	60	-	-	-	-	-	-	-	1.74
A.C.U.	"	131.31	34.50	2	120	0.5	1	4489	3721	5.43	0.178	0.378	1.36
12		125.88	34.20	3	240		1	5625	5476	3.98	0.119	0.342	1.29
		120.58	34.05	4	360		0.5	5625	5625	3.65	0.115	0.290	1.23
				1	50	-	-	-	-	-	-	-	-
A.C.U.	"	135.10	34.73	2	100	0.6	1	1369	1369	18.84	0.49	0.352	1.23
21		128.91	34.52	3	200		1	3135	3135	7.49	0.212	0.375	1.18
		123.71	34.40	4	300		0.5	3481	3481	6.21	0.190	0.352	1.07
				1	50	0.8	-	-	-	-	-	-	-
A.C.U.	"	123.83	34.95	2	100		1	3025	3025	7.16	0.225	0.345	1.048
22		116.27	35.04	3	200		1	3844	4096	4.97	0.167	0.379	0.833

Table 5.6 A.C. Series

Test No.	Consolidation Stress P_o KN/m^2	P_f KN/m^2	q_f KN/m^2	q/P	$\frac{\sigma'}{\sigma'_3}$	ε_1%	ε_v%	$\frac{\varepsilon_v}{\varepsilon_1}$
C.D. 13	200	278.28	264.85	0.950	2.33	14.2	4.91	0.346
C.D. 15	100	151.46	151.38	1.006	2.514	14.25	5.38	0.377
C.D. 17	150	227.34	232.01	1.02	2.547	14.0	6.44	0.46
C.D. 19	200	295.36	286.09	0.969	2.431	15.28	5.41	0.354

Table 5.7 I.C.D. Series

Test No.	Consolidation Stress P_o KN/m^2	P_f KN/m^2	q_f KN/m^2	q/P	$\frac{\sigma'_1}{\sigma'_3}$	A_f	$\varepsilon_1\%$
C.U.2	264	327	367	1.122	2.80	0.450	1.0
C.U.3	245	195	212	1.087	2.71	0.568	2.50
C.U.4	294	239	239	1.00	2.50	0.565	1.16
C.U.6	300	219	227	1.036	2.58	0.74	1.79

Table 5.8 I.C.U. Series (independent stress triaxial cell)

Test No.	Consolidation Stress P_o KN/m^2	P_f KN/m^2	q_f KN/m^2	q/P	$\frac{\sigma'_1}{\sigma'_3}$	A_f	$\varepsilon_1\%$
C.U.7	282	190.50	193.50	1.016	2.54	0.78	3.86
C.U.8	300	194.50	201.12	1.034	2.58	0.828	3.64
C.U.9	200	143.18	148.30	1.036	2.58	0.716	3.0
C.U.(1 11 (2	100 300	73.7 200.0	74.49 196.41	1.01 0.982	2.52 2.46	0.69 0.85	3.0 4.68
C.U. 16	150	95.75	110.75	1.157	2.88	0.81	6.20

Table 5.9 I.C.U. Series

Test No.	Consolidation Stress P_o KN/m²	P KN/m²	q KN/m²	q/P	$\frac{\sigma'_1}{\sigma'_3}$	A_f	ε_1%	$(\frac{\varepsilon_v}{\varepsilon_1})$
A.C.U.10	300	-	90	0.3	1.33	-	-	1.73
	-	292	150	0.514	1.620	0.243	0.928	-
	-	232	150	0.647	1.82	1.17	0.733	-
		231.63	179.2	0.774	2.04	0.78	1.14	-
Failure		223.75	210.74	0.942	2.37	0.71	1.30	-
		207.54	208.75	1.006	2.51	0.79	5.93	
A.C.U.12	360	-	180	0.50	1.60	-	-	1.23
		329.53	285.14	0.865	2.22	0.770	1.16	-
Failure		311.55	287.59	0.923	2.33	0.962	1.95	-
A.C.U.14	200	-	116	0.582	1.72	-	-	1.12
A.C.U.21	300	-	180	0.6	1.67	-	-	1.07
	-	295.30	236.11	0.800	2.09	0.431	0.278	-
Failure	-	255.83	242.76	0.949	2.39	1.069	2.61	-
		244.48	245.34	1.004	2.51	1.21	4.22	
A.C.U.22	200	-	160	0.8	2.09	-	-	0.833
		198.56	182.63	0.920	2.33	0.400	0.107	-
Failure	-	184.13	182.41	0.991	2.48	1.043	1.07	-

Table 5.10 A.C.U. Series

Test No.	Consolidation Stress σ'_3 KN/m^2	P KN/m^2	q KN/m^2	q/P	$\frac{\sigma'}{\sigma'_3}$	ε_1%	ε_v%	$(\frac{\varepsilon_v}{\varepsilon_1})$ *
C.P.18	100	100	0	0	1.0			4
	-	102.03	30.73	0.301	1.335	0.49	0.224	1.11
	-	103.97	44.37	0.427	1.50	1.14	0.669	0.91
		104.4	62.47	0.60	1.75	1.78	1.04	0.584
C.P.20	200	200	0	0	1.0	-	-	3.99
	-	200.7	62.08	0.309	1.35	1.3	0.73	1.04
	-	202.03	104.62	0.518	1.626	2.57	1.36	0.76
	-	199.91	124.0	0.62	1.78	3.23	1.65	0.59
Failure	-	195.29	196.36	1.006	2.51	8.23	2.10	0.255

* Values of $\varepsilon_v/\varepsilon_1$ are taken when the sample has been left under certain value of q for some time as it is evident from q - ε_1 plot

Table 5.11 I.C.P. Series

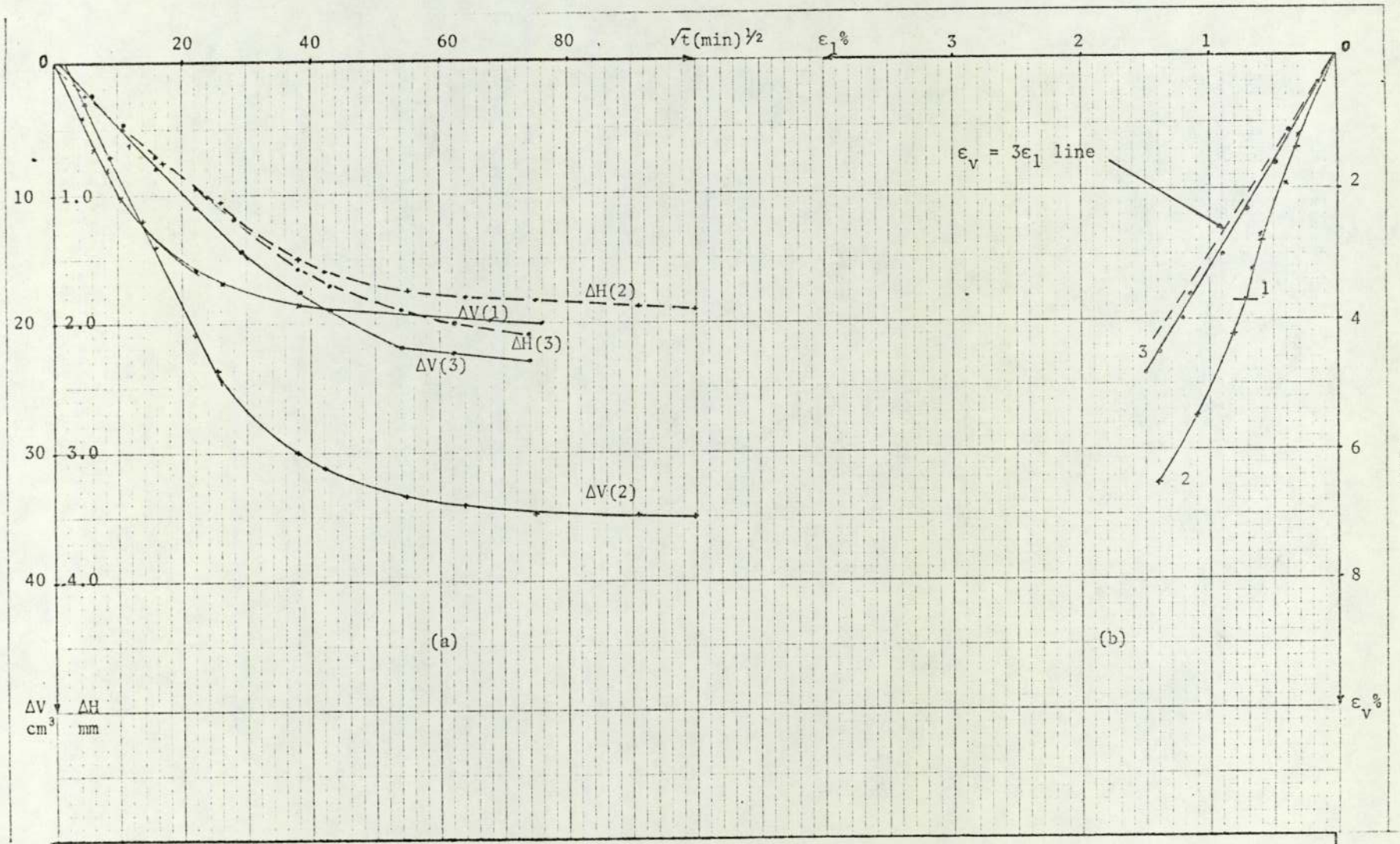

Fig.5.22 (a) Consolidation Curves for Test C.D.8 (See Table 5.4 for further details),(b) Strain path ε_v vs ε_1

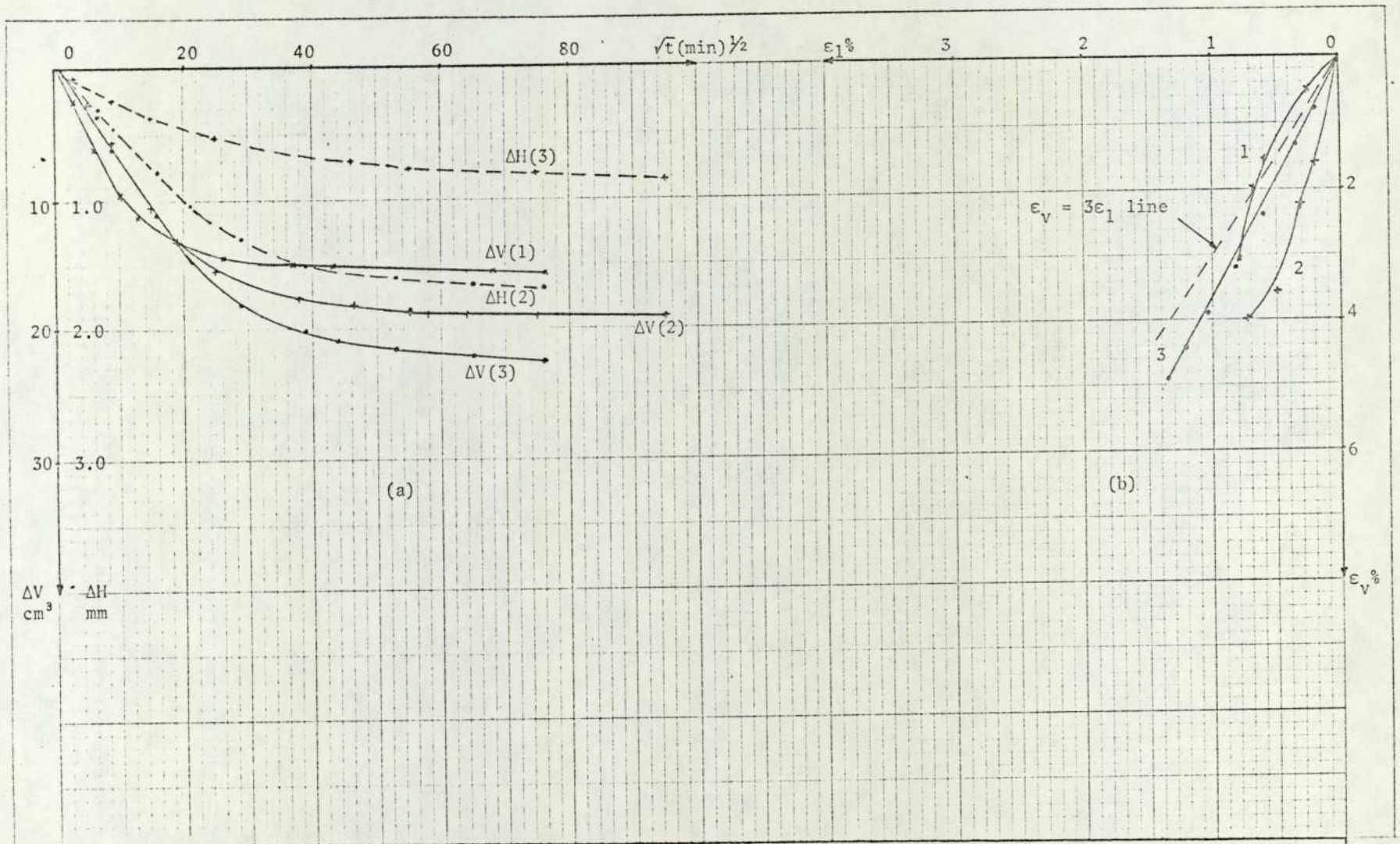

Fig. 5.23(a) Consolidation curves for test C.U.9 (see Table 5.4 for further details) (b) Strain path ε_v vs ε_1

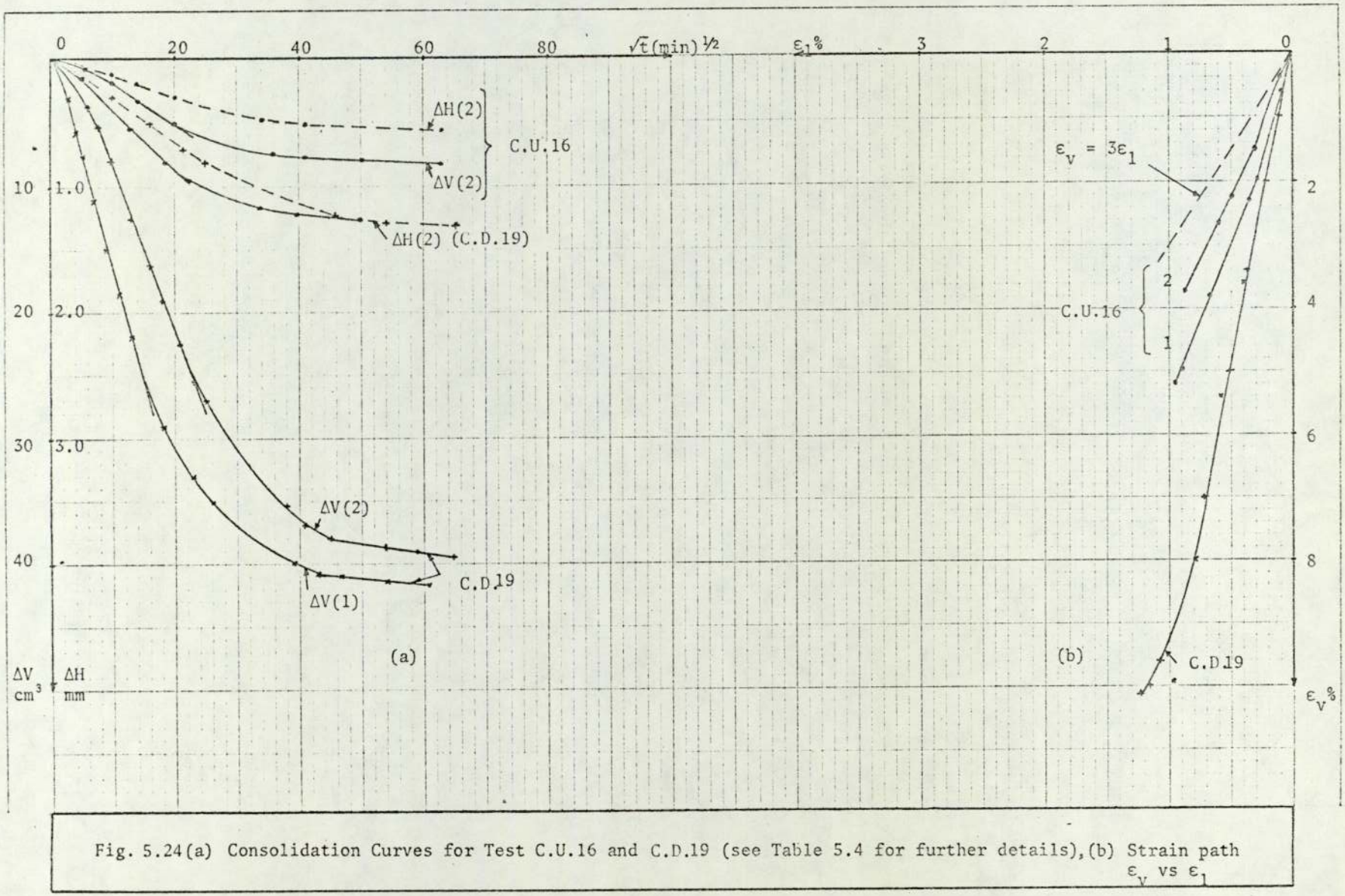

Fig. 5.24(a) Consolidation Curves for Test C.U.16 and C.D.19 (see Table 5.4 for further details), (b) Strain path ε_v vs ε_1

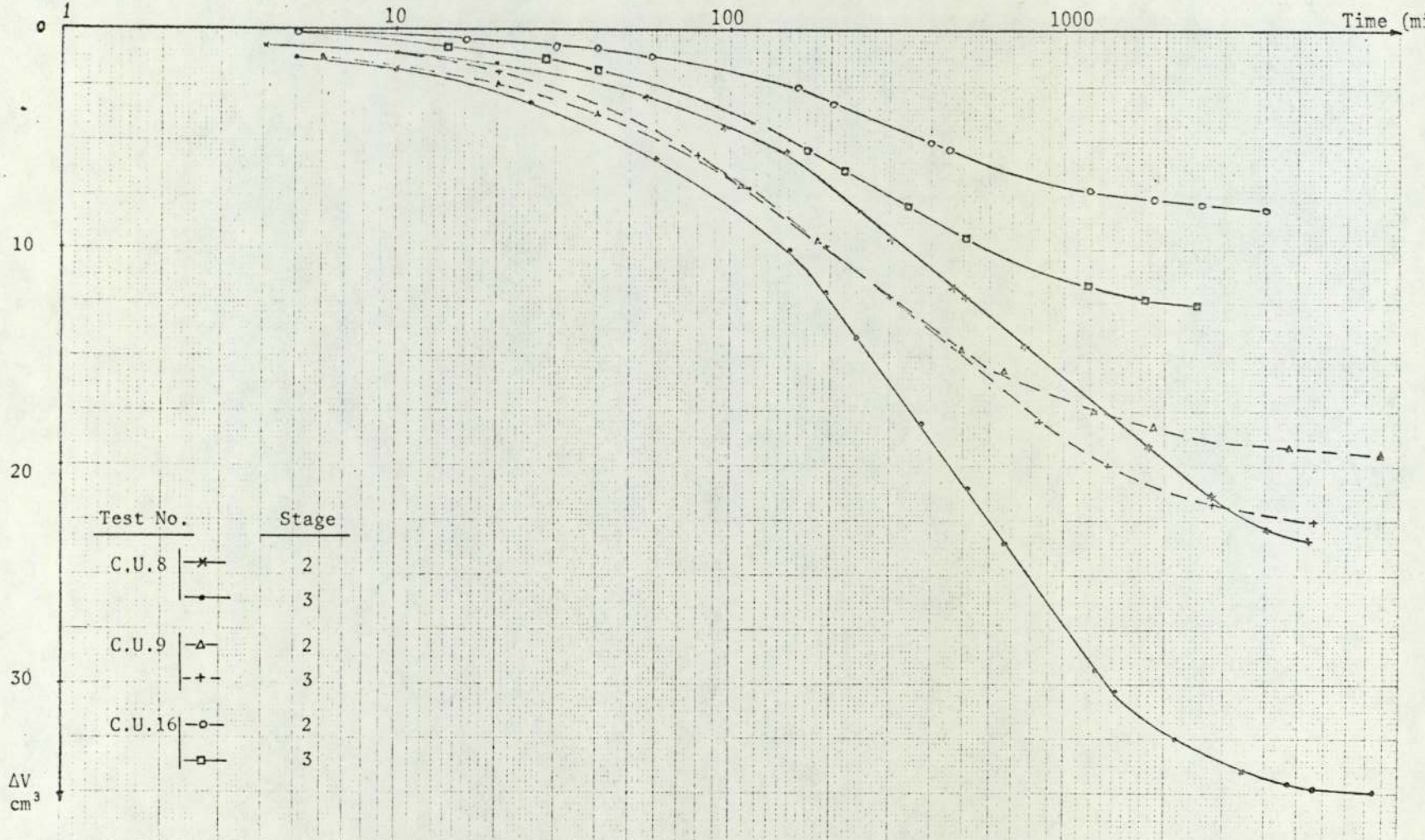

Fig. 5.2 5 Compression-logarithm time plots for I.C.A. & I.C.B. Series (See Tables 5.4 and 5.5)

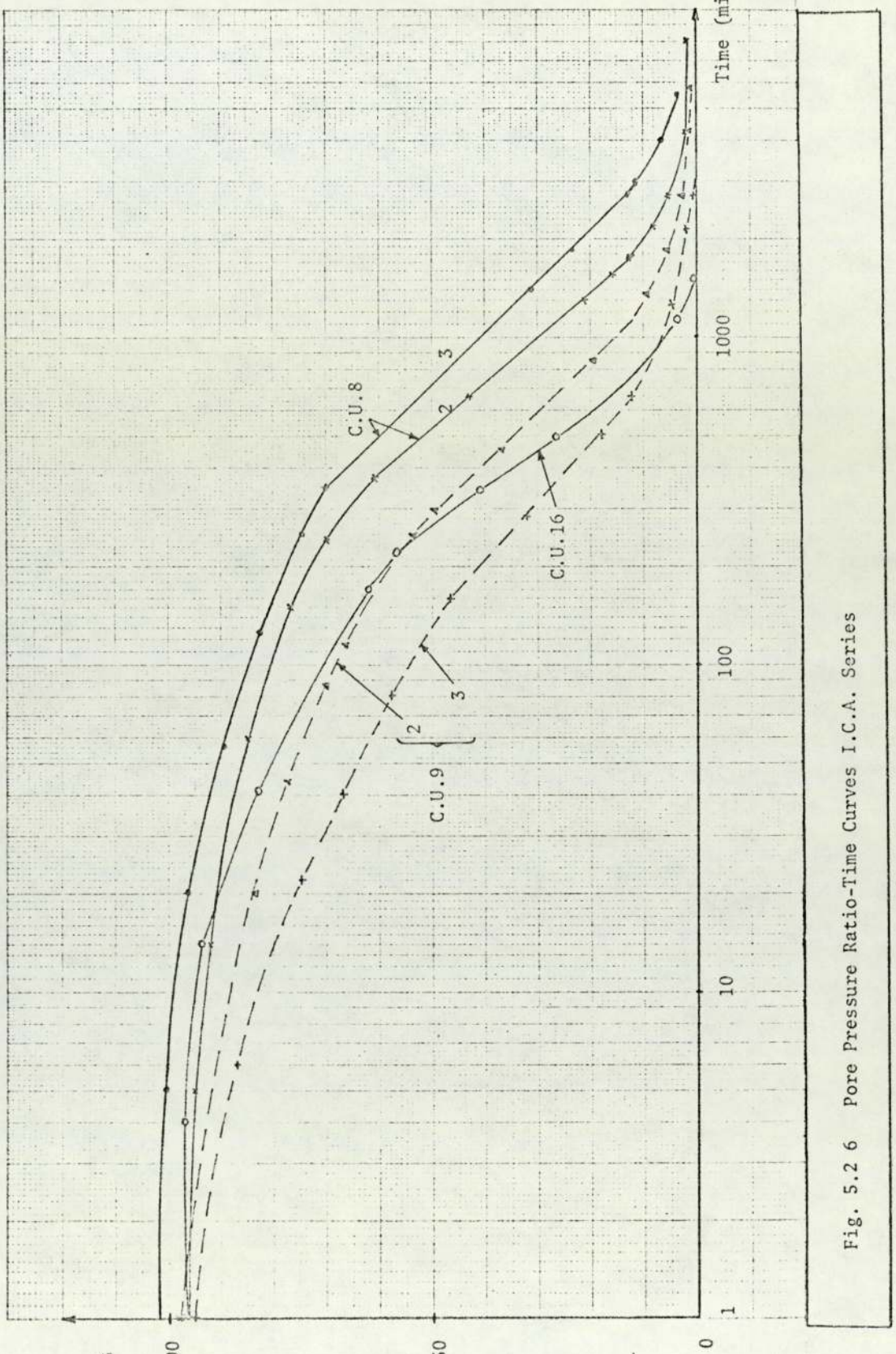

Fig. 5.2 6 Pore Pressure Ratio-Time Curves I.C.A. Series

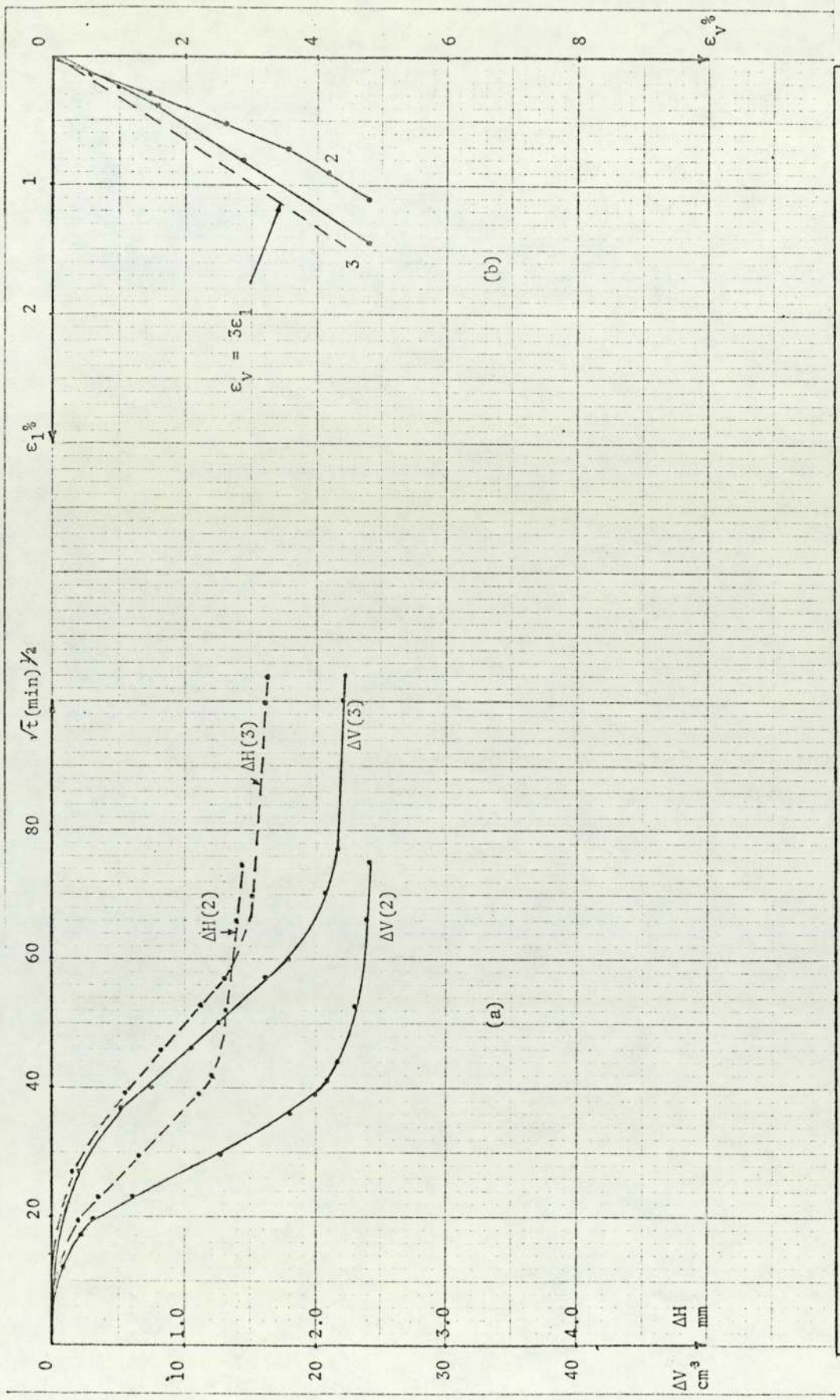

Fig.5.27(a) Consolidation Curves Test C.D.13 (See Table 5.5 for further details), (b) Strain path ε_v vs ε_1

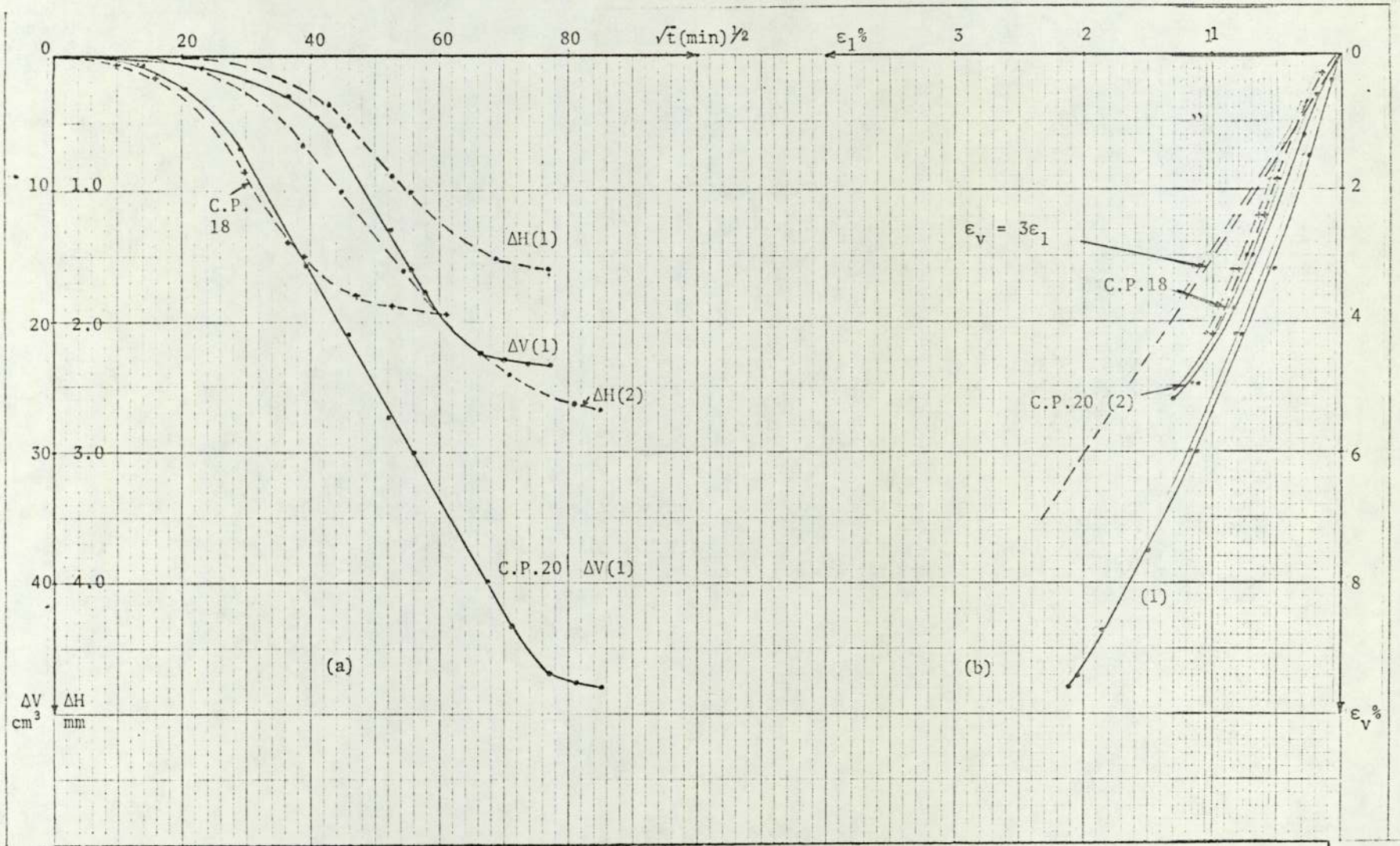

Fig.5.28(a) Consolidation Curves Test C.P.18 & C.P.20 (see Table 5.5 for further details), (b) Strain path ε_v vs ε_1

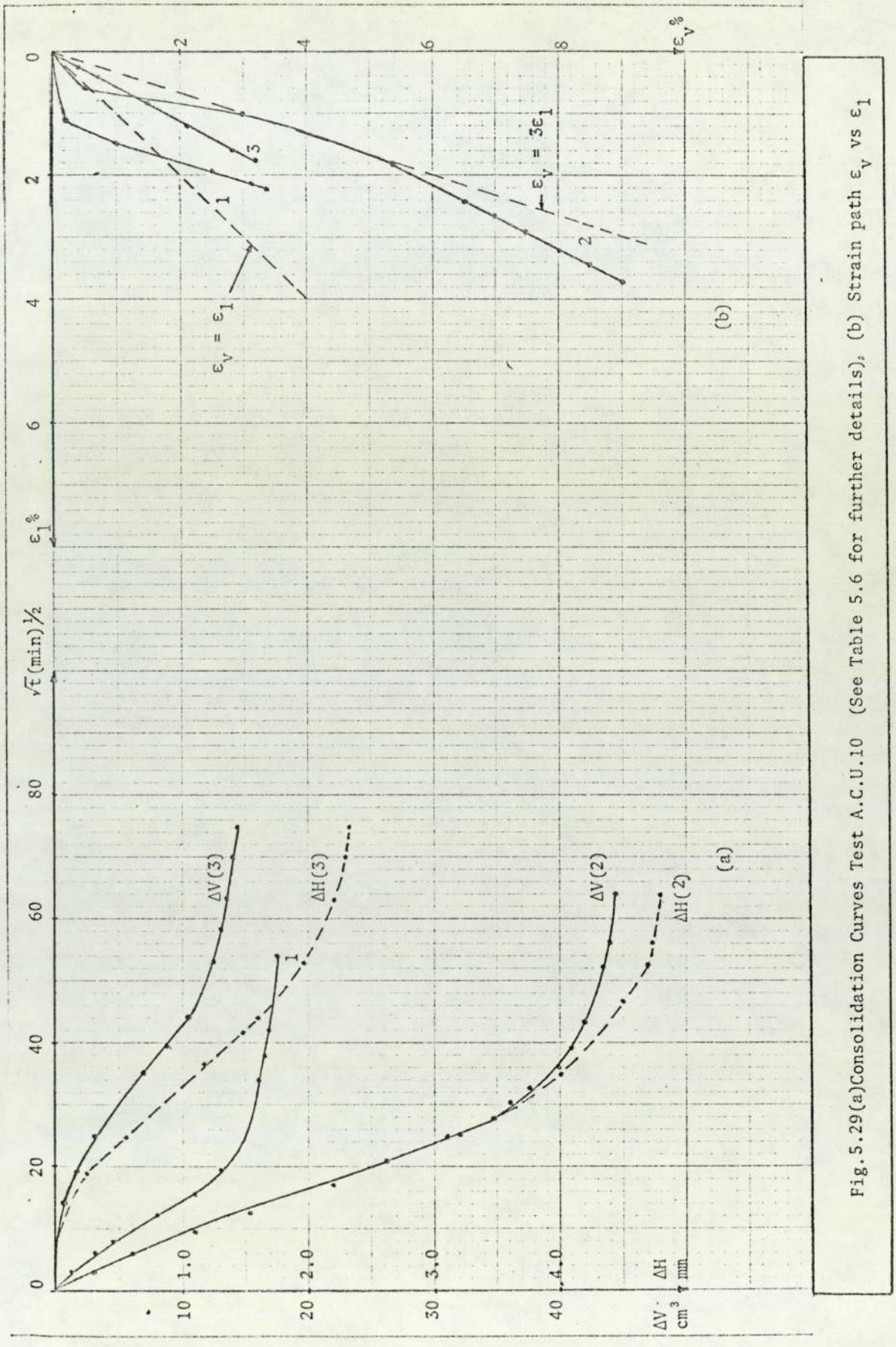

Fig. 5.29(a) Consolidation Curves Test A.C.U.10 (See Table 5.6 for further details), (b) Strain path ε_v vs ε_1

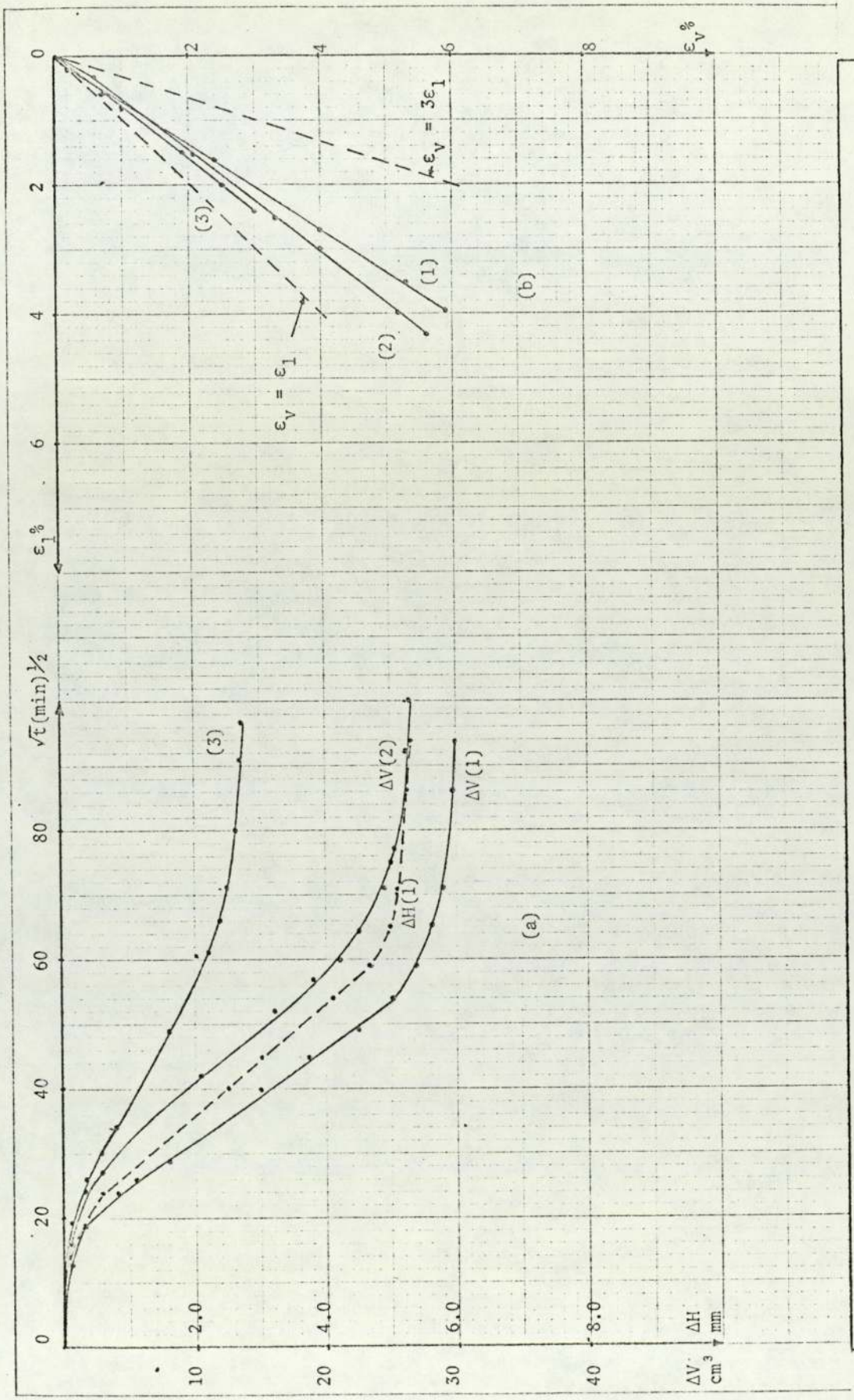

Fig.5.30(a) Consolidation Curves Test A.C.U.12 (See Table 5.6 for further details), (b) Strain path ε_v vs ε_1

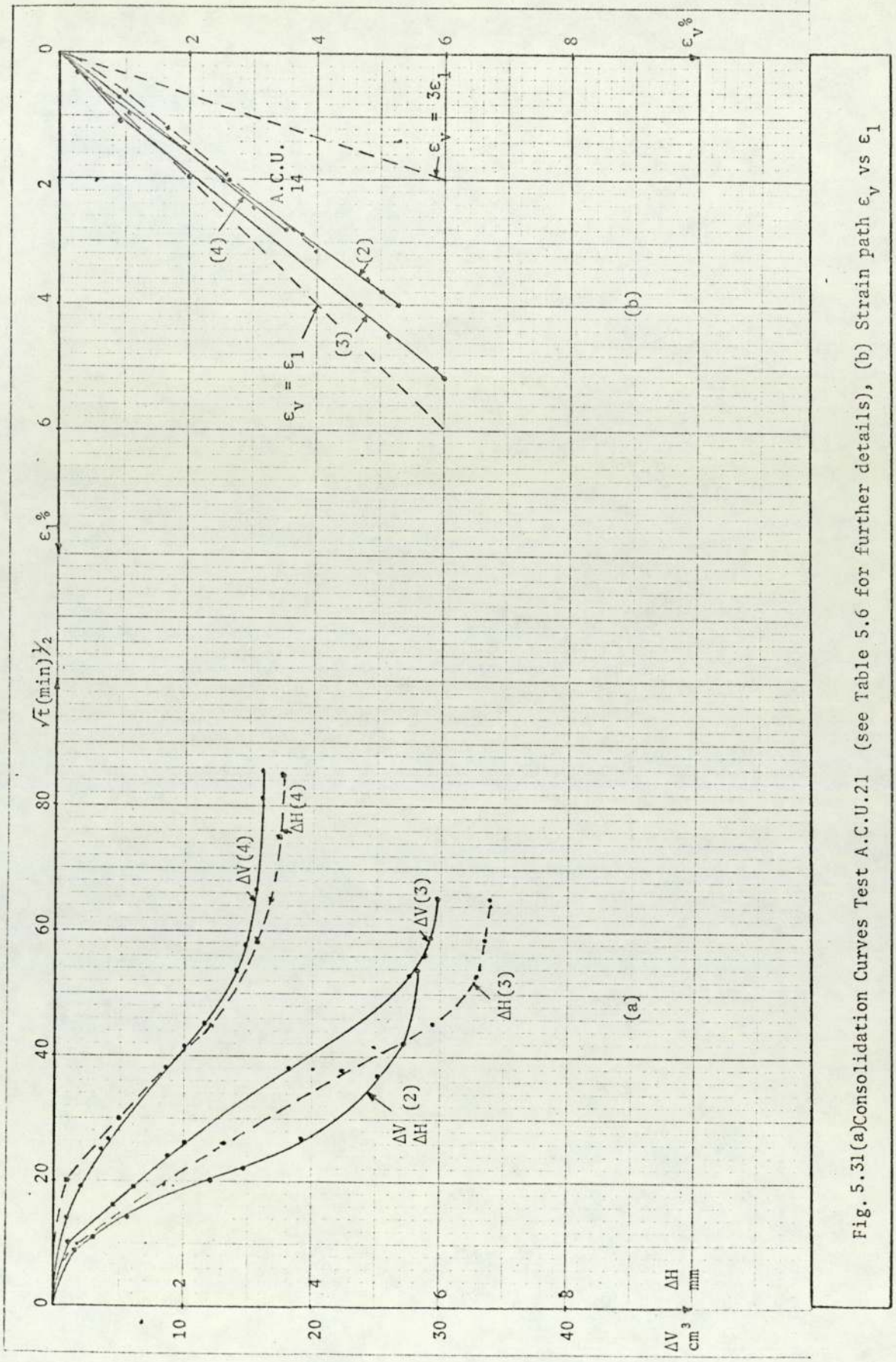

Fig. 5.31(a)Consolidation Curves Test A.C.U.21 (see Table 5.6 for further details), (b) Strain path ε_v vs ε_1

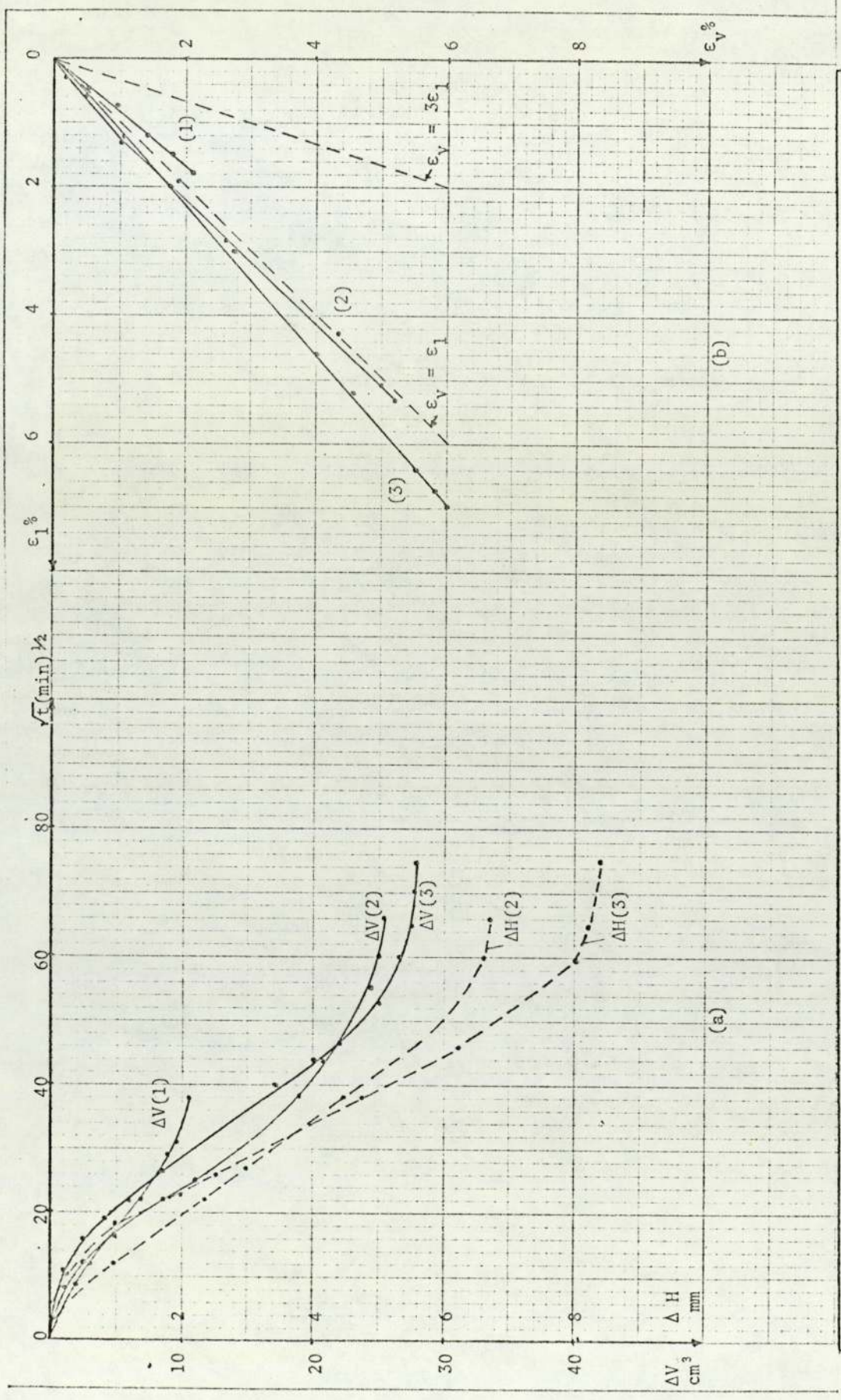

Fig. 5.32(a)Consolidation Curves Test A.C.U.22 (See Table 5.6 for further details), (b) Strain path ε_v vs ε_1

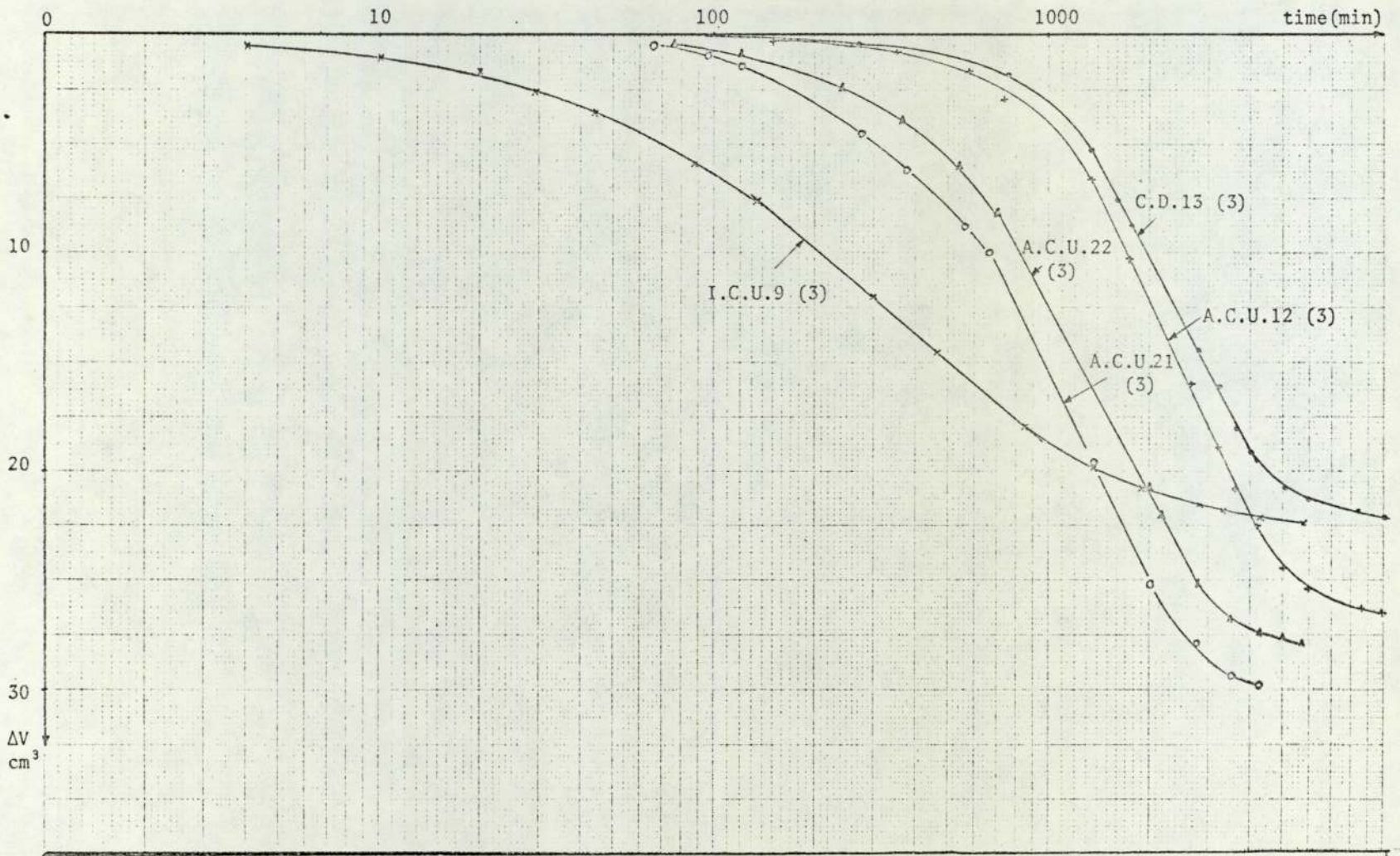

Fig. 5.33 Compression-logarithm of time for stress increment from P_1 = 100 KN/m^2 to P_2 = 200 KN/m^2 (increment 3)

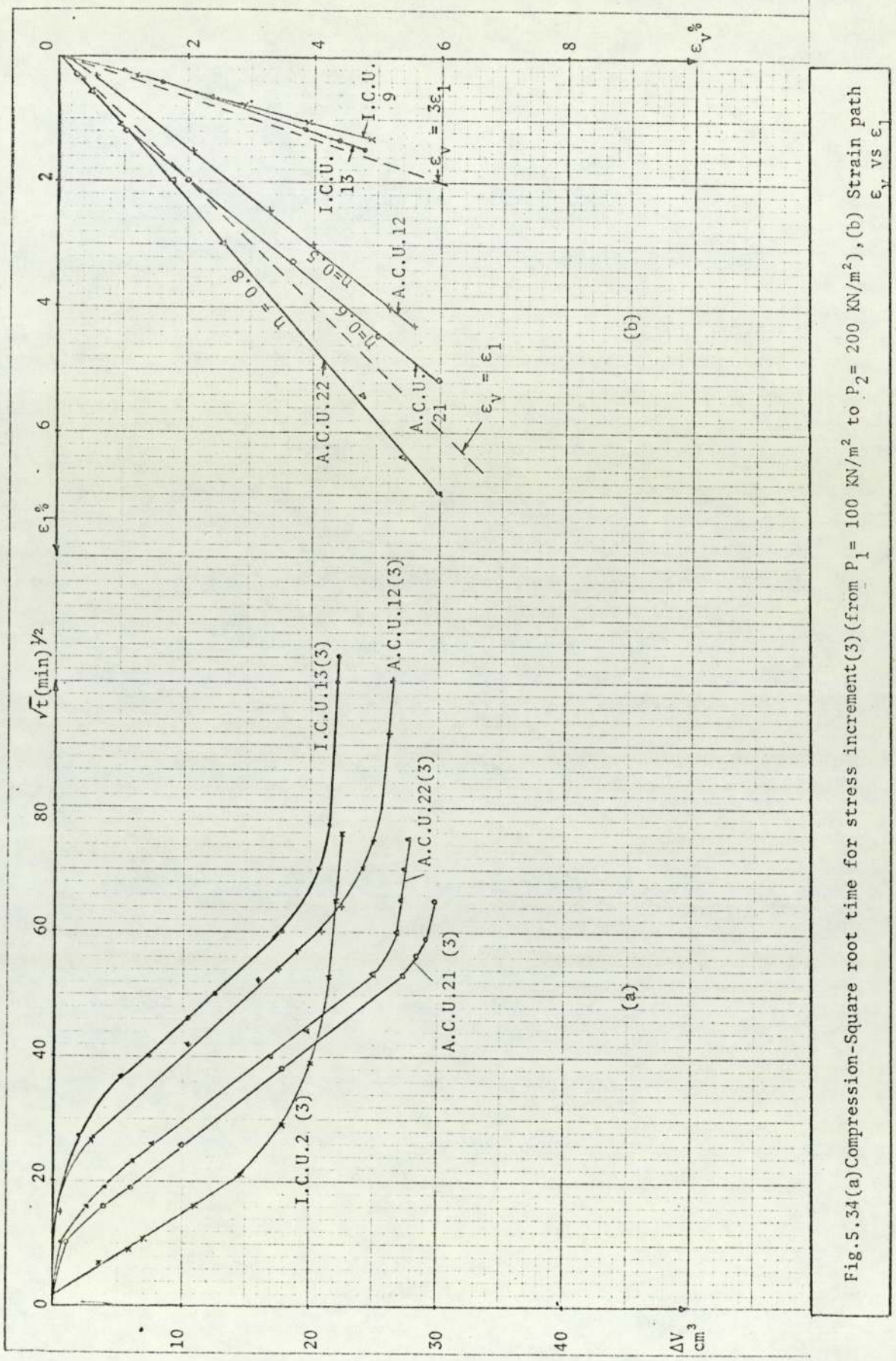

Fig.5.34(a)Compression-Square root time for stress increment(3)(from P_1= 100 KN/m^2 to P_2= 200 KN/m^2),(b) Strain path ε_v vs ε_1

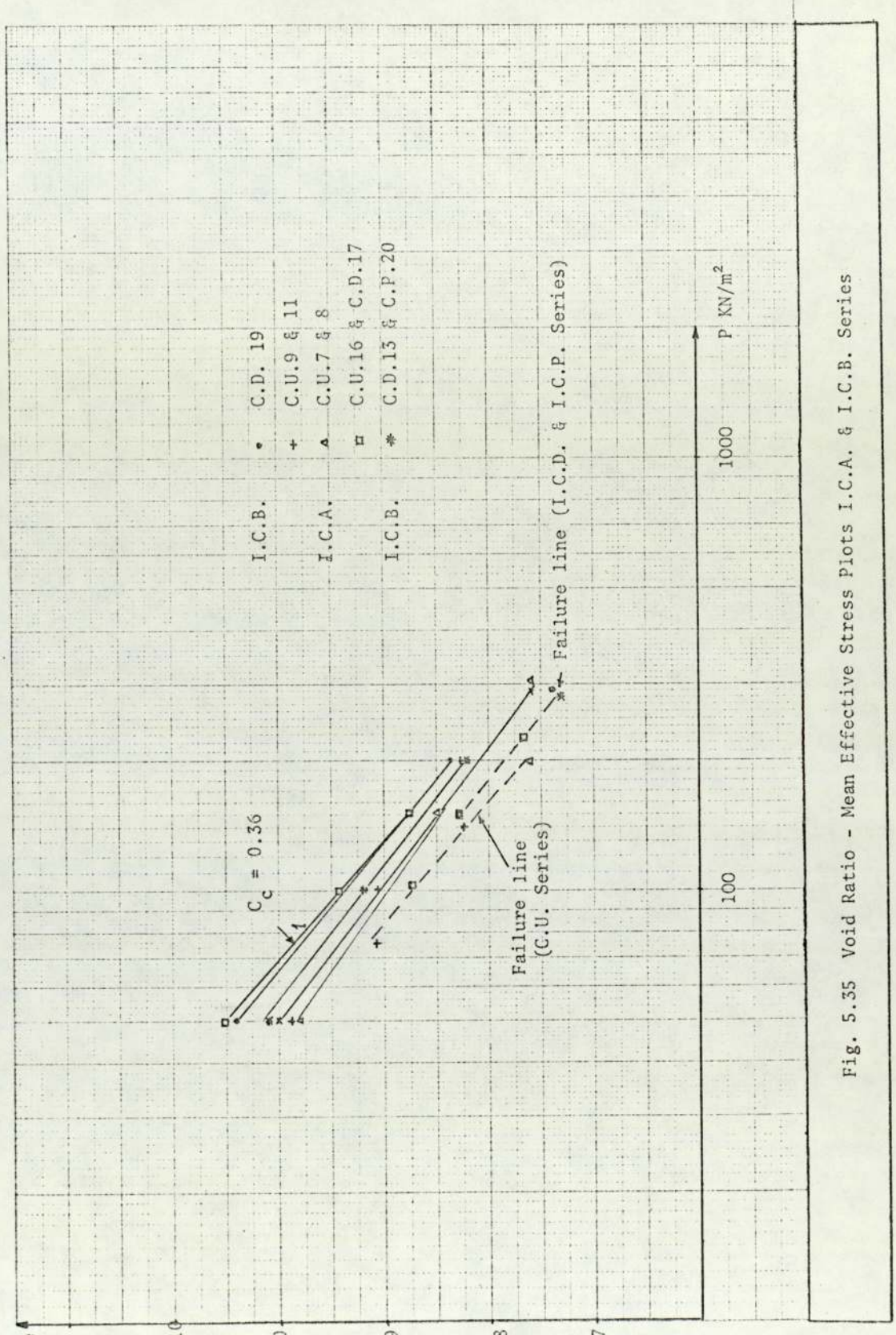

Fig. 5.35 Void Ratio - Mean Effective Stress Plots I.C.A. & I.C.B. Series

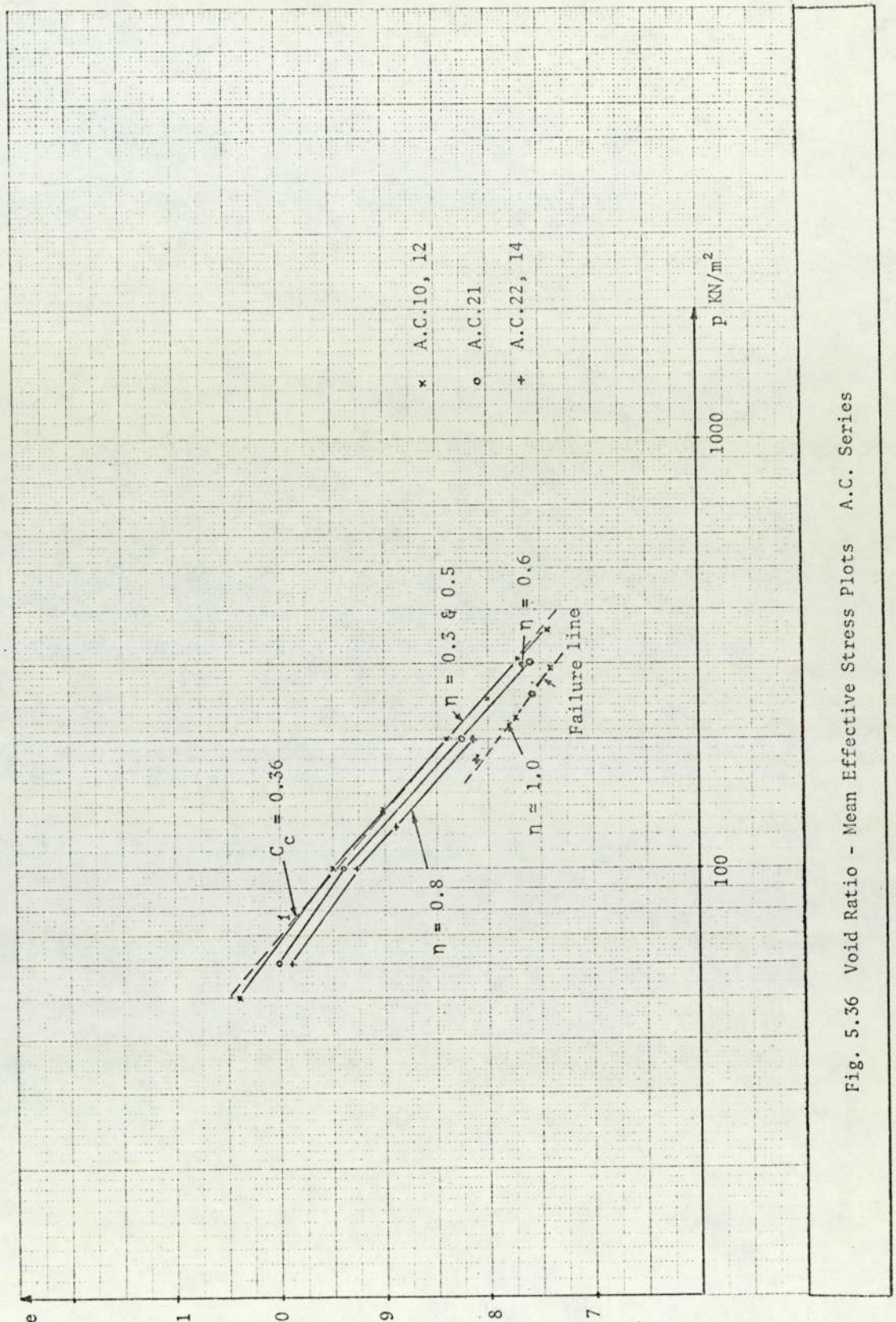

Fig. 5.36 Void Ratio - Mean Effective Stress Plots A.C. Series

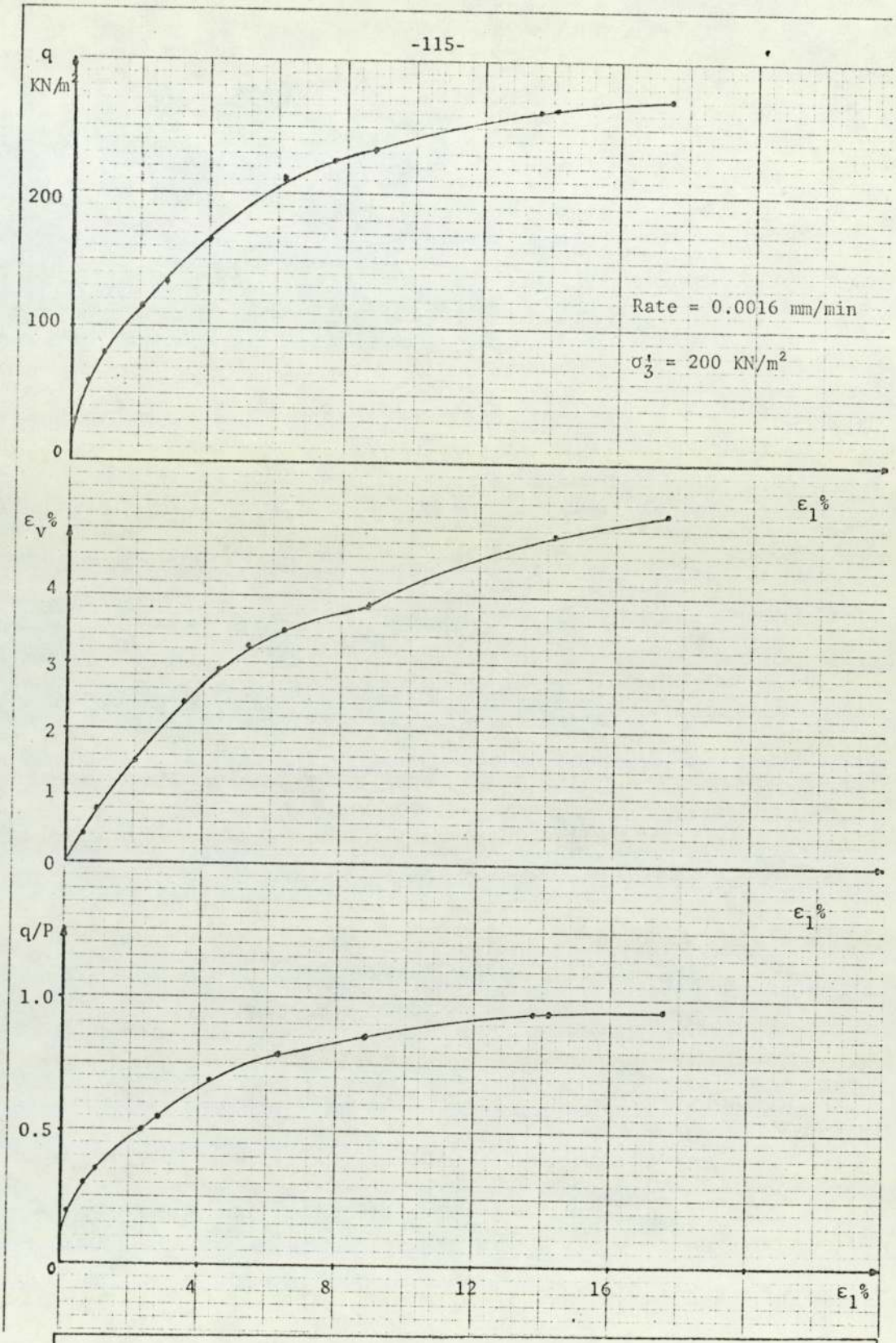

Fig. 5.37 Drained Shearing Stage C.D. Series (C.D.13)

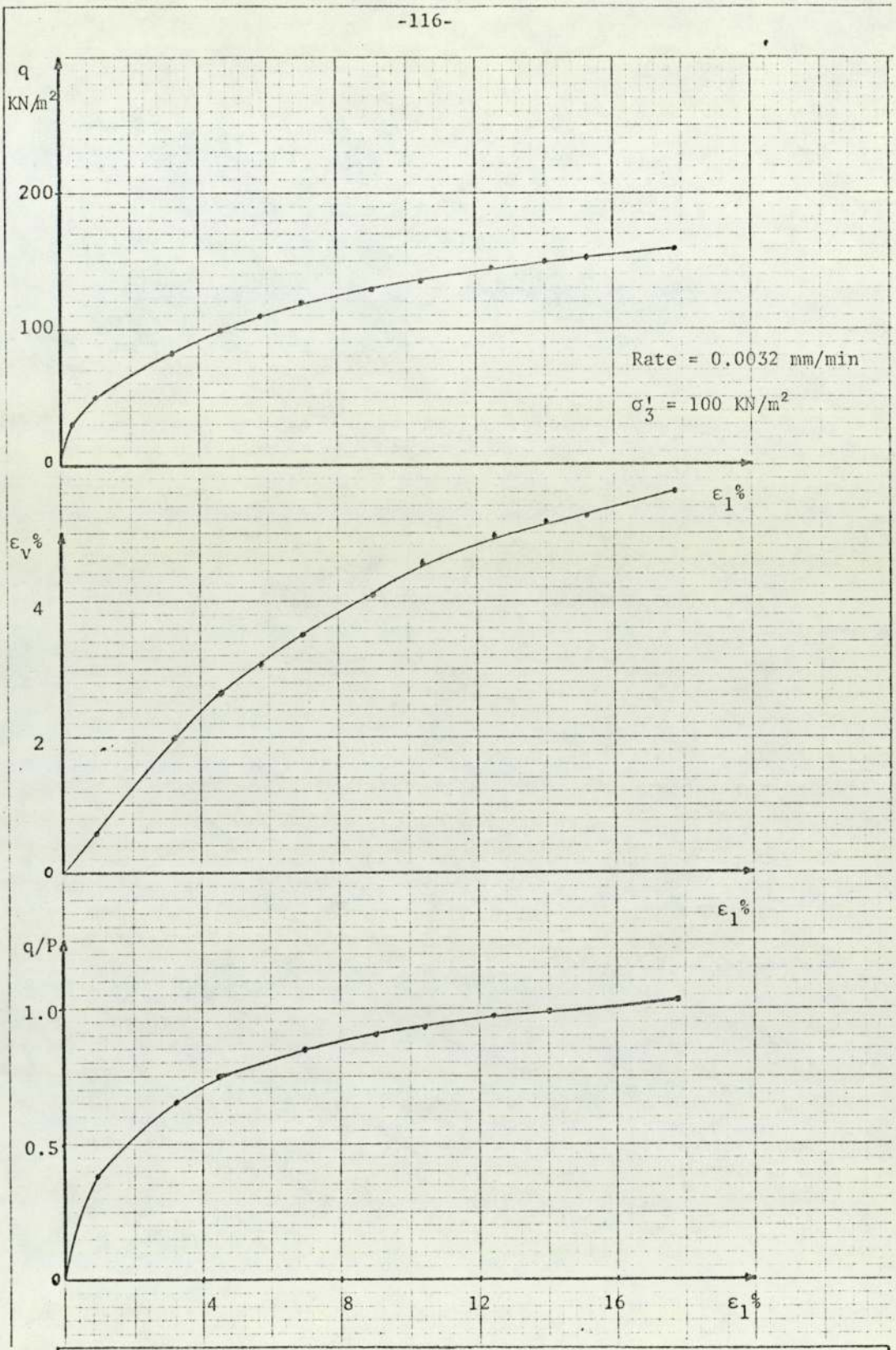

Fig. 5.38 Drained Shearing Stage C.D. Series (C.D.15)

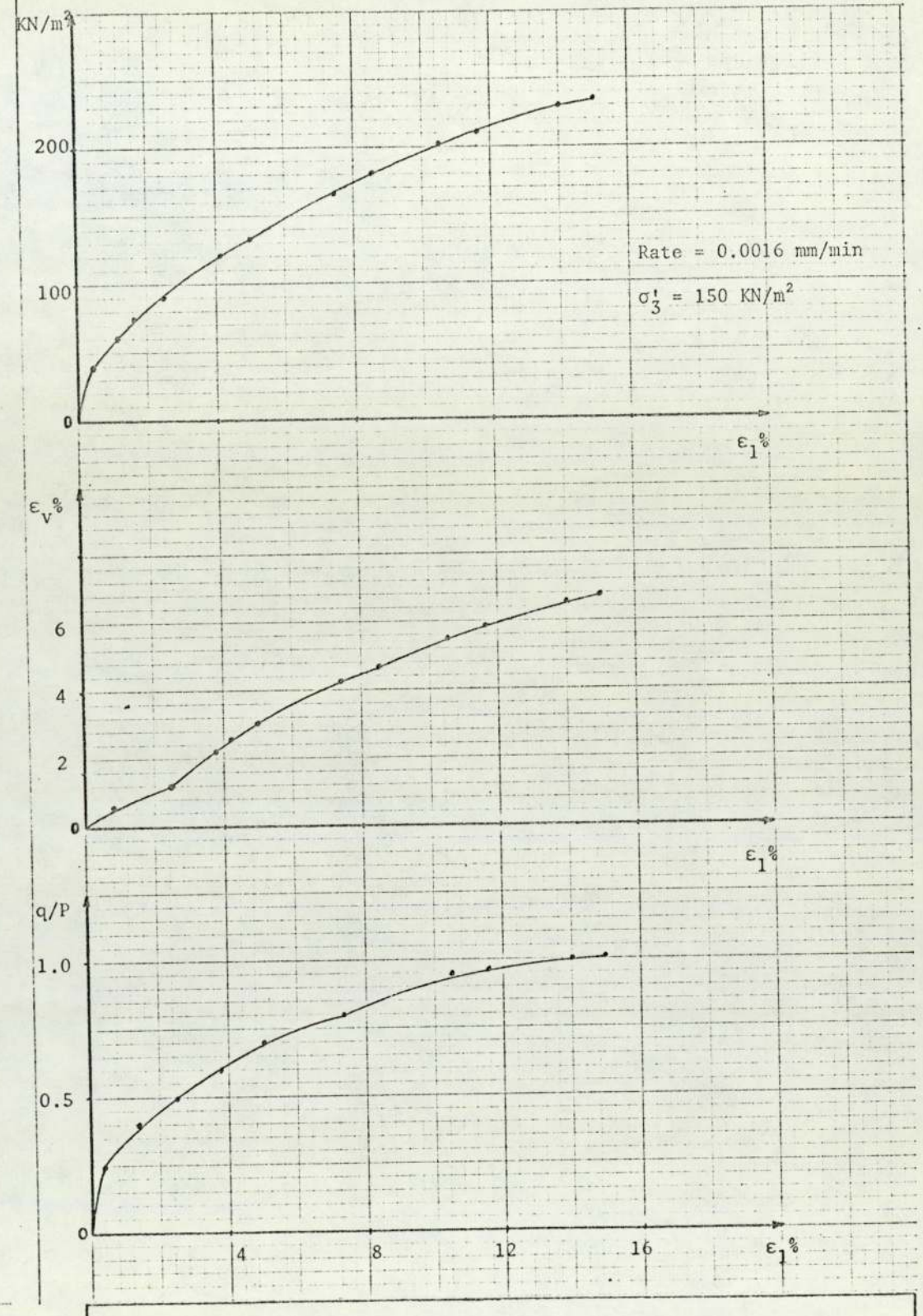

Fig. 5.39 Drained Shearing Stage C.D. Series (C.D.17)

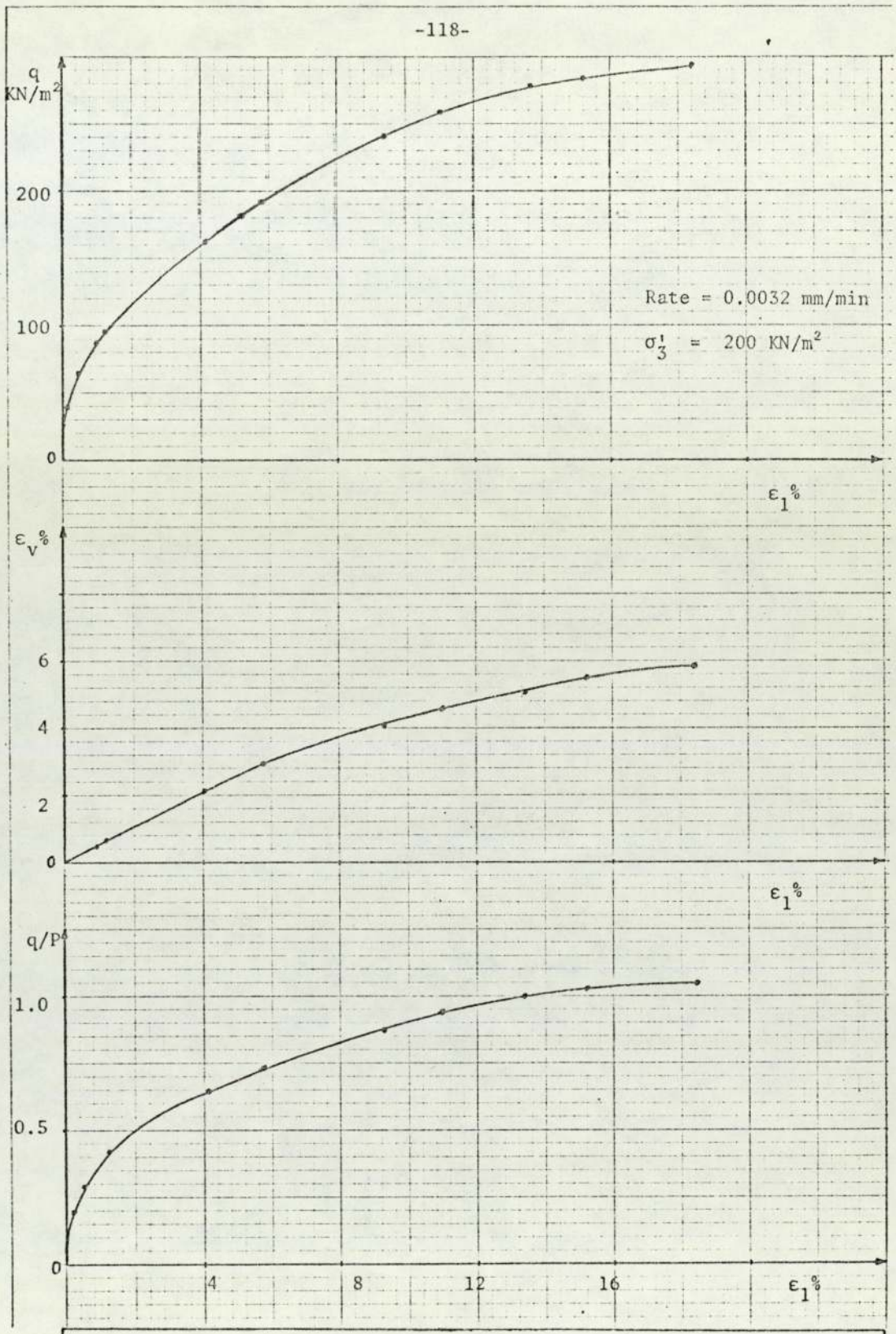

Fig. 5.40 Drained Shearing Stage C.D. Series (C.D.19)

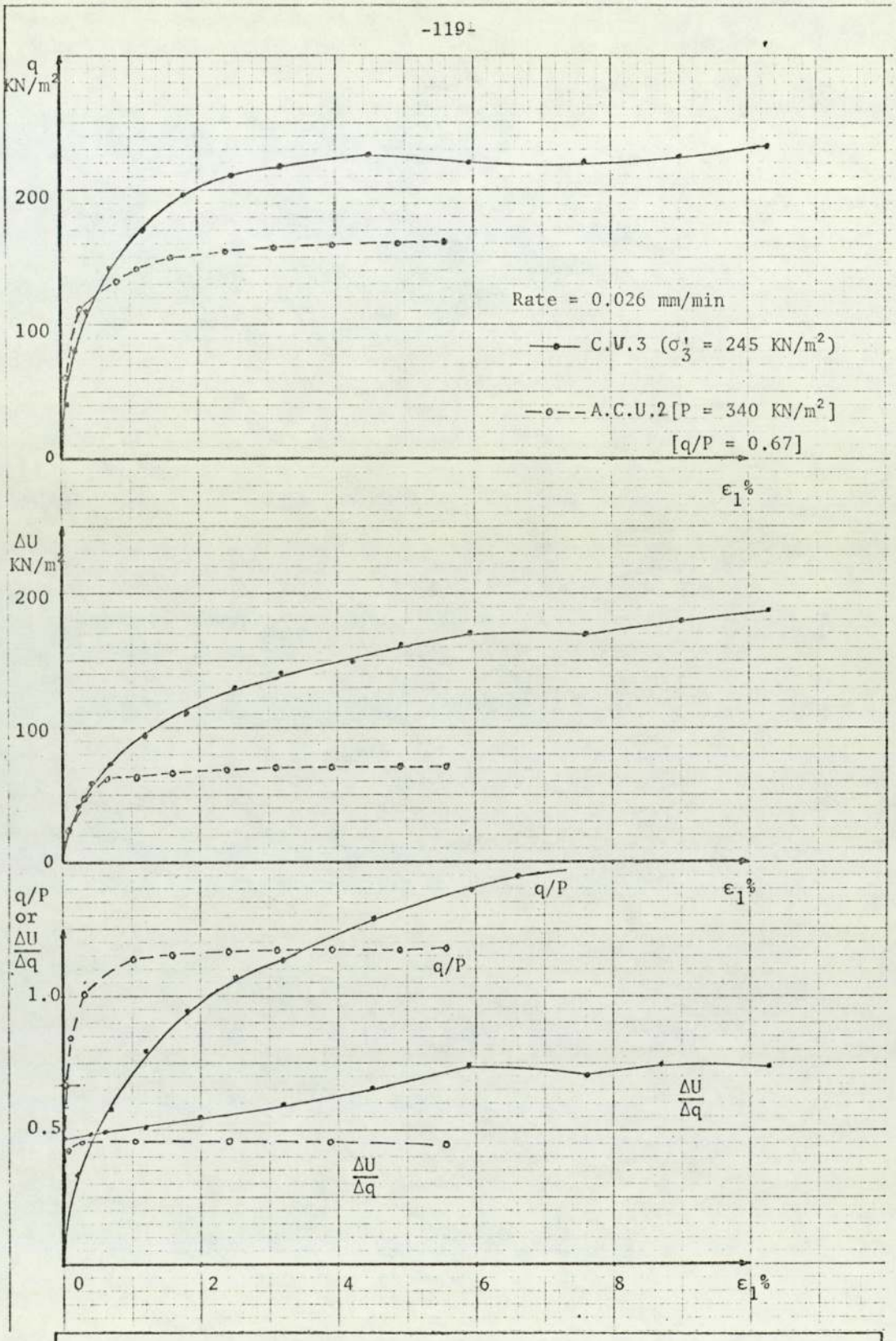

Fig. 5.41 Undrained Shearing Stage I.C.U. Series (A.C.U.2 & C.U.3)

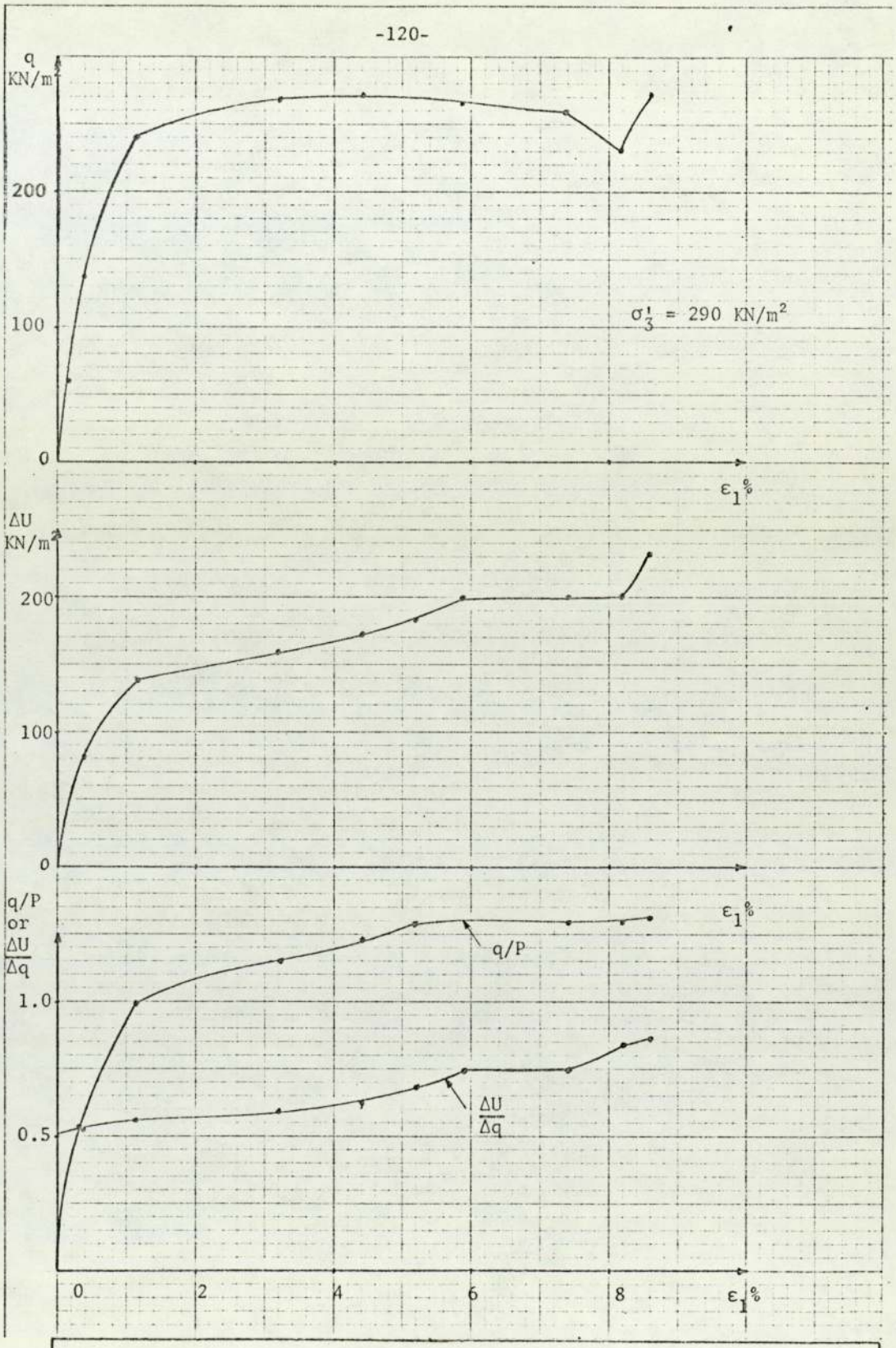

Fig. 5.42 Undrained Shearing Stage I.C.U. Series (C.U.4)

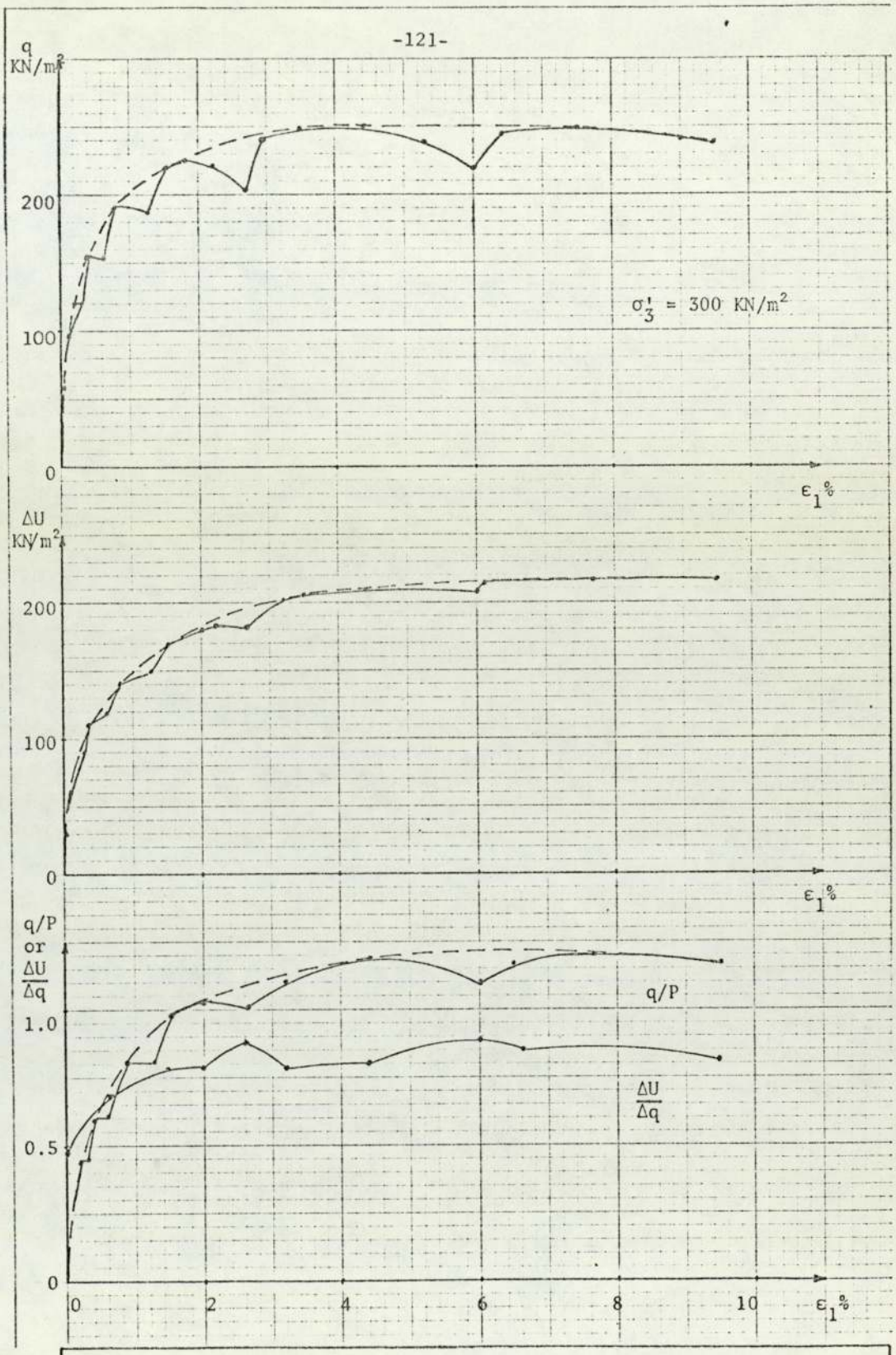

Fig. 5.43 Undrained Shearing Stage I.C.U. Series (C.U.6)

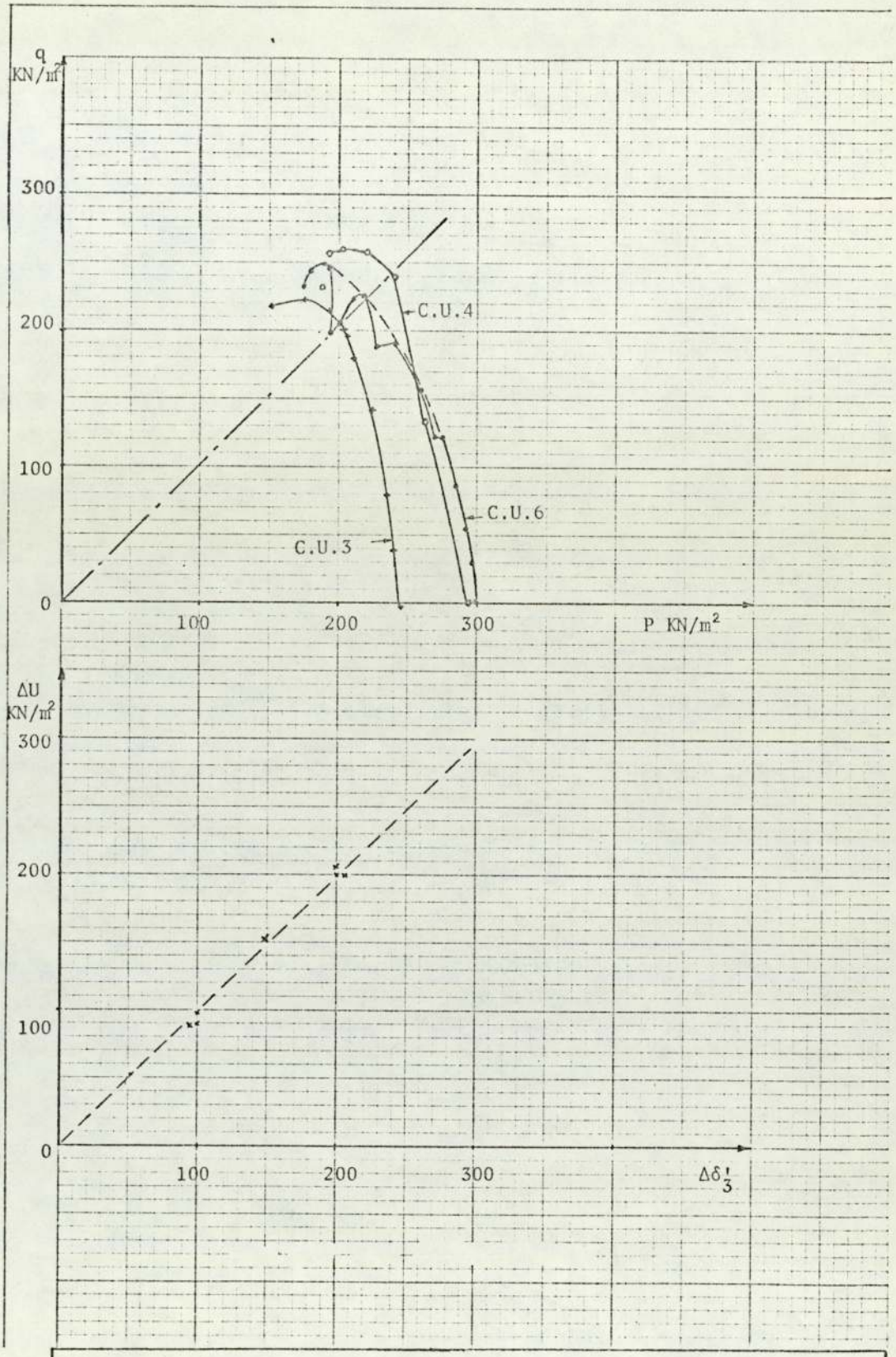

Fig. 5.44 C.U. Series Results

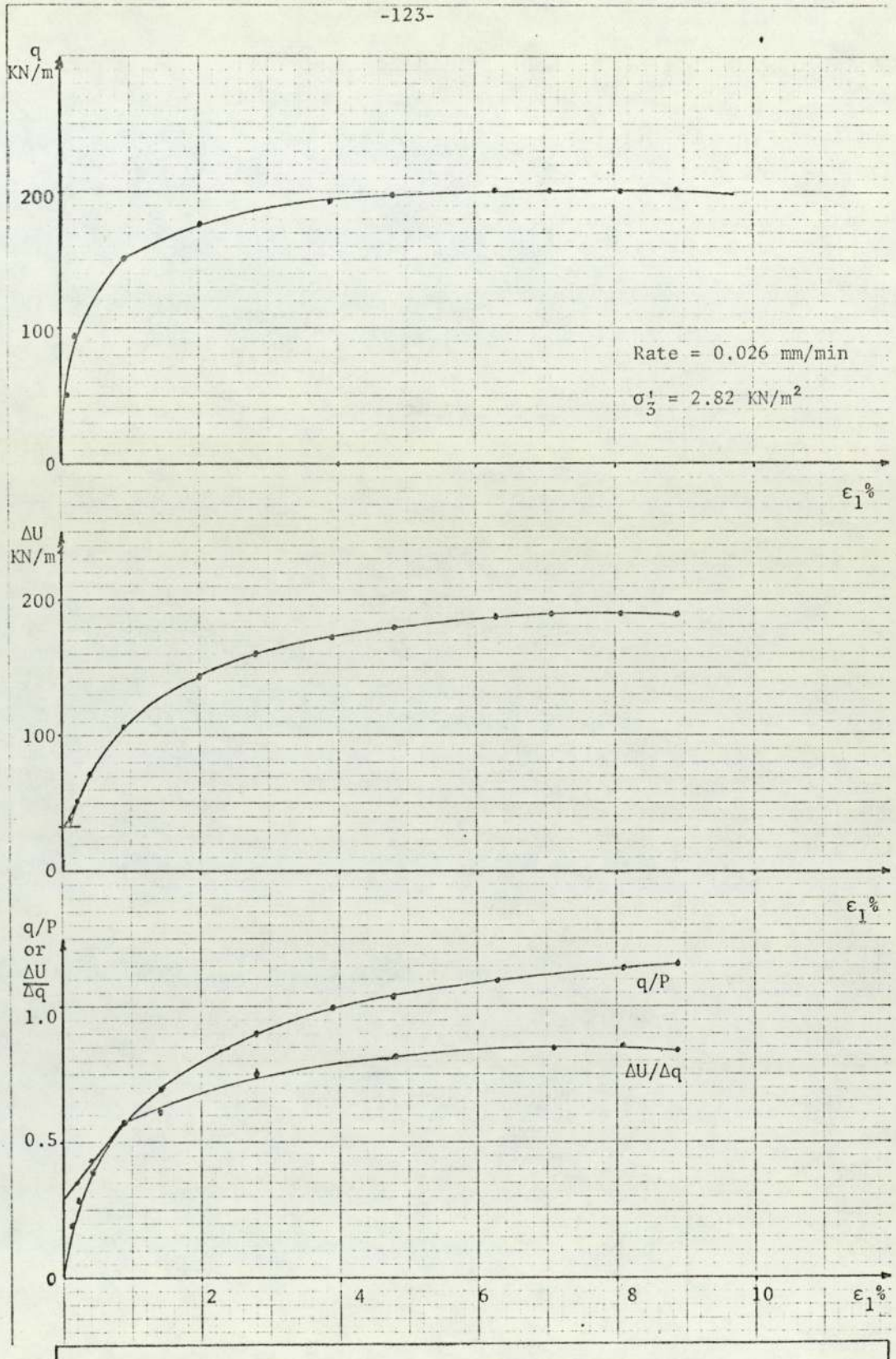

Fig. 5.45 Undrained Shearing Stage C.U. Series (C.U.7)

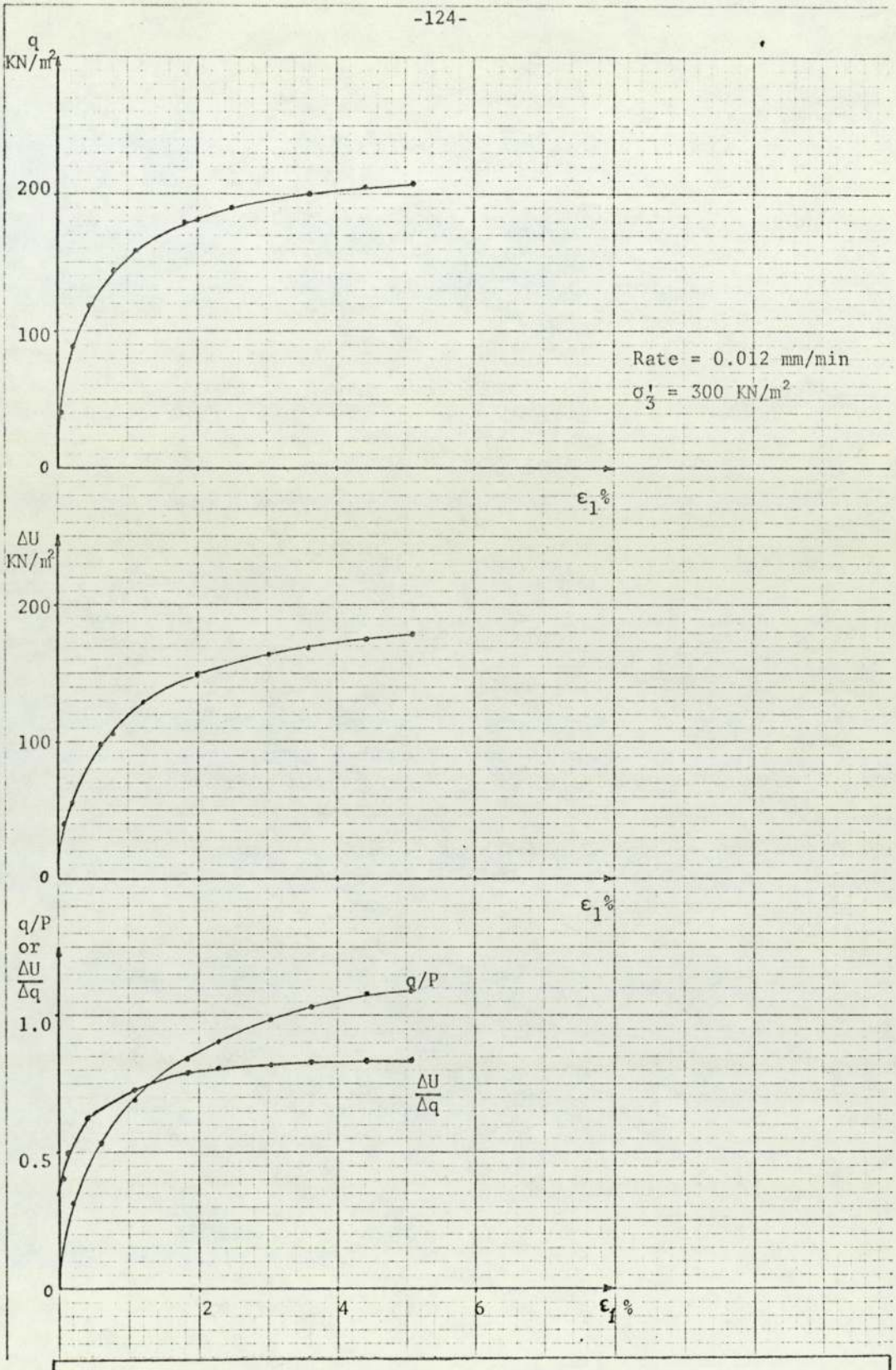

Fig. 5.46 Undrained Shearing Stage C.U. Series (C.U.8)

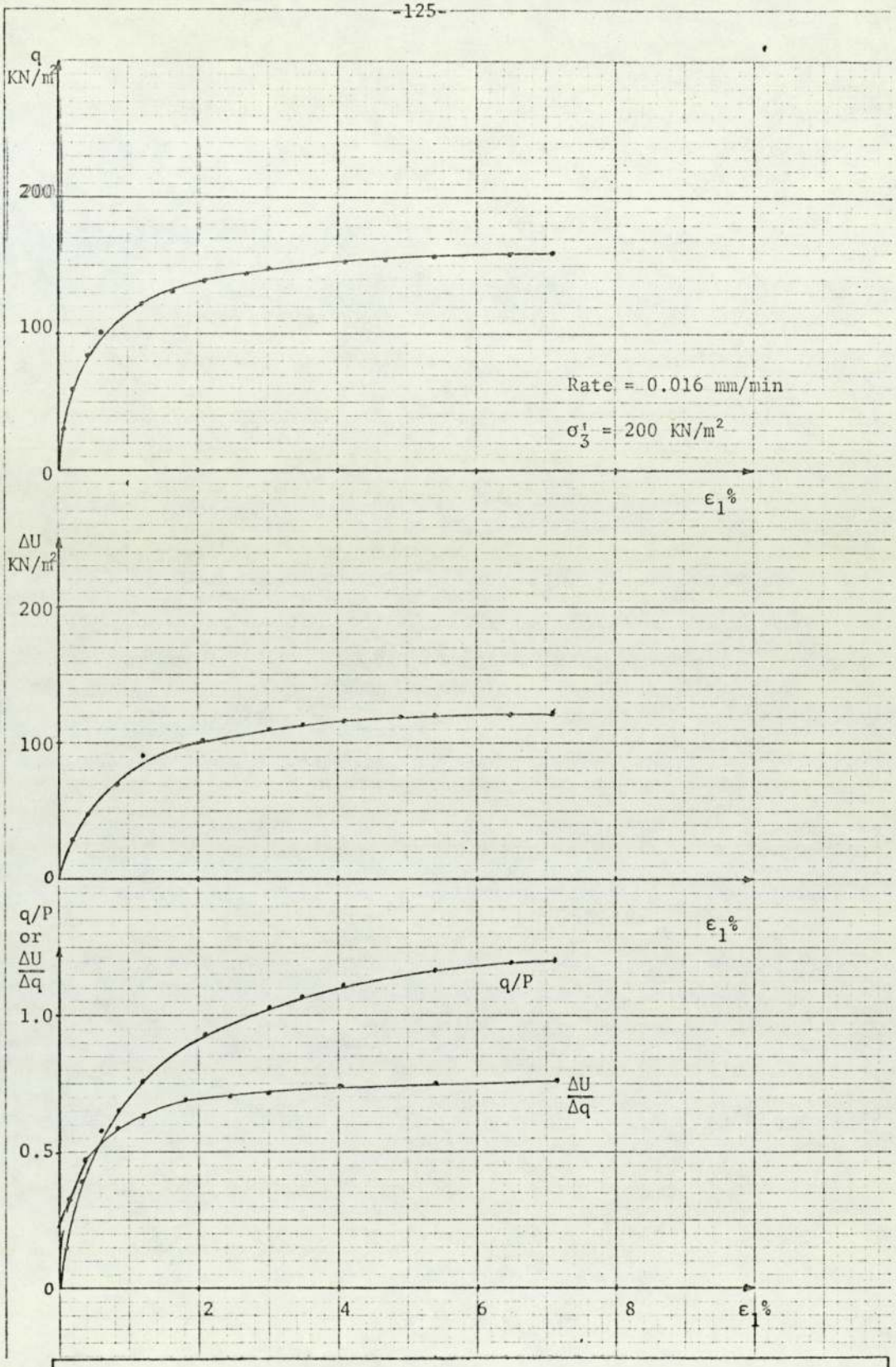

Fig. 5.47 Undrained Shearing Stage C.U. Series (C.U.9)

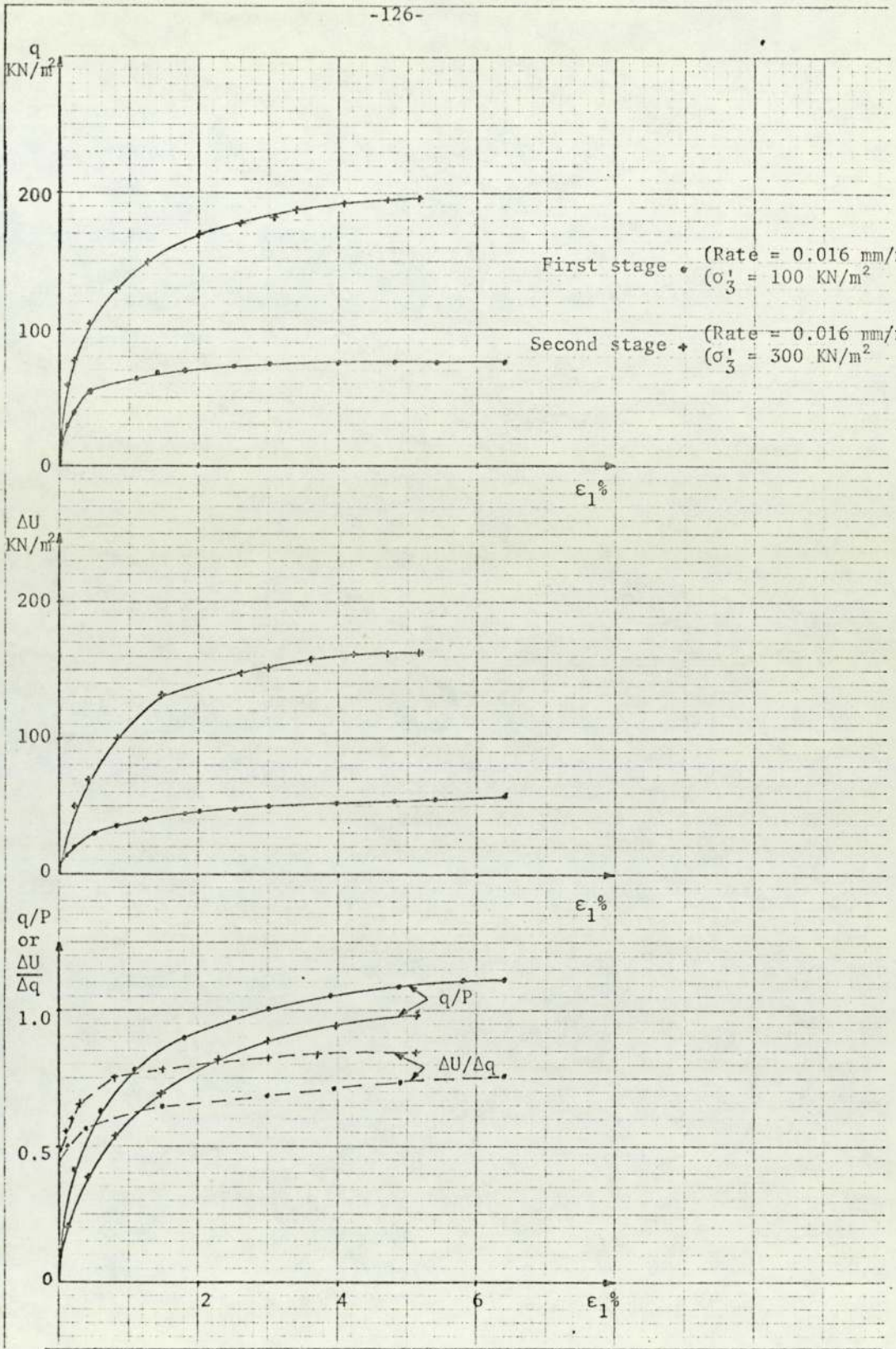

Fig. 5.48 Undrained Shearing Stage C.U. Series (C.U.11)

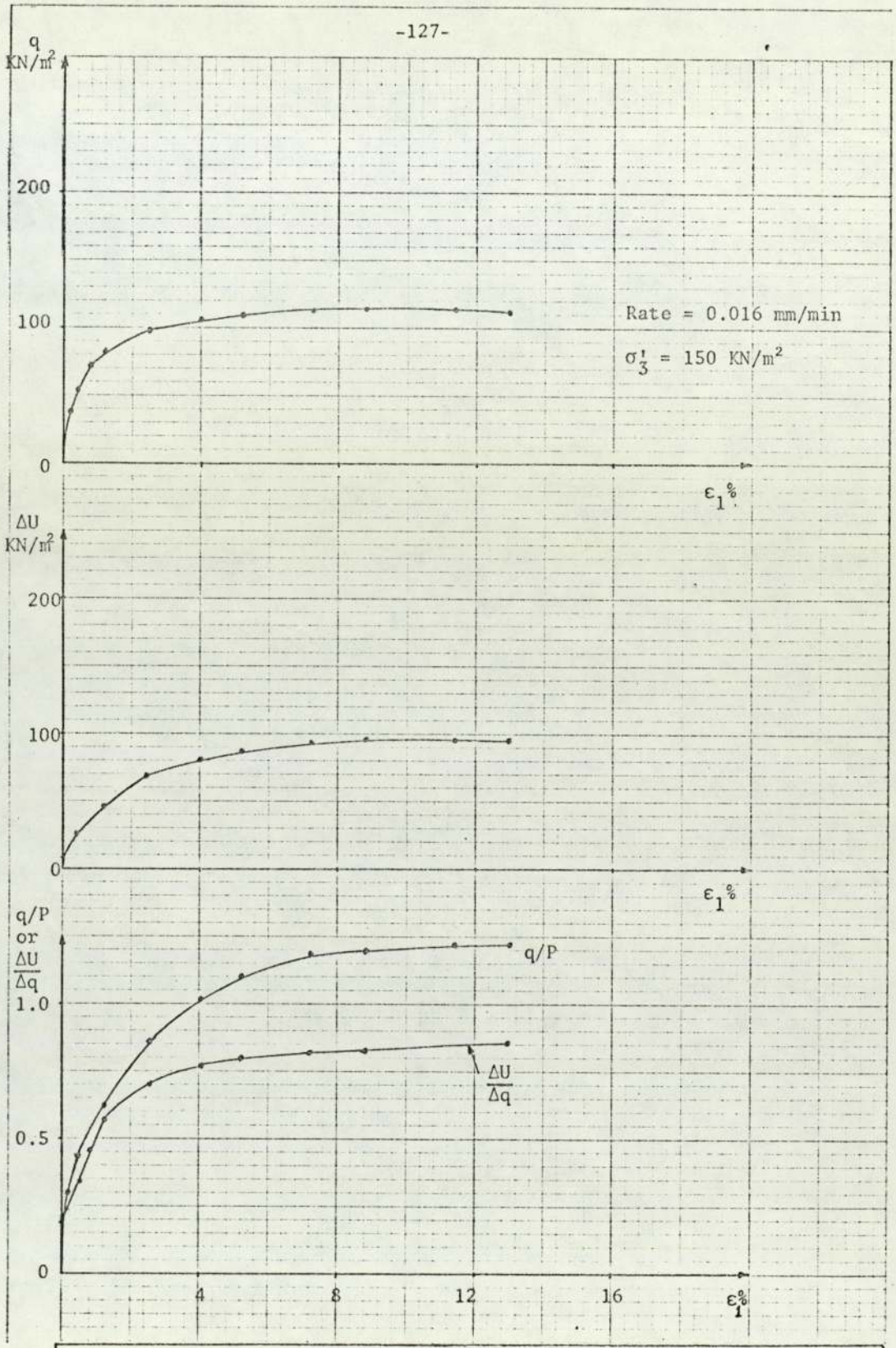

Fig. 5.49 Undrained Shearing Stage C.U. Series (C.U.16)

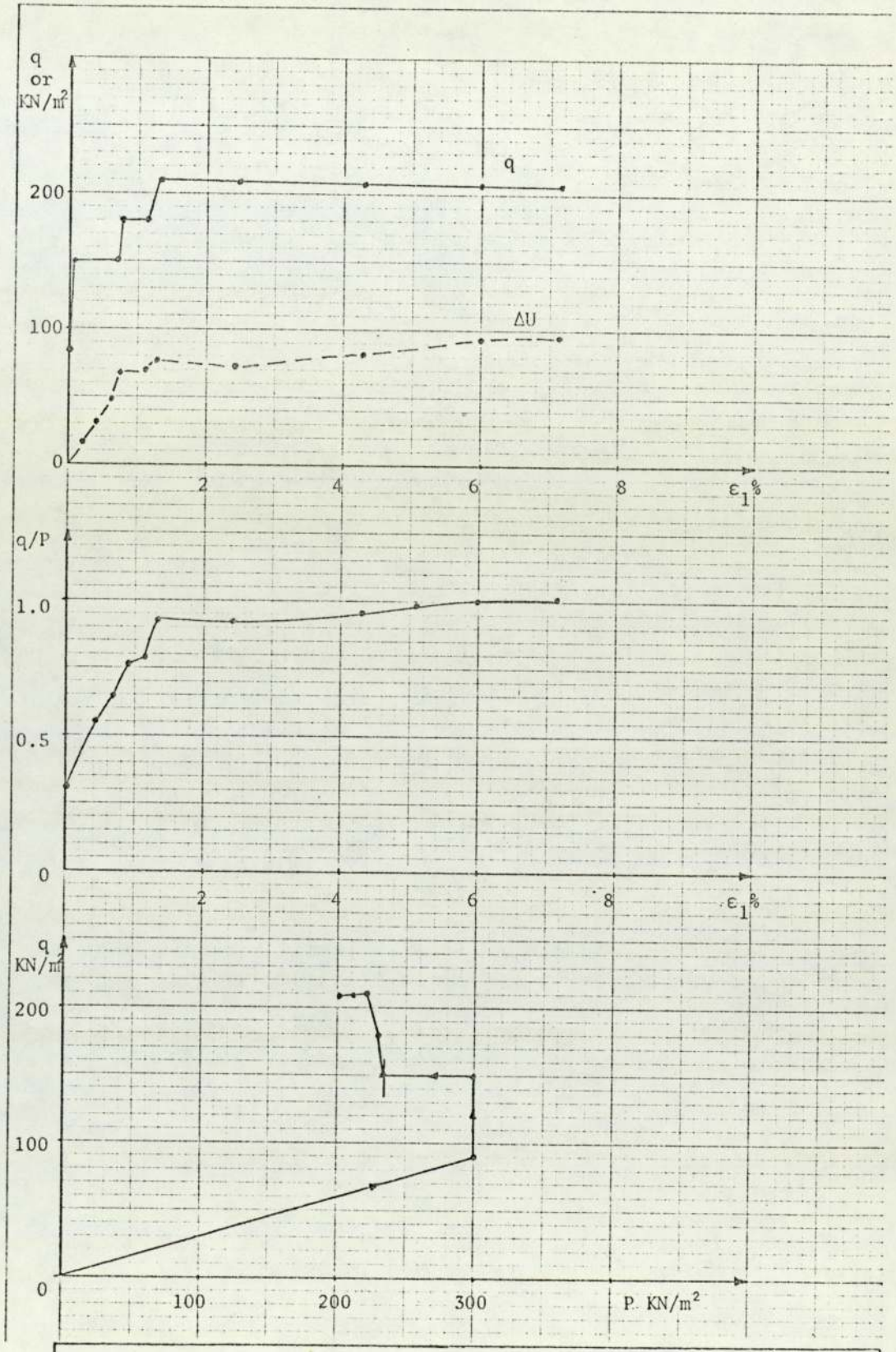

Fig. 5.50 Undrained Shearing Stage A.C.U.Series (A.C.U.10)

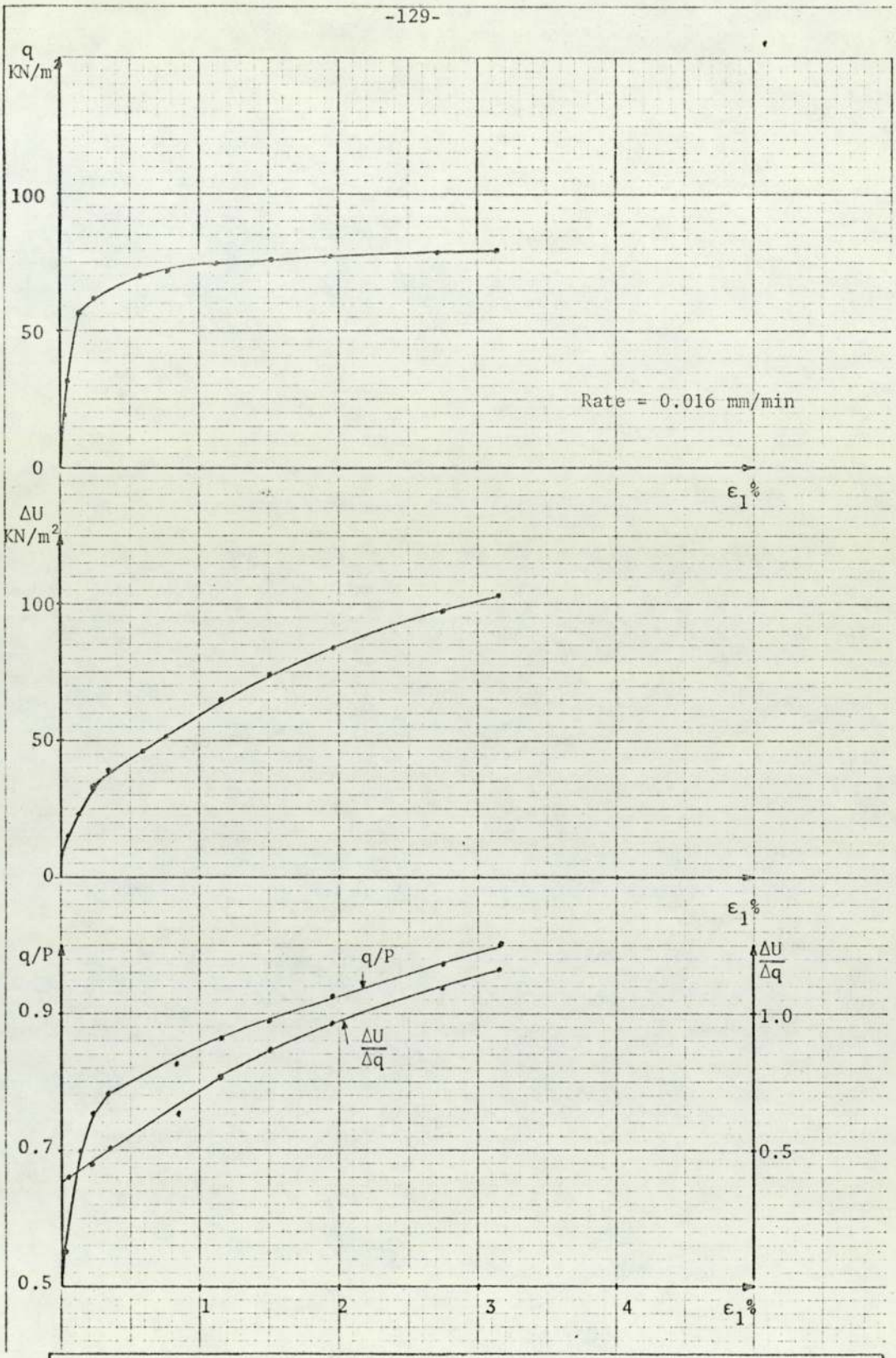

Fig. 5.51 Undrained Shearing Stage A.C.U.Series (A.C.U.12)

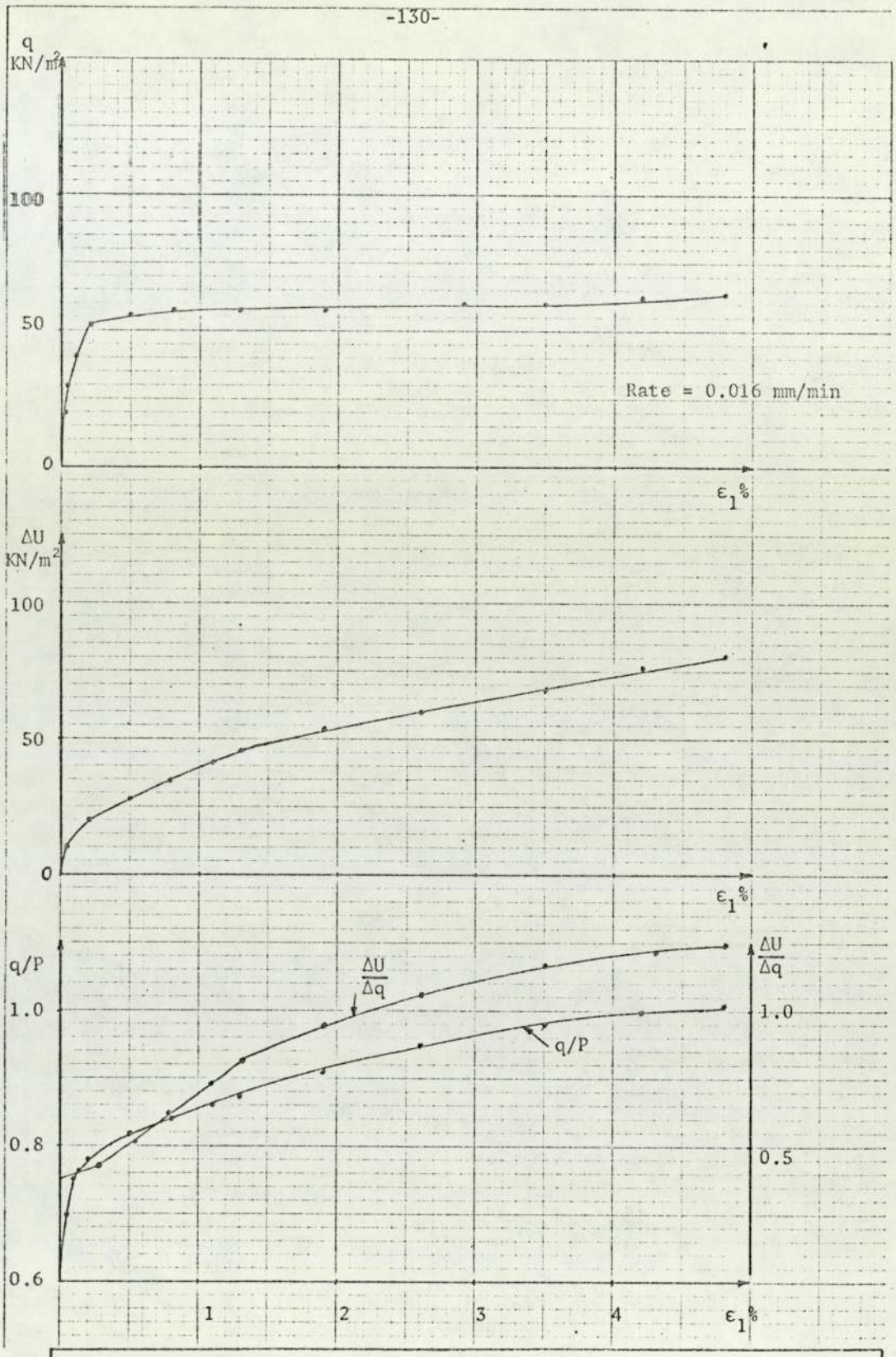

Fig. 5.52 Undrained Shearing Stage A.C.U.Series (A.C.U.21)

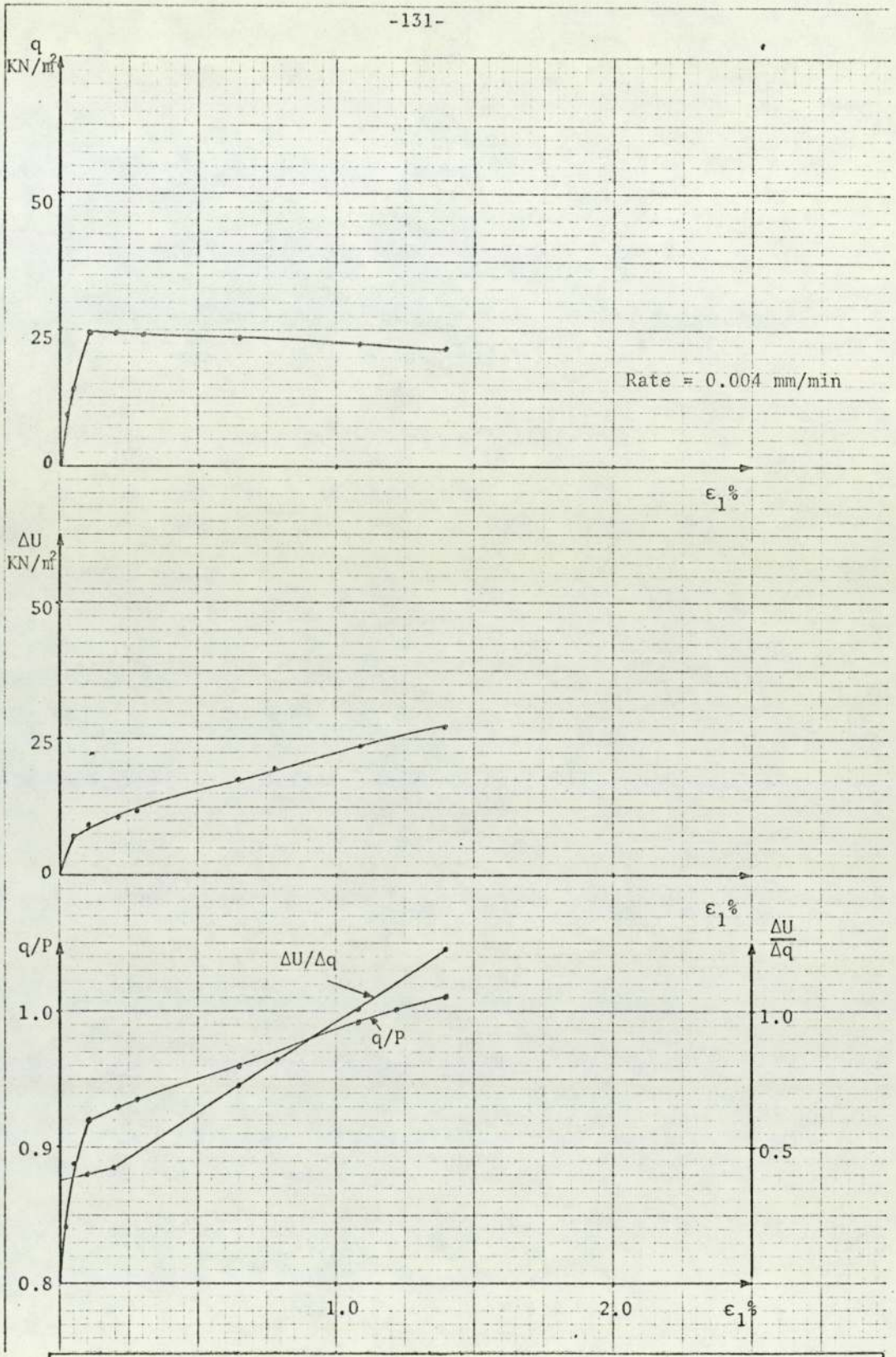

Fig. 5.53 Undrained Shearing Stage A.C.U. Series (A.C.U.22)

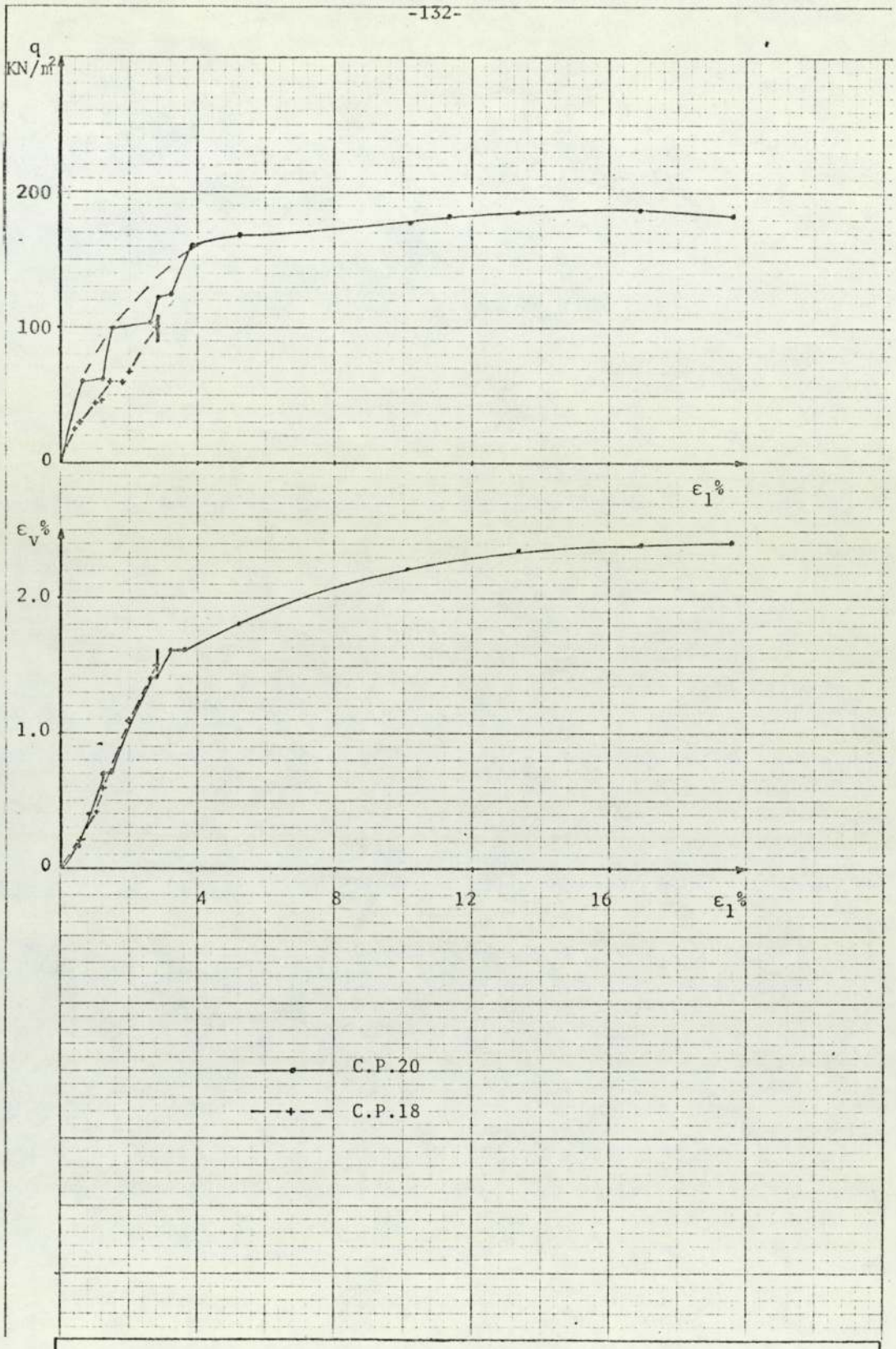

Fig. 5.54 C.P. Series (C.P.18 and C.P.20)

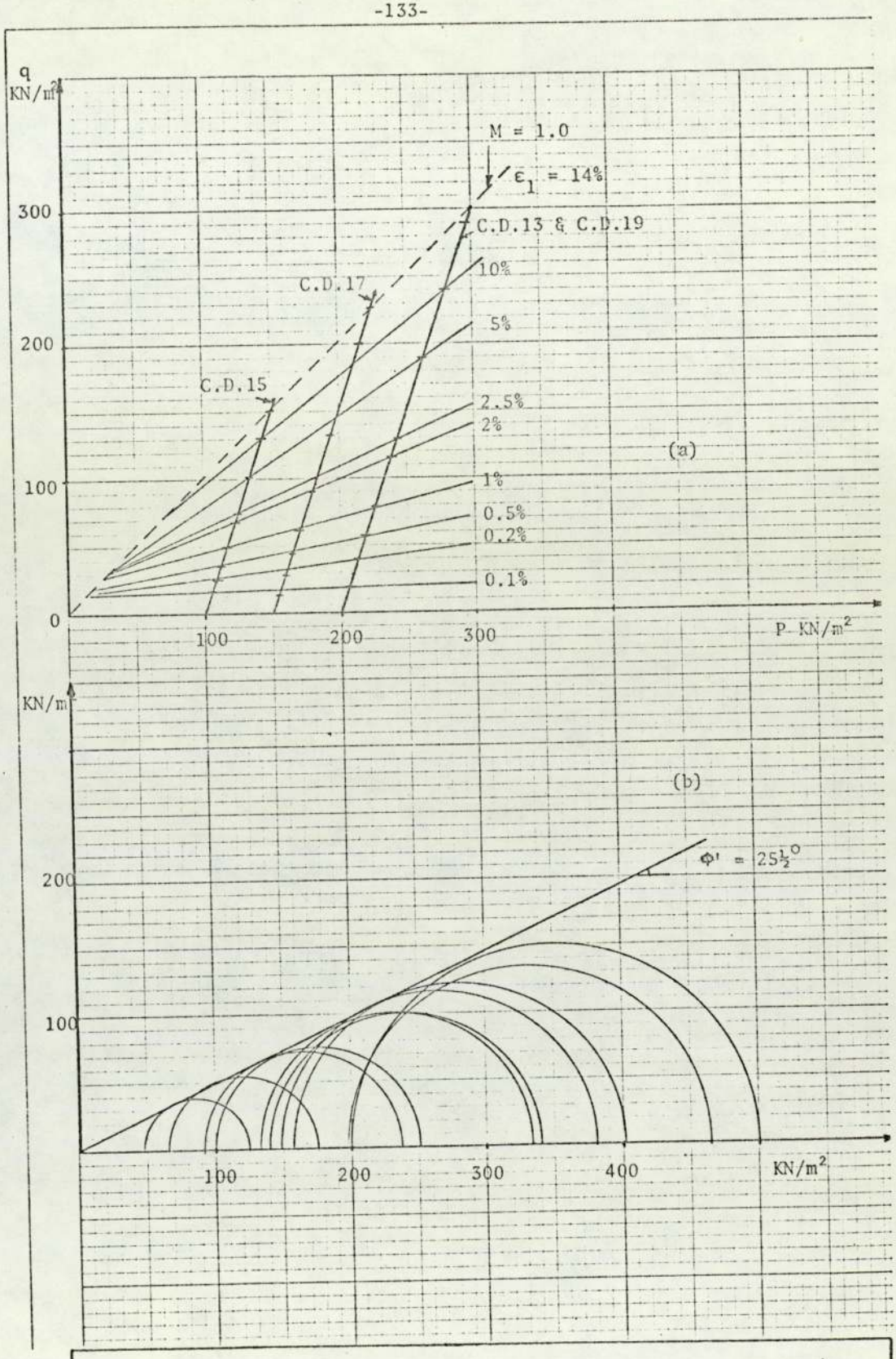

Fig. 5.55 I.C.D. Series and Mohr Circles from Drained and Undrained Tests

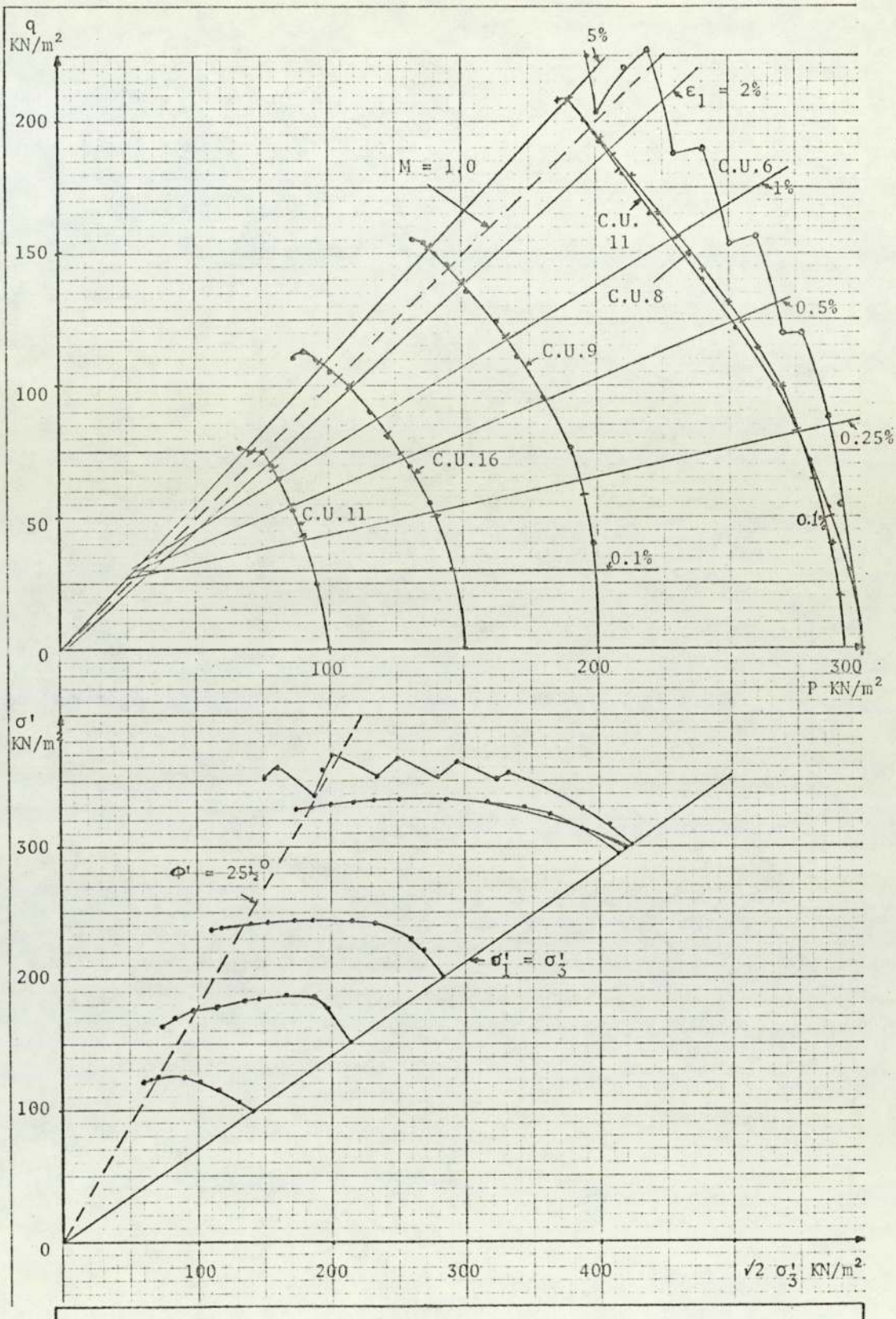

Fig. 5.56 I.C.U. Series (Stress Paths with strain contours)

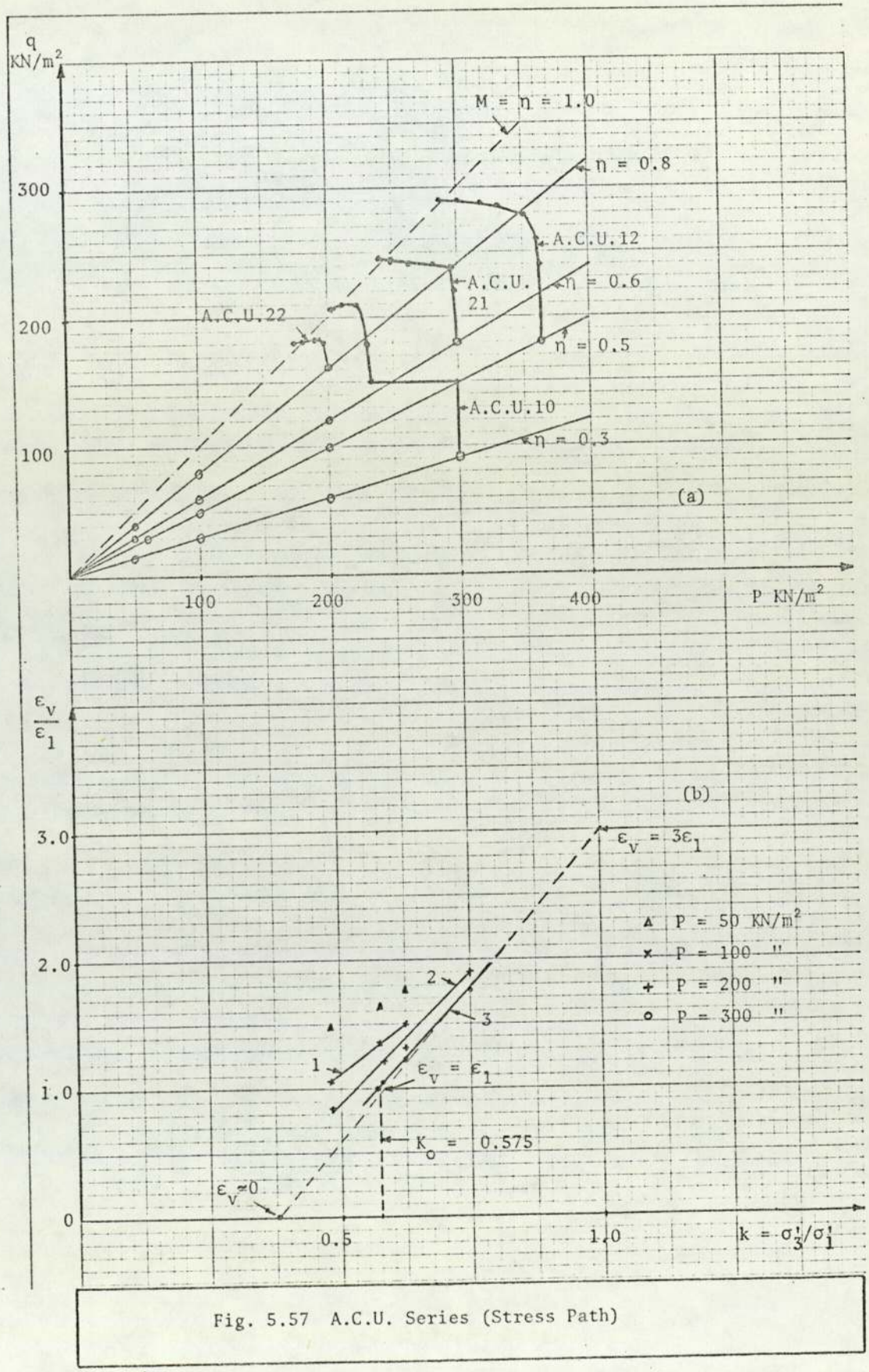

Fig. 5.57 A.C.U. Series (Stress Path)

CHAPTER SIX

DISCUSSION OF TEST RESULTS

6.1 Preparation of the remoulded Lias clay samples

All the samples were prepared from slurry at moisture contents well above the liquid limit (w_ℓ = 56%), and were initially consolidated in the tall oedometer; the extruded samples were firm enough for handling without any disturbance. Variation in the moisture content within the samples was small (see Chapter 4, Table 4.1), but due to the presence of variable side friction the samples consolidated under the same load did not have the same initial moisture content. The same unknown side friction prevented accurate evaluation of the compression index for the consolidation stage in the tall oedometer and the estimated values were rather high as compared with those obtained from the standard oedometer tests (Figs. 4.3 and 5.2).

6.2 Results of Oedometer Tests

The two types of consolidation tests (conventional and tests with measurement of the pore pressure at the base) yield almost identical results. The value of compression index, C_c, was between 0.34 and 0.4, and swelling index, C_s, was between 0.062 and 0.070. Variation of the load increment ratio, ($\frac{\Delta\sigma'}{\sigma'}$ = 1, 1/2 and 1/3) resulted in different values of the coefficient of consolidation, C_v, but had little effect on the values of C_c and C_s.

It is interesting to note that on the plots of e - logσ' the consolidation lines from different tests do not coincide (Fig. 5.2 and 5.11), but are almost parallel; it is especially marked in Fig. 5.2 where the initial preparation moisture contents were different

(between 58% and 75%). Thus it appears that the initial moisture content is one of the variables which produce a shift of the consolidation lines without a change in their gradient.

Another factor which affects the position of the e - logσ' plot is the degree of secondary consolidation. This is evident from the void ratio - effective stress plots with the rate of consolidation, $\frac{\delta e}{\delta t}$, as a third parameter (Fig. 5.14 and 5.17). As the rate of consolidation decreases these lines fall to the left of the line obtained at the end of the expulsion of the excess pore pressure. Hence the longer the time for creep strains to occur, the lower are the void ratios under the same stress. However, the consolidation lines with different rates of consolidation (or duration of time, Bjerrum, 1967) are parallel, and they present a family of $e = [e(\sigma')]_{t=const.}$ lines. The effects of secondary consolidation are discussed further in Section 6.4.

The results of tests with pore pressure measurement at the base showed smaller induced, initial, pore pressures than the applied stresses, particularly at high stress levels (Fig. 5.9 and 5.10). This is consistant with observations by others (e.g. Lowe, 1974) and is due to the combined effect of factors such as: (a) flexibility of the measuring devices, (b) immediate expulsion of water from the top of the sample, (c) decrease in soil stresses due to the side friction, and (d) a small, immediate increase in the effective stress which occurs even in saturated samples (Leonard et al, 1964 and Barden, 1965). The time for 90% consolidation, t_{90}, obtained from the pore pressure dissipation curves, were much higher than those obtained by the curve

fitting methods, and were not conclusive.

The predictions of the consolidation strains from Gibson and Lo's theory are compared with the experimental results in Figs. 5.20 and 5.21. It can be seen that there is a good agreement in the initial stage of the tests and in the secondary consolidation range, but not in the transitional stage.

6.3 Results of Triaxial Tests

These results are discussed under separate headings of consolidation tests and shearing tests.

6.3.1 Consolidation Tests

The isotropic consolidation tests were carried out with different drainage conditions, sample heights and different modes of application of load increments (gradual or incremental). Whereas in anisotropic consolidation tests the drainage conditions and heights were kept constant and load increment was gradual (see Chapter 5).

The following points are evident from the results in Figs. 5.22 to 5.36.

(a) The coefficient of consolidation $(C_v)_a$ and $(C_v)_r$ for I.C.B. and A.C. series are much smaller compared with the I.C.A. series. The transitional zone in the compression - time curves are shorter for I.C.B. and A.C. series compared with the I.C.A. series; but the gradient of the tail of the curves (secondary consolidation range) is identical for all series (e.g. see Fig. 5.33).

(b) Volume changes have increased with the increase of $\eta=q/p$ in anisotropic tests under the same mean effective stress increment (Fig. 5.32). Thus a higher value of q results in a smaller value of the void ratio, e, under the same mean effective stress, p.

(c) The $\varepsilon_v - \varepsilon_1$ relationship is shown in Figs. 5.22 to 5.32; for each test the $\varepsilon_v/\varepsilon_1$ ratio is usually constant during primary and secondary consolidation stage of each test. Theoretically, in isotropic conditions, the strain ratio $\varepsilon_v/\varepsilon_1$ is equal to 3 and the shear strain 'ε' is equal to zero (if the soil is isotropic and stresses are isotropic). This has not been the case in the isotropic stress conditions, in which, generally, the ratio $\varepsilon_v/\varepsilon_1$ was found to be greater than 3, particularly in the stress range used in preparation of the samples in the tall oedometer. But at higher stress levels it decreased and approached the theoretical value of 3 (see Tables 5.4 and 5.5).

For anisotropic consolidation tests the strain ratio $\varepsilon_v/\varepsilon_1$ was found to be dependent on the value of $\eta=q/p$ (or ratio σ'_1/σ'_3), but again, at low stress levels, it was influenced by the previous stress history and only approached constant values (dependent on η) at higher stress levels (Fig. 5.57).

It was thought that this phenomenon is due to the influence of the initial anisotropy induced in the sample during the one-dimensional consolidation in the tall oedometer. Results indicate that for one-dimensionally consolidated samples under mean stresses of between 50 and 62 KN/m^2, the previous stress history is erased at isotropic stresses of about 200 KN/m^2, i.e. in this case a stress of up to 4 times the initial stress is needed to erase the stress history

of the sample.

The void ratio - mean effective stress, e - logp, plots shown in Fig. 5.35 and 5.36 indicate a linear relationship between e and logp (or ε_v and logp);

$$e - e_o = C_c \log \frac{p}{p_o} \qquad (6.1)$$

values of C_c are between 0.3 and 0.4 for the I.C.A. series and between 0.33 and 0.4 for the I.C.B. series. The consolidation lines show a considerable scatter, partly because of small errors in the initial volume measurements, and partly due to different types of loading and the amount of secondary consolidation. For anisotropic tests (Fig.5.36) the consolidation lines are parallel, with a definite shift to the left, due to an increasing amount of shear strain ($\eta = q/p$ increases from 0.3 to 0.8); the lines approach and are parallel to the state-of-failure line where $q/p = M \simeq 1$. Two different state-of-failure lines are shown in Fig. 5.35 : one was obtained from undrained (I.C.U.) and the other from drained (I.C.D.) and p constant (I.C.P.) tests. The state-of-failure line in Fig. 5.36 was obtained from the A.C.U. tests.

The drained and undrained state-of-failure lines do not coincide as is generally known. But the former is almost coincident with the anisotropically consolidated undrained line shown in Fig. 5.36. It has been reported by Henkel and Sowa (1964) that the failure lines are different for K_o and isotropically consolidated undrained tests (failure being taken at the maximum q).

6.3.1.1 Shear deformations during anisotropic consolidation

If the ratio of plastic shear strains to volumetric strains during these tests is taken as :

$$\frac{\varepsilon_p}{(\varepsilon_v)_p} = \frac{\varepsilon - \varepsilon_r}{\varepsilon_v - (\varepsilon_v)_r} \qquad (6.2)$$

and if the elastic (or recoverable) strain ε_r is negligible, then $\varepsilon = \varepsilon_p$ and using equations (2.42) and (2.49), we obtain :

$$\frac{\varepsilon}{(\varepsilon_v)_p} = \frac{1}{(1 - \frac{k}{\lambda})} \left(\frac{\varepsilon_1}{\varepsilon_v} - \frac{1}{3}\right) \qquad (6.3)$$

Values of $\frac{\varepsilon}{(\varepsilon_v)_p}$ and $\frac{\varepsilon}{\varepsilon_v}$ for anisotropic consolidation are plotted against the stress ratio $\eta = q/p$ in Fig. 6.1. The relationships are linear, but do not pass through the origin possibly because of the stress-history of the samples (the total strain ratio line in Fig. 6.1 corresponds to the line (3) in Fig. 5.57b).

From equation (6.3) it is evident that if $(\varepsilon_v)_p$ is related to the mean effective stress in terms of :

$$(\varepsilon_v)_p - (\varepsilon_v)_{po} = (\lambda - k) \log_e \frac{p}{p_o} \qquad (6.4)$$

and:

$$\frac{\varepsilon}{(\varepsilon_v)_p} = f(\eta) = \text{constant} \qquad (6.5)$$

then

$$\varepsilon = f(\eta)\ (\lambda - k) \log_e \frac{p}{p} \qquad (6.6)$$

Hence for any other stress path during anisotropic consolidation the volumetric strains and shear strains can be obtained (if the values

λ, k and $f(\eta)$ are known for the soil).

6.3.2 Shear Tests

(a) Drained Tests (I.C.D. Series)

Since the investigation of the behaviour of remoulded Lias clay was also concerned with obtaining the basic soil parameters, conventional drained and undrained tests were carried out.

Results of four drained tests are presented in Chapter 5, and the stress path with strain contours are shown in Fig. 5.55a.

The stress-strain curves q vs ε_1 and $\eta = q/p$ vs ε_1 (Figs. 5.37 - 5.40) exhibit steep initial gradients which flatten out at large axial strains. The initial steep gradients are due to the build up of small pore pressure at the bottom of the sample (drainage from the top), necessary for drainage to proceed. These pressures were not allowed to increase above 20 KN/m^2 by adjusting the rate of strain. When the volume change slowed down (close to the q_{max}), the pore pressure was seen to drop.

Since failure could not be defined in terms of q_{max} or $(q/p)_{max}$, as these were not reached before the samples were deformed beyond a reasonably cylindrical shape, failure was assumed to have occurred at a point at which the incremental strain ratio ($\Delta\varepsilon_v/\Delta\varepsilon_1$) became almost constant (this approximately corresponded to ε_1 = 14% and ε_v between 5 and 6%).

For drained tests, the value of stress ratio at failure $(q/p)_f = M$ falls between 0.95 and 1.0. The common tangent plotted to the Mohr circles shown in Fig. 5.55b, for stresses at failure from the drained and undrained tests give $c' \simeq 0$ and $\phi' = 25.5^{o}$.

(b) Undrained Tests (I.C.U. Series)

The first series of undrained tests were carried out in the Independent Stress Cell. They include C.U.2 and C.U.3 (strain-controlled) and C.U.4 and C.U.6 (stress-controlled) tests (Figs. 5.41 - 5.44).

The C.U.2 test was an anisotropically consolidated test, whereas all the other tests were isotropically consolidated. The rest of the strain controlled undrained tests were carried out in a standard Triaxial Cell (Figs. 5.45 - 5.49).

Stress-strain curves from undrained tests (q vs ε_1) show steeper initial gradients for stress-controlled tests than those for strain-controlled tests. The curves from the former tests flatten suddenly at certain values of q (with q/p still rising), whereas in the latter tests they curve gradually. In strain-controlled tests at large strains, q reaches its maximum value, or increases slightly, while q/p is still increasing; this is because the pore pressure, u, still increases.

In this range $\delta q = \delta u$ (small increments) but total $\Delta q \neq \Delta u$. This state was considered to correspond to the state-of-failure.

The value of A (pore pressure coefficient) was found to vary between 0.27 and 0.4 at the start of the tests, and between 0.7 and 0.85 at failure. It was thought that this behaviour could be due to the fast rate of strain, but when a test was run at a very slow rate (C.U.8), a similar phenomenon was observed (the original rate was calculated according to Bishop and Henkel, 1957) - it is possible that for large samples during shearing the pore pressure at mid-plane of the sample is higher than at the ends where it was monitored.

Recorded values of $(q/p)_f = M$ for undrained tests were between 0.98 and 1.1 (for C.U.16 test, where $H_o/D_o = 1$, M = 1.15). Results of the undrained stress-path plotted in the q-p plane (Fig. 5.56a) show a near vertical initial part for the stress-controlled tests, but for strain-controlled tests they are oblique and fall below the former curves.

It is interesting to note that the strain contour of $\varepsilon_1 = 0.1\%$ on the q-p plane for both drained and undrained tests (with the exception of C.U.8 test) is horizontal (Figs. 5.55a and 5.56a), and the rest of the lines radiate from the point of intersection of $\varepsilon_1 = 0.1\%$ line and M = 1 line. This is possibly due to the influence of the previous stress-history of the soil.

(c) Constant mean effective stress tests (I.C.P. Series)

Results of the two tests shown in Fig. 5.54 show similar stress-strain curves to those of the drained tests (Figs. 5.37 - 5.40), but with smaller volumetric and shear strains at failure. The evaluated value of $(q/p)_f$ = M for Test C.P.20 was approximately equal to 1.

6.3.3 Anisotropically Consolidated Undrained Tests (A.C.U. Series)

In this series of tests stress-strain curves (q vs ε_1) rise sharply, reaching the maximum value at small strains, and then either remain constant or fall, depending on the value of the q/p ratio (Figs. 5.50 - 5.53). The former applies to small q/p ratios and the latter to high q/p ratios.

Shear strains at the maximum values of q were small (see Table 5.10) compared with those observed in the I.C.U. series. The pore pressure increment and the stress ratio q/p was found to increase even after the deviator stress 'q' had reached its maximum; this was not due to the rate of loading as this was very slow (0.016 mm/min - Test A.U.22 performed at a quarter of this rate of strain and the same behaviour was observed).

During the time that the q reached its maximum the rise in the pore pressure was small, and the values of the pore pressure coefficient A at the start of the tests were between 0.4 and 0.5 (similar high values of A were reported for overconsolidated clays by Simon and Som, 1969, and Thomas, 1973). Beyond the peak values of q the pore pressure

and stress ratio q/p were still increasing, but the soil was undergoing large shear deformations under an almost constant deviator stress. From these results it is apparent that an anisotropically, normally consolidated clay, when sheared in an undrained manner, behaves as an overconsolidated soil, i.e. as a rigid-plastic material rather than a plastic (strain hardening) material.

If the points of maximum q are to be taken as the failure points, then smaller values of ϕ' and M are obtained (in this case $\phi' = 23^{o}$ and $M \simeq 0.9$) than those evaluated for the I.C.U. series - see section 6.4(a). This type of behaviour for anisotropically consolidated samples of remoulded clay was reported elsewhere (Ladd, 1965, R Khera et al, 1967). The values of ϕ' and M taken at maximum q/p values are 25.5^{o} and 1.0 respectively and the value of $A_f \simeq 1$ or greater than one at these points. The state-of-failure line for this series plotted in Fig. 5.36 for the case of $M = (q/p)_f = 1.0$ is close to the state-of-failure line obtained from the I.C.D. series and lies above the I.C.U. state-of-failure line (see Section 6.3.2).

The observed difference between the state-of-failure lines of the I.C.U. and I.C.D. - A.C.U. series (Figs. 5.35 and 5.36) is contrary to the assumption made in the critical state theory. The possible sources of this difference are :

(a) That large shear strains experienced by the soil during anisotropic consolidation or drained shearing alter its structure, thus affecting the void ratios.

(b) In the undrained tests pore pressure was measured at the top and bottom of the specimen and for large samples it is possible that the pore pressure at mid-height of the sample (failure zone) was higher than it was at the ends.

It is conceivable that if large shear deformations were allowed, with relation to the size of the samples, these lines could coincide and approach a common critical void ratio (C.V.R.) line.

6.4 Secondary Consolidation Deformations

One of the objects of the present work was to study the secondary deformations in both oedometer and triaxial tests. The subject has been thoroughly investigated in the one-dimensional consolidation tests (see references in Section 2.2) but not in the three-dimensional consolidation or in shearing tests (Walker, 1969).

In the present work the results from the triaxial tests were unfortunately inconclusive. This was partly due to the difficulties of performing a sufficient number of triaxial tests (because of the time taken in testing of large samples) and partly due to the difficulties of maintaining constant temperature in the laboratory.

The available results are those from isotropically and anisotropically consolidated tests and from one p-constant test and oedometer tests. The secondary deformations are considered

as the rate of deformation or the rates of volumetric and shear strains; the volumetric strains, ε_v, and the shear strains, ε_1, are strain invarients as defined in Section 2.4. These rates of strain are considered in terms of the gradients of the ε_v and ε_1 vs logt plots, where they appear as straight lines; the gradient defines a logarithmic rate of strain (α in equation 2.33), which is related to the true rate of strain by equation (2.34).

The rates of volumetric strains, $\alpha_{\varepsilon_v} = 2.3t \frac{d\varepsilon_v}{dt}$, and shear strains, $\alpha_\varepsilon = 2.3t\frac{d\varepsilon}{dt}$, are plotted against the stress ratio q/p in Fig. 6.2. Results of the strain rates from oedometer tests are also shown in Fig. 6.2, where stress ratio q/p is calculated using the value of $K_o = 0.575$ and volumetric strain rates from Fig. 5.14 and 5.17. Fig. 6.2 indicates that the volumetric strain rate is independent of stress ratio, i.e. $\alpha_{\varepsilon_v} \simeq$ constant and shear strain rate is increased linearly with the stress ratio, i.e. $\alpha_\varepsilon \propto \eta$ (Walker, 1969 reports the same behaviour for stress controlled drained tests on Kaolin).

6.5 Predictions of Strains for Different Stress Paths

In this section the results of the anisotropically consolidated tests are used to predict strains for other tests.

In Fig. 6.3(a) shear strains from drained and undrained tests (in both tests samples were consolidated to the same consolidation stress p, see Fig. 6.5(a)), are plotted in the form of the undrained shear strains $\varepsilon_u = \varepsilon_1$ against drained shear strains $\varepsilon_d = \varepsilon_1 - \frac{\varepsilon_u}{3}$. It is seen that for the tall samples ($H_o/D_o = 2$) a linear relationship exists between these two strains, defined by $\varepsilon_d = 4.3\ \varepsilon_u$; test results from one test on a short sample $H_o = D_o$ also show linear relationship but of different gradient. Similar results from P-constant and undrained tests (with $H_o/D_o = 2$) shown in Fig. 6.3(b) give a linear relationship $\varepsilon_{p(const)} = 2.5\varepsilon_u$.

Following the suggestion made by Roscoe and Poorooshasb (1963) that for normally consolidated clays for any stress increment the total shear strain ε is made up of two parts, one associated with a change in the stress ratio $\eta = q/p$ (at constant volume), ε_u, and the other, with an increase in the mean stress p (at constant η), ε_η, one can write that :

$$\varepsilon = [\varepsilon_u]_{v = \text{const}} + [\varepsilon_\eta]_{\eta = \text{const}} \qquad (6.6)$$

If this is true, then separately obtained values of ε_u (from a series of undrained tests) and ε_η (from a series of anisotropically consolidated tests) can be used to obtain shear strains, ε, of a

soil subjected to any stress increment. Volumetric strains, ε_v, can be calculated from the e - logp plots (Fig. 1, Lewin, 1975).

Knowing the ratio of $\varepsilon_d/\varepsilon_u$ the strains ε_u can be determined if ε_η are known (Lewin, 1975). If in equation (6.6) ε is the shear strain for a drained stress path, then $\varepsilon_d = \varepsilon_u + \varepsilon_\eta$, and hence one can write :

$$\varepsilon_u = \frac{\varepsilon_\eta}{(\varepsilon_d/\varepsilon_u - 1)} \qquad (6.7)$$

Therefore shear strains during a drained test or for any stress increment in the q-p plane resulting in plastic strains can be calculated if only the values of ε_η and $\varepsilon_d/\varepsilon_u$ are known; and associated volumetric strains can be calculated if C_c (compression index) is known. Comparison of the shear strains from drained and p-constant tests and calculated strains according to equation (6.6) are shown in Fig. 6.4a and show a very good agreement. Volumetric strains along a drained stress path calculated according to equation (6.1) are shown in Fig. 6.4b (the isotropic and anisotropic consolidation lines are parallel, Fig. 5.36). The observed volumetric strains from drained tests are greater than predicted at values of $\eta < 0.3$ and smaller than predicted values at $\eta > 0.7$.

6.5.1 Path Dependency of Strain Increments for Normally Consolidated Lias Clay

The behaviour of a normally consolidated soil as a work-hardening material leads to the hypothesis of the existence of a plastic potential (Section 2.4.3); this implies that the normality law could be applied to the soil. But it has been argued and proved by Lewin (1973, 1975)

that for normally consolidated soils the plastic potential is not a unique surface in a stress space: different plastic potential exists for different stress histories. Thus plastic potential of an anisotropically consolidated soil is different to that of an isotropically consolidated soil (the latter has been found to correspond to the undrained stress path, Lewin, 1975).

For normally consolidated Lias clay the directions of strain vectors obtained from three different tests (isotropically consolidated drained tests, p-constant test and anistropically consolidated undrained tests) are shown in Fig. 6.5b. The strain directions (ε vs ε_v) are plotted for different values of $\eta = q/p$ from the above tests.

The results show that the directions of the strain vectors for anisotropic tests differ markedly from those of p-constant and drained tests (the latter two being closer together). Thus it indicates that for remoulded Lias clay different plastic potentials exist (if plastic potential surfaces are constructed from the strain directions using the normality condition) as observed by Lewin (1973) for the slate dust.

6.5.2 Other Predictions for Remoulded Lias Clay

From the series of anisotropically consolidated tests the value of K_o (coefficient of earth pressure at rest $\varepsilon_2=\varepsilon_3=0$) was evaluated to be 0.575. This is compatible with 0.569 obtained from the empirical expression of $K_o = 1 - \sin\phi'$ (Jacky, 1948). From the Modified Cam-clay model (Roscoe and Burland, 1968), a value of 0.7 is predicted for K_o.

The predictions of the undrained stress path and shear strains using the Modified Cam-clay and Cam-clay model are compared with the experimental results in Fig. 6.6a. The observed stress path only corresponds with the predicted curve from the modified theory at early stages ($\eta < 0.5$); and there is not a close agreement with the Cam-clay predictions.

In Fig. 6.5b the strain increment ratios, $\frac{\varepsilon}{(\varepsilon_v)_p}$, obtained from anisotropic consolidation tests, consolidated drained tests and p-constant tests, are compared with the predicted values according to the Modified Cam-clay and Cam-clay model. This comparison shows a marked difference between the observed and predicted strain ratios, particularly for the results of the the anisotropic test; the drained and p-constant strain ratios are very close. This again implies that if the plastic potentials are constructed from the strain increment directions they are different for two cases of isotropically and anisotropically consolidated samples.

In conclusion, it can be stated that for remoulded Lias clay the magnitude of both the volumetric and shear strains, for any stress path, can be predicted reasonably from the knowledge of C_c, ε_η and the strain ratio $\varepsilon_d/\varepsilon_u$, but because of the existence of different plastic potentials for the soil, directions of the resultant strain vector cannot be predicted from the information; neither can be predicted accurately by the Modified Cam-clay theory.

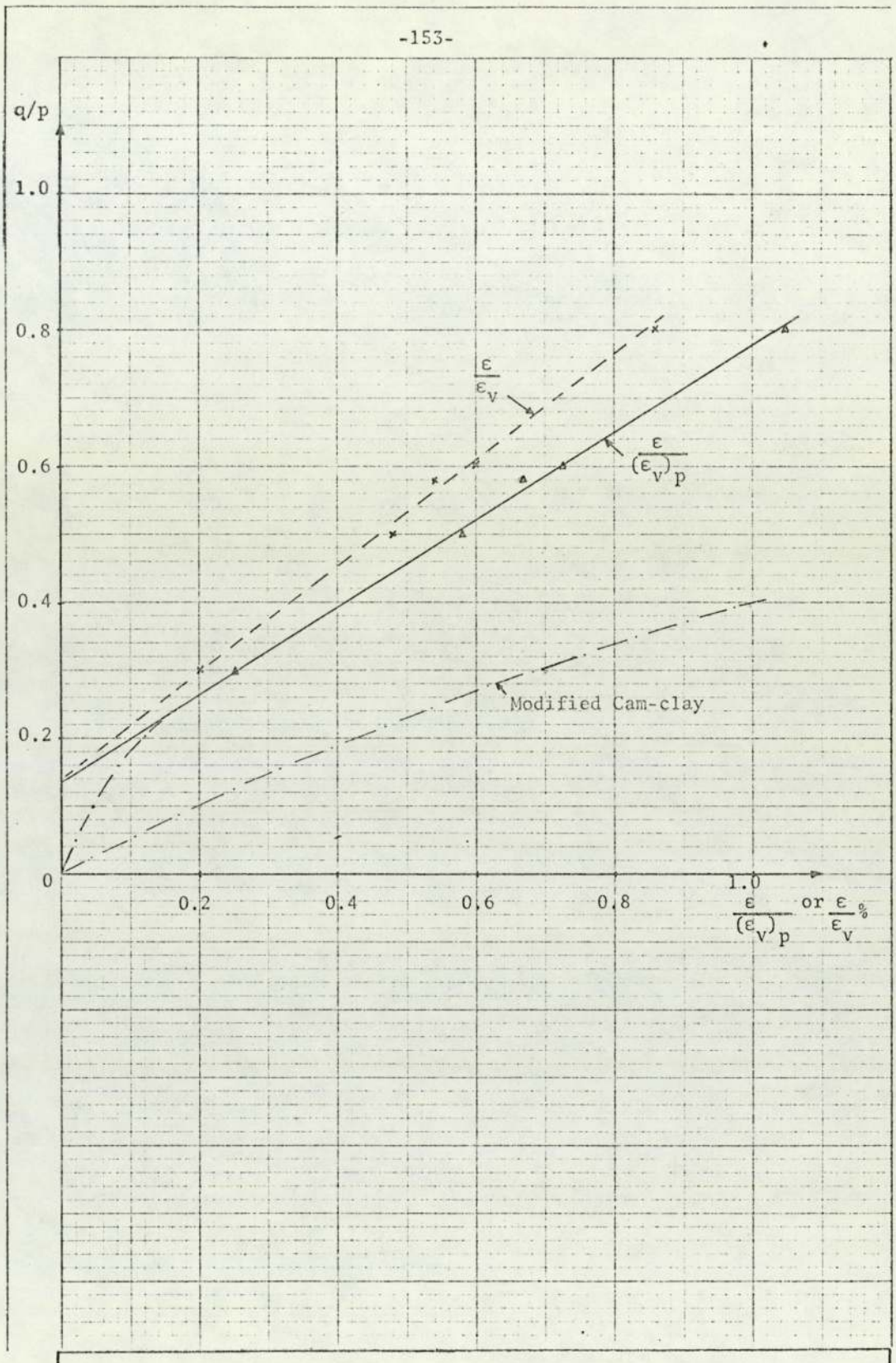

Fig. 6.1 Strain ratio vs stress ratio
(anisotropically consolidated samples)

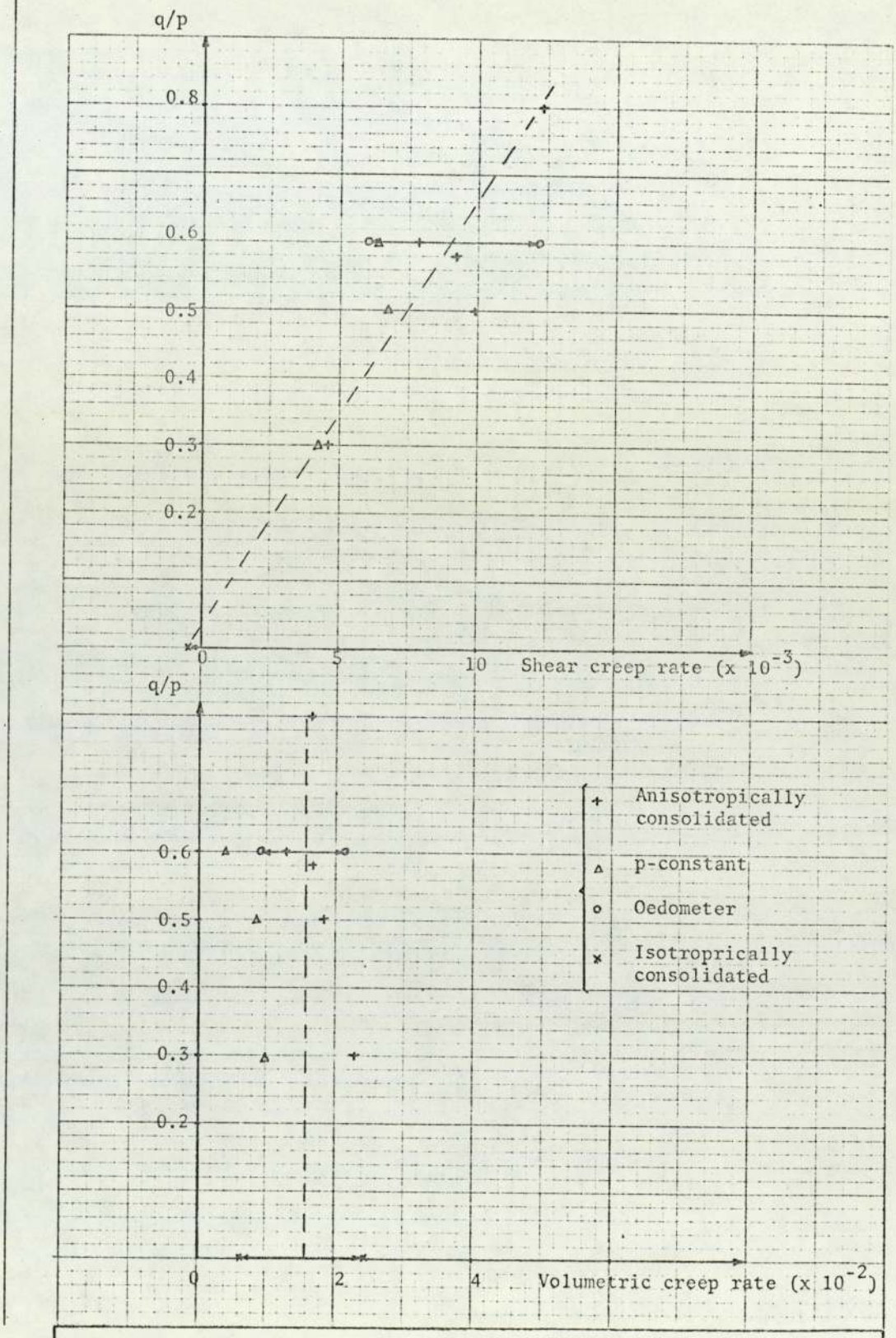

Fig. 6.2 Creep rate of strain vs stress ratio - during secondary consolidations

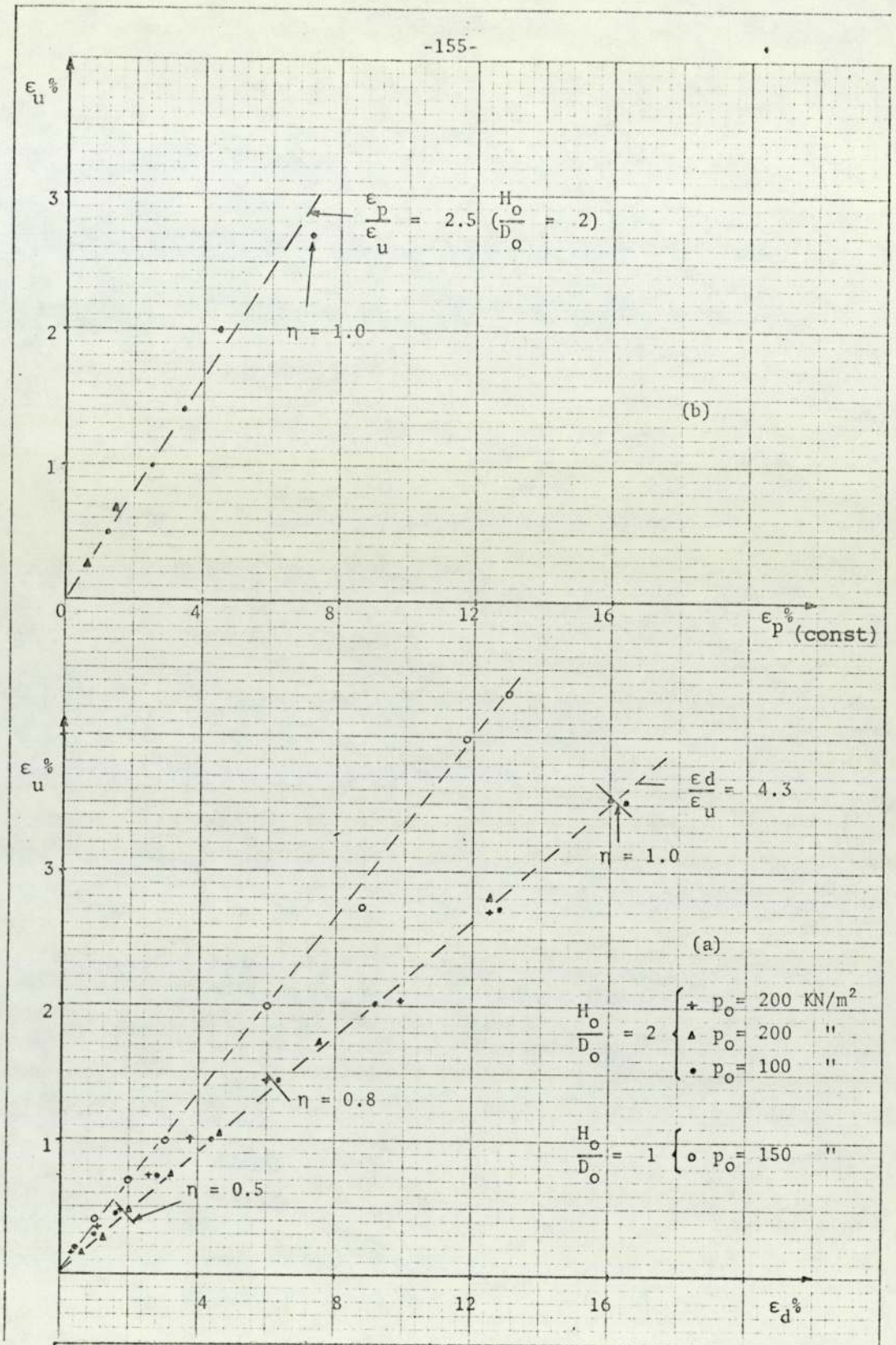

Fig. 6.3 Comparison of shear strains in drained and undrained tests

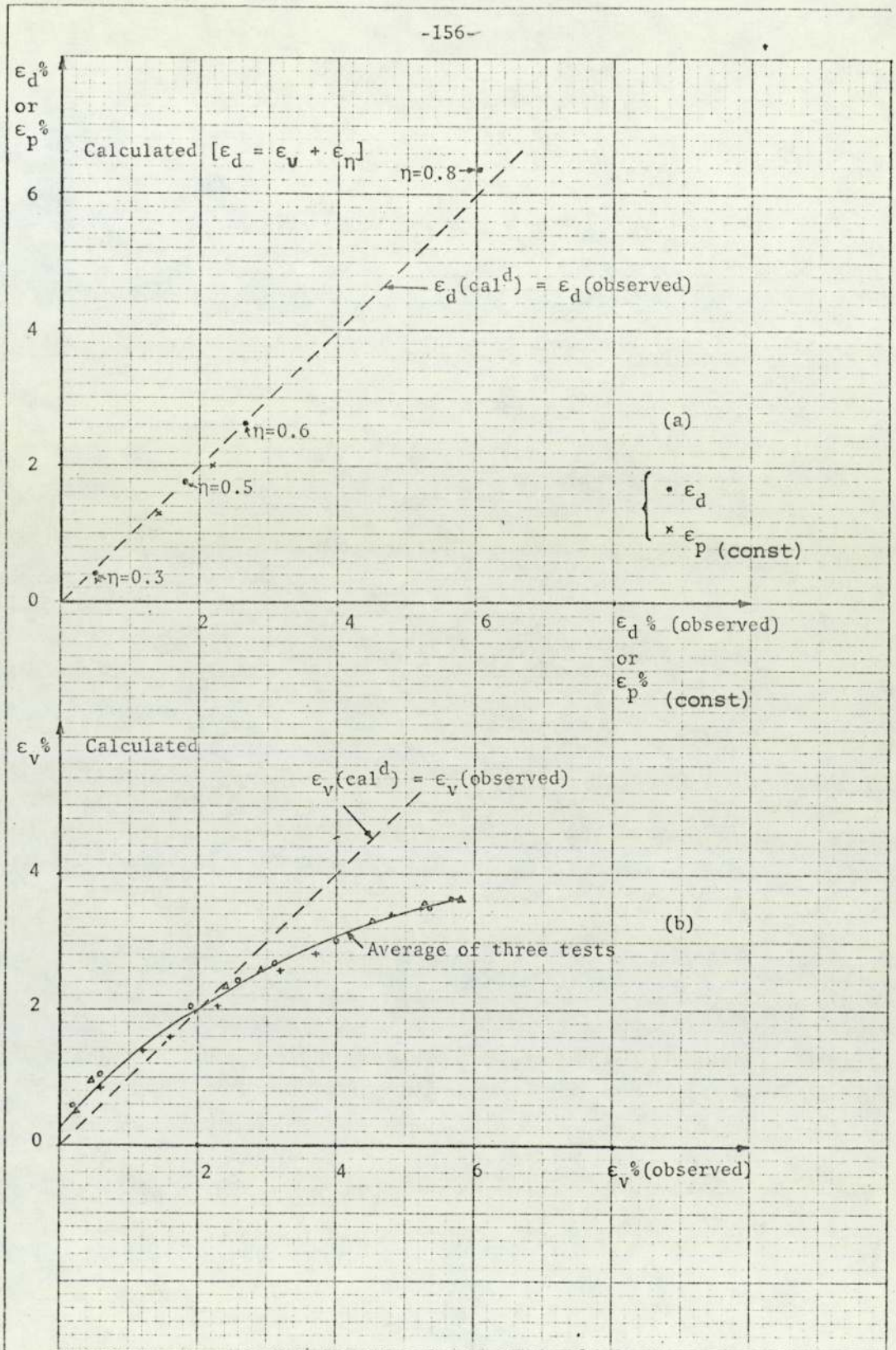

Fig. 6.4 Comparison between calculated and observed strains (drained and p-constant tests)

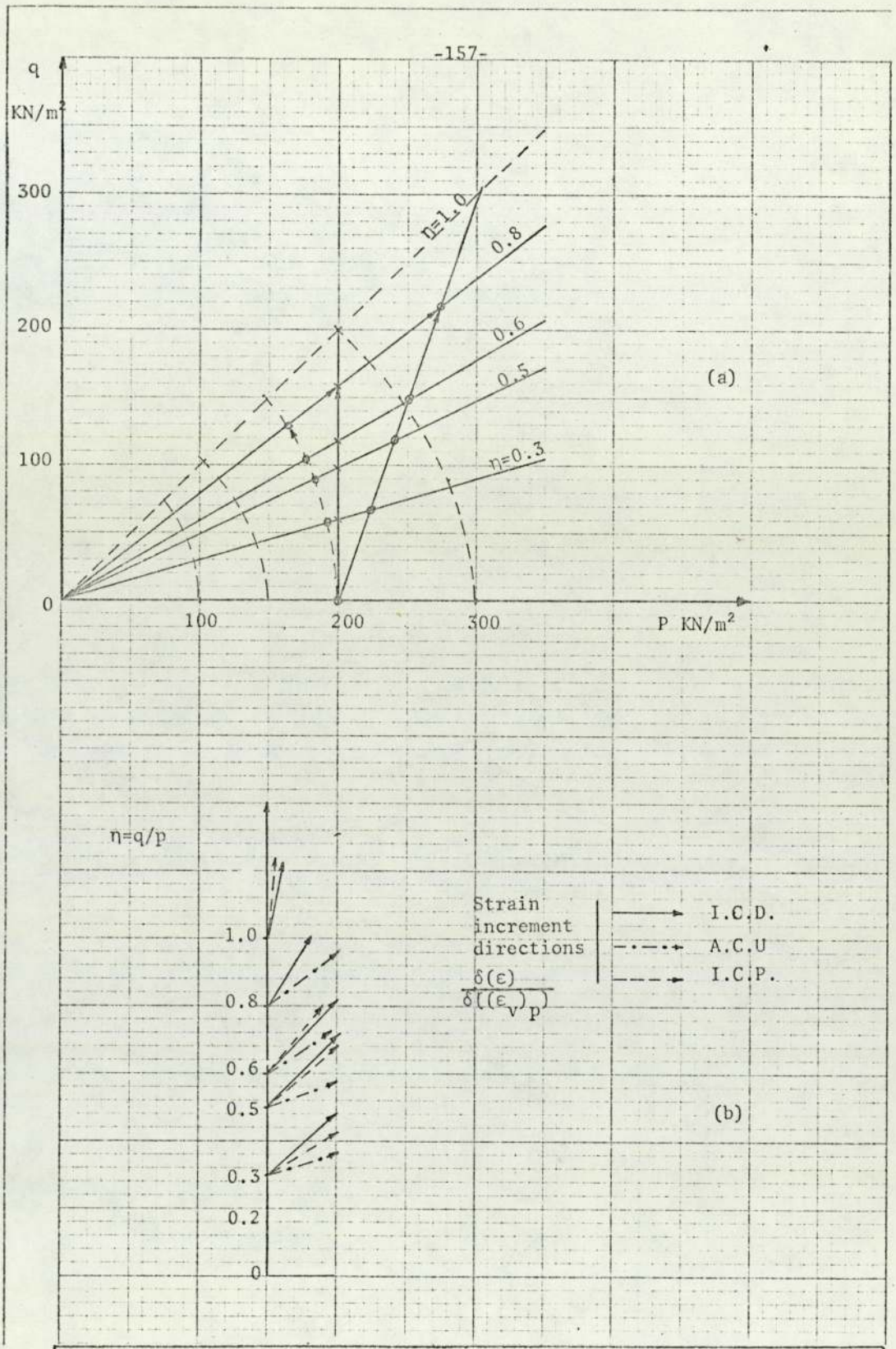

Fig. 6.5 (a) stress paths, (b) strain increment directions

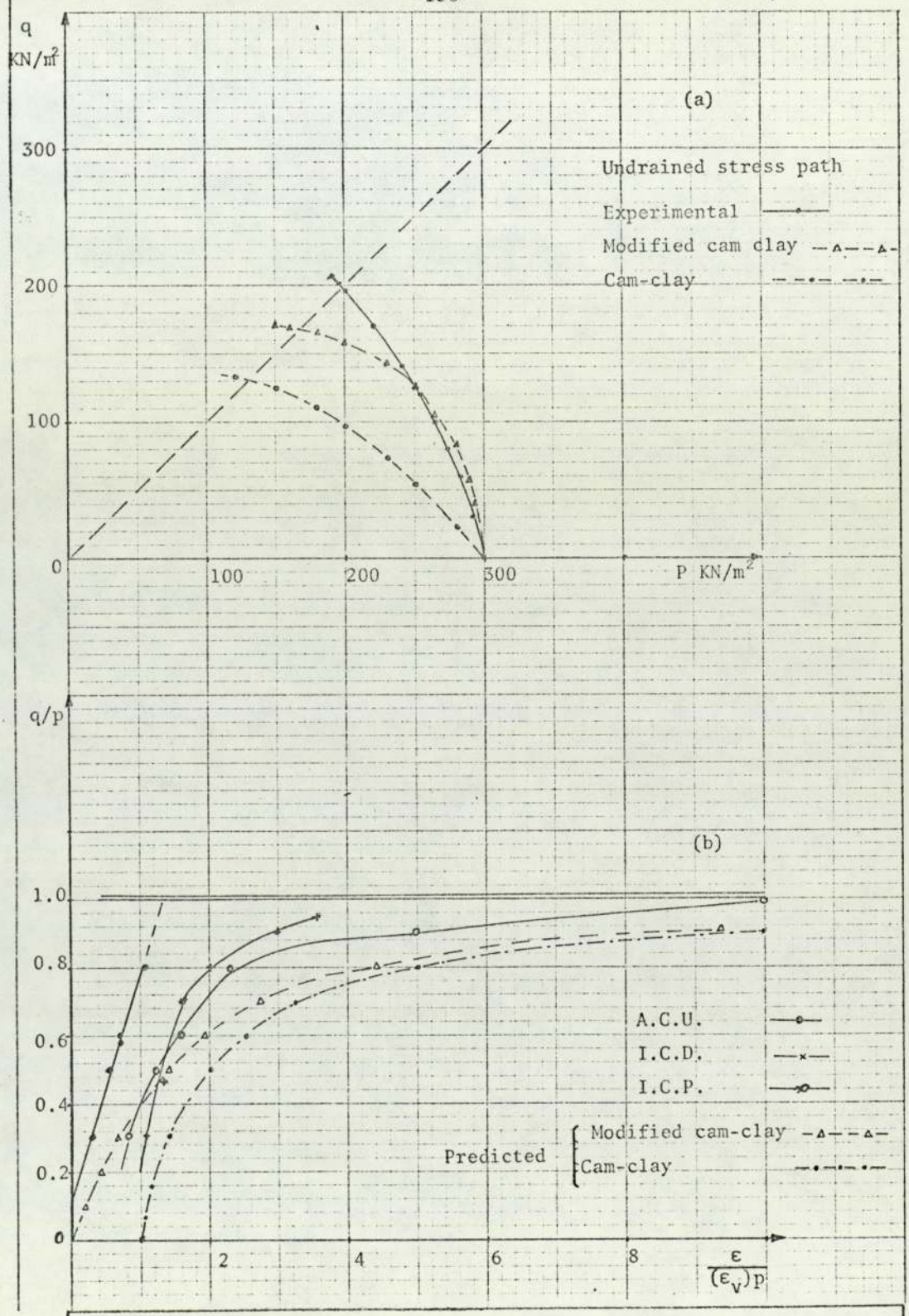

Fig. 6.6 (a) comparison of undrained stress path
(b) stress ratio vs strain ratio

CHAPTER SEVEN

GENERAL SUMMARY OF CONCLUSIONS

7.1 General Summary of Conclusions

This work is concerned with the stress-strain behaviour of saturated remoulded Lias clay and was executed under the following three main headings according to the testing programme outlined in Chapter 3.

(I) Sample preparation and evaluation of the basic physical soil parameters of the Lias clay.

(II) Investigation of soil deformation and pore pressure development in one-dimensional consolidation together with observations of the creep strains and their predictability.

(III) Study of the stress-strain behaviour of the soil when subjected to stress paths simulated in a triaxial apparatus under controlled strain and stress loading and investigation of theoretical methods of prediction of this behaviour.

(I) The findings in this section are summerized below :

(a) The initial moisture content of the clay (mixing water content) had an effect on the void ratio - effective stress relationship. The higher the initial moisture contents, the higher the moisture content under the same consolidation stress (Fig. 5.2).

(b) The initial one-dimensional consolidation of the soil in the tall oedometer induced a certain degree of anisotropy in the samples. Isotropic stresses of up to four times the initial consolidation

stress were needed to eliminate this stress history.

(c) Mechanical soil properties obtained from different tests and used in theoretical predictions are :

Compression index: $C_c = 0.33 - 0.40$

Swelling index: $C_s = 0.06 - 0.072$

Drained shear strength parameters: $c' = 0$, $\phi' = 25.5^o$ and $M \simeq 1.0$

(II) In section (II) the following points were investigated experimentally and the results were compared with the theories introduced in Chapter 2 :

(a) The effect of the rate of consolidation $(\frac{de}{dt})$, as a third variable, on the consolidation lines on the e - logp; it was confirmed that the lines were getting closer as the rate of consolidation decreased. This suggests that there must be an ultimate line in the e - logp plane unique to any soil beyond which no further compression takes place. The scope of the creep investigations in triaxial apparatus was curtailed (see Section 6.4), but the available results shown in Fig. 6.2 indicate that the volumetric strain rate is independent of stress ratio (or deviatoric stress) and shear strain rate is increasing linearly with the stress ratio.

(b) A solution of the one-dimensional consolidation based on a saturated Kelvin body model (Gibson and Lo, 1961) was examined. It was found that once the final strain was chosen the predicted consolidation strains during the secondary consolidation (end of the pore pressure dissipation) were in good agreement with the experimental results, but the primary consolidation strains were not predicted well.

(III) In section III the following points were investigated and conclusions are drawn upon the observations in each case :

(a) Parallelism of the isotropic and anisotropic consolidation lines on the e - logp plot.

Anisotropic consolidation lines were parallel and moved towards the state-of-failure line as the value of $\eta = q/p$ increased (Fig.5.36). In most cases (including the isotropic test) some anisotropy present in the smaples (effect of initial one-dimensional consolidation) resulted in a scatter of the results at low stresses after which the slopes of the consolidation lines became the same, but the lines were bodily displaced (Fig. 5.35).

(b) The state-of-failure line on the e - logp plot.

The state-of-failure lines from undrained and drained tests did not coincide whereas the latter coincided with the failure line obtained from the anisotropic undrained tests.

In drained tests there was continuing volume decrease at failure and in undrained tests continuing pore pressure increase at failure. In anisotropically consolidated undrained tests, maximum q was reached at small strains while the pore pressure and q/p ratio continued to increase. It appears, therefore, that the state-of-failure lines obtained at large shear strains are tending to a limit which is possibly the C.V.R. line.

(c) From the anisotropic consolidation tests a linear relationship between the strain ratio ($\frac{\varepsilon}{(\varepsilon_v)_p}$) and stress ratio, q, was established (Fig. 6.1).

(d) There is also a linear relationship between drained shear strains, ε_d, and undrained shear strains, ε_u, for samples consolidated to the same mean effective stress p. The ratio of $\varepsilon_d/\varepsilon_u$ (for samples with H_o/D_o ratio of 2) was found to be equal to 4.3.

(e) The shear strains for any stress paths can be accurately predicted using the expression $\varepsilon = \varepsilon_\eta + \varepsilon_u$, but the volumetric strain predictions are not so good and tend to underestimate the strains at or close to the failure. It was concluded that for normally consolidated clays, shear strains for any stress path (producing plastic strains) can be predicted from the knowledge of the $\varepsilon_d/\varepsilon_u$ ratio and ε_η.

(f) Experimental results were used to investigate the basic energy equation (2.54) of the Modified Cam-clay model. It was found that the model did not give good predictions of the strain ratios in the anisotropic consolidation, but better agreement was obtained with the results of the p-constant tests.

Undrained stress path predicted from the model did not coincide with the experimental results as failure was approached (Fig. 6.6); theoretical results predicted A_f values greater than one.

(g) Effect of stress history on the strain increment vector

The investigation of the incremental strain vector directions showed that they are dependent on the loading history of the samples and, therefore, if plastic potentials for the case of isotropically and anisotropically consolidated samples are constructed, from the strain increment directions at any point, they are different. This implies that if the same stress increment vector is applied to the two soils, at the same point in a stress plane, the resultant strain vector will have different directions.

7.2 Suggestions for Further Research

It is apparent that a stage has been reached in investigation of the behaviour of remoulded soils where it would be advantageous to examine the effect of different stress paths on their microstructure. It is, therefore, suggested that studies should be made to establish the importance of the effects of the structure of the soil on the yielding and deformation. The same applies to investigation of the creep phenomenon.

With reference to the specific results presented in this work, cyclic loading (unloading and reloading) tests should be carried out in constant stress ratio consolidation and p-constant and drained tests, to check the time dependent and recoverable and irrecoverable strains and the assumption that $\varepsilon_r = 0$.

In investigation of the incremental stress-strain relationship, the stresses should be taken beyond the point of influence of the stress history of the soil including the effect of the secondary consolidation deformations, i.e. large stress probes should be used.

Finally, it must be pointed out that no advantage was gained from testing of large (70 mm diameter) samples of remoulded soil; in fact considerable time would have been saved if smaller (38 mm diameter) samples had been tested.

REFERENCES

REFERENCES

ANAGOSTI, P (1963). 'Stress, Deformations and Pore Pressure in Triaxial Tests Obtained By A Suitable Rheological Model'. Proc. Eur. Conf. S.M. & F.E. Wieshaden, Vol. 1, pp. 1-6.

BARDEN, L and McDERMOTT, J W (1965). 'Use of Free Ends in Triaxial Testing of Clays'. Journal of S.M. & F.E., Proc. A.S.C.E. 1965, S.M.6.

BARDEN, L (1965). 'Consolidation of Clay with Non-Linear Viscosity'. Geotechnique. Vol. 15. pp. 345-362.

BENNETT, D H (1975). Private Communications. The University of Aston in Birmingham.

BENNISON, G M and WRIGHT, A E (1969). 'Geological History of The British Isles'. Edward Arnold Limited, London.

BIOT, M A (1941). 'General Theory of Three-Dimensional Consolidation'. J. of Applied Physics, Vol. 12, pp. 155-164.

BIOT, M A (1956). 'Theory of Deformation of a Porous Viscoelastic Anisotropic Solid'. J. of Applied Physics, Vol. 27, No. 5, pp. 459-467.

BISHOP, A W and HENKEL, D J (1962). 'The Measurement of Soil Properties in the Triaxial Test'. Arnold 1962.

BJERRUM, L (1967). 'Engineering Geology of Normally Consolidated Marine Clays as Related to Settlement of Buildings'. Geotechnique, Vol. 17, p. 81.

BURLAND, J B (1965). 'The Yielding and Dilation of Clay'. Correspondence, Geotechnique, Vol. 15, pp. 211-214.

BURLAND, J B (1972). 'A Method of Estimating Pore Pressure and Displacement Beneath Embankments on Soft, Natural Clay Deposits'. Proc. Roscoe Memorial Symp., Cambridge. pp. 505-536, Foulis.

CALLADINE, C R (1963). 'Correspondence on a Theoretical and Experimental Study of Strains in Triaxial Tests on Normally Consolidated Clays'. Geotechnique, Vol. 13, pp. 15-23.

CALLADINE, C R (1971). 'A Microstructure View of the Mechanical Properties of Saturated Clay'. Geotechnique, Vol. 21, pp. 391-415.

COULTHARD, M (1975). 'Petrology of Weathered Lower Lias Clay'. Ph.D. Thesis, The University of Aston in Birmingham.

CRAWFORD, C B (1965). 'The Resistance of Soil Structure to Consolidation'. Can. Geotech. J. Vol. II, No. 2, pp. 90-97.

DRUCKER, D C, HENKEL, D J and GIBSON, R E (1957). 'Soil Mechanics and Work-Hardening Theories of Plasticity'. A.S.C.E. Transactions, Vol. 122, pp. 338-346.

DRUCKER, D C (1964). 'Concept of Path Independency and Material Stability for Soils'. I.U.T.A.M. Symposium, Grenoble, Rheology and Soil Mechanics. Berlin, pp.23-46.

GIBSON, R E and LO, K Y (1961). 'A Theory of Consolidation for Soils Exhibiting Secondary Compression'. Norwegian Geotechnical Institute - Publication No. 41.

HENKEL, D J and SOWA, V A (1964). "The Influence of Stress History on Stress Path in Undrained Triaxial Tests on Clay'. A.S.T.M. Special Publication, No. 361, pp.280-292.

HENKEL, D J (1959). 'The Relationship between Strength, Pore Water Pressure and Volume Change Characteristics of Saturated Clays'. Geotechnique. Vol. 9, p. 119.

HILL, R (1950). 'The Mathematical Theory of Plasticity', Oxford.

KHERA, R P & KRIZEK, R J (1967). 'Strength Behaviour of an Anisotropically Consolidated Remoulded Clay'. Highway Research Record, 190, pp 8-18.

LADD, C C (1965). "Stress-strain Behaviour of Anisotropically Consolidated Clays During Undrained Shear'. Proc. Sixth Int. Conf. Soil Mech. 1. p.282.

LEONARD, G A and RAMIAH, B K (1960). 'Time Effects in the Consolidation of Clays'. A.S.T.M. Special Technical Publication 254, pp. 116-130.

LO, K Y (1961). 'Stress-strain Relationship and Pore Water Pressure Characteristics of a Normally Consolidated Clay'. Proc. 5th Int. Conf. S.M. & F.E. Paris, Vol. 1, pp. 219-224.

LEWIN, P I and BURLAND, J B (1970). 'Stress Probe Experiments on Saturated Normally Consolidated Clay'. Geotechnique, Vol. 20, pp.38-56.

LEWIN, P I (1973). 'The Influence of Stress History on the Plastic Potential'. Proc. Symp. on plasticity and soil mechanics. Cambridge. pp. 96-106.

LEWIN, P I (1975). 'Plastic Deformation with Induced Anisotropy'. Istanbul Conference on S.M. & F.E. (Proceedings).

LOWE, J (1974). 'New Concept in Consolidation and Settlement Analysis'. Proc. Am. Soc. Civ. Engrs. Vol. 100, No. CT6, pp. 574-611.

McKINLAY, D G (1961). 'A Laboratory Study of Rates of Consolidation in Clays with Particular Reference to Conditions of Radial Pore Water Drainage'. Proc. 5th Int. Conf. S.M. & F.E., Paris, Vol. 1, pp. 225-229.

MITCHELL, R (1970). 'On the Yielding and Mechanical Strength of Leda Clay'. Can. Geotech. Jour. Vol. 7, pp. 297-312.

NAMY, D L (1970). 'An Investigation of Certain Aspects of Stress-Strain Relationship for Clay Soils'. PhD Thesis, Cornell University, Ithaca.

NASSERI, S (1972). 'Laboratory Investigation of Residual Strength of Lias Clay from Blockley, Gloucestershire'. MSc The University of Aston in Birmingham.

ROSCOE, K H, SCHOLFIELD, A N and WROTH, C P (1958). "On the Yielding of Soils', Geotechnique, Vol. 8, pp. 22-53.

ROSCOE, K H and POOROOSHASB H B (1963). 'A Theoretical and Experimental Study of Strains in Triaxial Compression Tests on Normally Consolidated Samples'. Geotechnique, Vol. 13, pp. 19-38.

ROSCOE, K H, SCHOLFIELD, A N and THURIRAJAH, A (1963). 'Yielding of Clays in State Wetter Than Critical', Geotechnique, Vol. 13, p.227.

ROSOE, K H and BURLAND, J B (1968). 'On The Generalized Stress-strain Behaviour of "Wet" Clay'. Symposium on Engineering Plasticity, pp. 535-609. Cambridge University Press.

ROWE, P W and BARDEN, L (1964). 'Importance of Free Ends in Triaxial Testing'. Proc. A.S.C.E., Vol. 90, S.M.I., pp.1-27.

SCHOLFIELD, A N and WROTH, C P (1968). 'Critical State Soil Mechanics'. London, McGraw-Hill.

SCOTT, R F (1963). 'Principles of Soil Mechanics'. Addison-Wesley Publishing Co. Ltd.

SIMON, N E and SOM, N N (1969). 'The Influence of Lateral Stresses on the Stress Deformation Characteristics of London Clay'. Proc. 7th Int. Conf. S.M. & F.E., Mexico.

SKEMPTON, A W and SOWA, V A (1963). 'The Behaviour of Saturated Clays during Sampling and Testing'. Geotechnique, Vol. 13, pp. 269-290.

ŠUKLJE, L (1969). 'Rheological Aspects of Soil Mechanics'. Wiley-Interscience, London.

ŠUKLJE, L (1963). "The Equivalent Elastic Constants of Saturated Soils Exhibiting Anisotropy and Creep Effects'. Geotechnique, Vol. 13, pp. 291-309.

TAN, T K (1964). 'Determination of the Rheological Parameters and the Hardening Coefficients of Clay'. I.U.T.A.M. Symposium, Grenoble. Rheology and Soil Mechanics. Berlin, pp. 256-270.

TAYLOR, D W and MERCHANT, W (1940). 'A Theory of Clay Consolidation Accounting for Secondary Consolidation'. J. Maths and Physics, Vol. 19, pp. 167-185.

TERZAGHI, K (1943). 'Theoretical Soil Mechanics', Wiley, New York.

THOMAS, C P (1973). 'Mechanical Properties of Heavily Overconsolidated Clays'. PhD Thesis, The University of Aston in Birmingham.

WALKER, L K (1969). 'Secondary Compression in the Shear of Clays'. Proc. A.S.C.E. Vol. 95, S.M.I. pp. 167-188.